DOE/NASA/0119-81/1
NASA CR-165271
MTI 81TR3

AN EXPERIMENTAL EVALUATION OF OIL PUMPING RINGS

Martin W. Eusepi
Jed Walowit
Maurice Cohen
Mechanical Technology Incorporated

April 1981

Prepared for
NATIONAL AERONAUTICS AND SPACE ADMINISTRATION
Lewis Research Center
Under Contract DEN 3-119

for
U.S. DEPARTMENT OF ENERGY
Conservation and Solar Applications
Office of Transportation Programs

MECHANICAL TECHNOLOGY INCORPORATED

968 ALBANY – SHAKER ROAD
LATHAM, NEW YORK 12110
Phone (518) 785-2211 · TWX 7104438150

April 9, 1981

U.S. Department of Energy
Conservation and Solar Applications
Office of Transportation Programs
Washington, D.C. 20545

Attention: Mr. R.E. Cunningham
Mail Stop 6-1

Subject: Contract No. DEN3-119
Final Report

Dear Mr. Cunningham:

Pursuant to the reporting requirements of the subject contract, we have herewith enclosed the Final Report incorporating the several requested modifications and comprising one (1) reproducible master and ten (10) copies.

We have also enclosed six (6) copies of the endorsed Document Release Authorization and have, on this date, distributed additional copies of the Final Report to each individual named on the attached listing.

Please address any questions you may have concerning the distribution named herein to the undersigned at 518/785-2476.

Sincerely,

Henry V. Foley

Henry V. Foley
Senior Contract Administrator

HVF:sen
attachments

cc: See attached distribution list

DOE/NASA/0119-81/1
NASA CR-165271
MTI 81TR3

AN EXPERIMENTAL EVALUATION OF OIL PUMPING RINGS

Martin W. Eusepi
Jed Walowit
Maurice Cohen
Mechanical Technology Incorporated
Latham, New York 12110

April 1981

Prepared for
National Aeronautics and Space Administration
Lewis Research Center
Cleveland, Ohio 44135
Under Contract DEN 3-119

for
U.S. DEPARTMENT OF ENERGY
Conservation and Solar Applications
Office of Transportation Programs
Washington, D.C. 20545
Under Interagency Agreement EC-77-A-31-1040

TABLE OF CONTENTS

TABLE OF CONTENTS (Cont'd)

LIST OF FIGURES

LIST OF FIGURES (Cont'd)

LIST OF TABLES

This Page Intentionally Left Blank

1.0 SUMMARY

As a means of increasing the understanding of pumping ring behavior, a reciprocating tester incorporating variable stroke (in steps) and frequency (continuous) was built, and three hydrodynamic pumping ring designs were evaluated. Within the scope of this program, pumping rings made from three materials were evaluated under the following conditions: a constant clamping pressure of 10.3 MPa (1500 lb/in.^{2}) at reciprocating frequencies of 10, 35 and 45 Hz and at strokes of 25.4 mm(1.00 in.), 38.1 mm(1.50 in.) and 50.8 mm (2.00 in.).

The three pumping ring materials that were tested included Tin-Based Babbit, (SAE 11), Bearing Bronze (SAE 660) and Mechanical Carbon Graphite (Union Carbide Grade CNF-J). Of these three materials, the Tin-Based Babbitt with an elastic modulus of E = 5.24 x 10^4 MPa (7.6 x 10^6 lb/in.^{2}) produced the best results by generating pressures to 11.0 MPa (1600 lb/in.^{2}). The Mechanical Carbon Graphite with a lower elastic modulus of 2.27 x 10^4 MPa (3.3 x 10^6 lb/in.^{2}) also produced good results, but could only pump to 8.24 MPa (1200 lb/in.^{2}). The Bearing Bronze rings, with an elastic modulus of 9.65 x 10^4 MPa (14 x 10^6 lb/in.^{2}), were the stiffest of the rings tested; they would not close-in on the shaft and could not pump above 0.790 MPa (115 lb/in.^{2}).

Friction forces generated by the rubbing of the pumping rings on the test shaft reached a maximum of 71.2 N (16 lb) per ring, and produced a maximum power loss of 1.61 kW (2.17 hp) at 45 Hz. The low friction loss produced by the pumping rings was also reflected in the limited temperature rise experienced by both the rings and the high-pressure discharge oil.

In conjunction with the experimental evaluation, an analysis of the pumping ring design was developed. This analytical solution, which combines the axisymmetric shell equation with the Reynolds equation for isothermal conditions, produced theoretical pressure-flow curves that closely approximate the experimental data. The results of this work for the Mechanical Carbon Graphite rings showed experimental pumping pressure reaching 8.24 MPa

(1200 lb/in.^{2}) with the analysis indicating reasonable agreement. Improvements to the theoretical treatment of local temperature and time effects should greatly increase the prediction of pumping ring behavior.

2.0 INTRODUCTION

Although the Stirling engine has been in existence for many years, only recently has a more intensive effort been applied for its improvement (ref. 1). A critical engine area for which improvement is warranted is dynamic rod sealing, and, in particular, the external rod seal by which gas and oil spaces are separated. It is in this area, concentrating specifically on the hydrodynamic oil pumping ring, that this report is directed.

Several investigators have examined the pumping ring both analytically (ref. 2), (ref. 3) and experimentally (ref. 4). The general conclusion reached from the literature is that, in fact, very little pumping ring performance data exist and that the connection between performance and theoretical prediction has not been entirely made; thus, it is difficult to adequately predict performance or to extend designs for improved efficiency.

The objectives of this program were to provide a test vehicle for evaluating oil pumping rings, and to perform tests on pumping ring designs supplied to the program. As presently constructed, the pumping ring tester not only can accommodate the specific pumping ring design supplied as part of this program, but can be easily converted to test many other designs. The report that follows discusses the pumping ring tester design, identifies the pumping rings that were tested, and presents the experimental results of the tests conducted. An analysis of the specific ring design tested is included in this report to complement the experimental results.

This Page Intentionally Left Blank

3.0 TEST APPARATUS

The test apparatus, designed and constructed to meet the requirements of this program, is based on the following parameters:

- Rod Diameter: D = 19.0 mm (0.750 in.)
- Rod Stroke: S = 25.4 mm (1.00 in.)
  S = 38.1 mm (1.50 in.)
  S = 50.8 mm (2.00 in.)
- Rotational Speed: N = Variable over the range
  $10 \leq N \leq 60$ Hz
- Low-Pressure Pumping Ring Supply:
  20W40 Oil at 49°C (120°F) at pressures to 0.41 MPa (60 lb/in.^{2})
- Ring Closure Pressure: P_o = 10.3 MPa (1500 lb/in.^{2})

3.1 Test Vehicle Design

The test vehicle, which was built in modular units, is best described by referring to the assembly drawing shown as Figure 1. In this figure, only the test head parts are illustrated. At the lower end, a crosshead (1), driven by a connecting rod (2), applies reciprocating motion to the test rod (3). The crosshead is guided as it reciprocates by a crosshead sleeve (4). A lower housing (5), which serves as a foundation for the remainder of the apparatus, includes a manifolding system for providing oil to the crosshead sleeve.

The upper end of the crosshead (1) contains a female taper, which is matched to the taper ground on the end of the test shaft (3). Although the taper is sized for locking, a retaining clip (6) is also provided to assure that no relative axial motion exists between the crosshead and the test rod during tester operation. The remaining tester elements situated above the housing constitute the portion of the tester designed to house the oil pumping rings.

Mounted directly on the lower housing is a lower guide-bearing housing (7), which is designed with a special piloting arrangement to provide excellent radial positioning with low axial friction. Sandwiched between the bearing housing and the lower housing are three load cells (8) to be used for friction

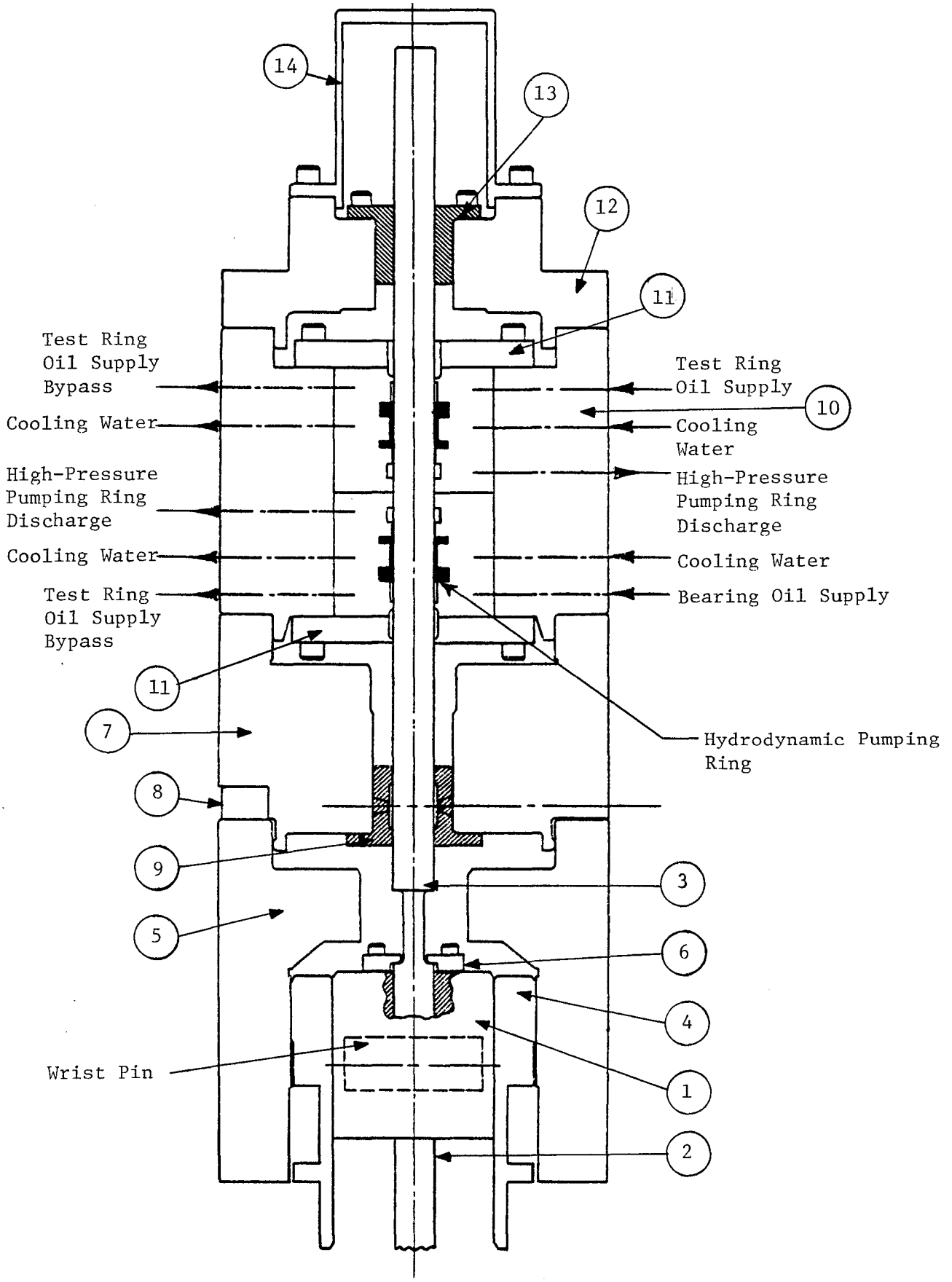

Fig. 1 Test Head Assembly

measurements. The guide bearing (9) is an externally pressurized, pocketed design, which is supplied with the same oil as the pumping rings, thereby eliminating the need for special seals. The oil supply to the guide bearing is adjustable to provide hydraulic shimming of the test rod for alignment purposes. Additionally, the guide bearing functions to provide shaft cooling, which results from the oil exiting the bearing; this design eliminates the need for any auxiliary cooling systems.

Situated above and tightly piloted to the lower bearing housing is the oil pumping ring cartridge housing (10). This housing provides the mounting system for two, identical test cartridges (11), which, in turn, house the pumping rings. This portion of the test rig is designed so that all the facilities necessary to input and control the oil entering and exiting the pumping ring cartridges are connected to or pass through the cartridge housing; the relative locations of all the passages are identified on Figure 1.

A second bearing housing (12), which contains a guide bearing (13) identical in design and operation to the lower guide bearing (9), is tightly piloted to the cartridge housing (10) to ensure proper bearing alignment. A simple cap (14) closes this upper bearing housing.

Each housing of the tester is provided with interconnecting passages to allow oil to drain back to the tester crankcase. The crankcase assembly, shown in Figure 2, contains a crankshaft (1) that is supported on a pair of automotive-type sleeve bearings (2). An oil seal (3) is provided at the point where the crankshaft penetrates the crankcase for connection to a driver. The crankcase is split horizontally to allow for changing crankshafts. Removable counterweights (4) permit balancing of the crankshaft when changing either the reciprocating mass or the crank throw.

The connection between the test head (shown in Figure 1) and the crankcase is made by bolting the two parts together at the surface indicated on Figure 2.

The crankshaft assembly is bolted to a separate base that contains a variable-speed electric motor. A gear tooth belt connects the drive motor to the

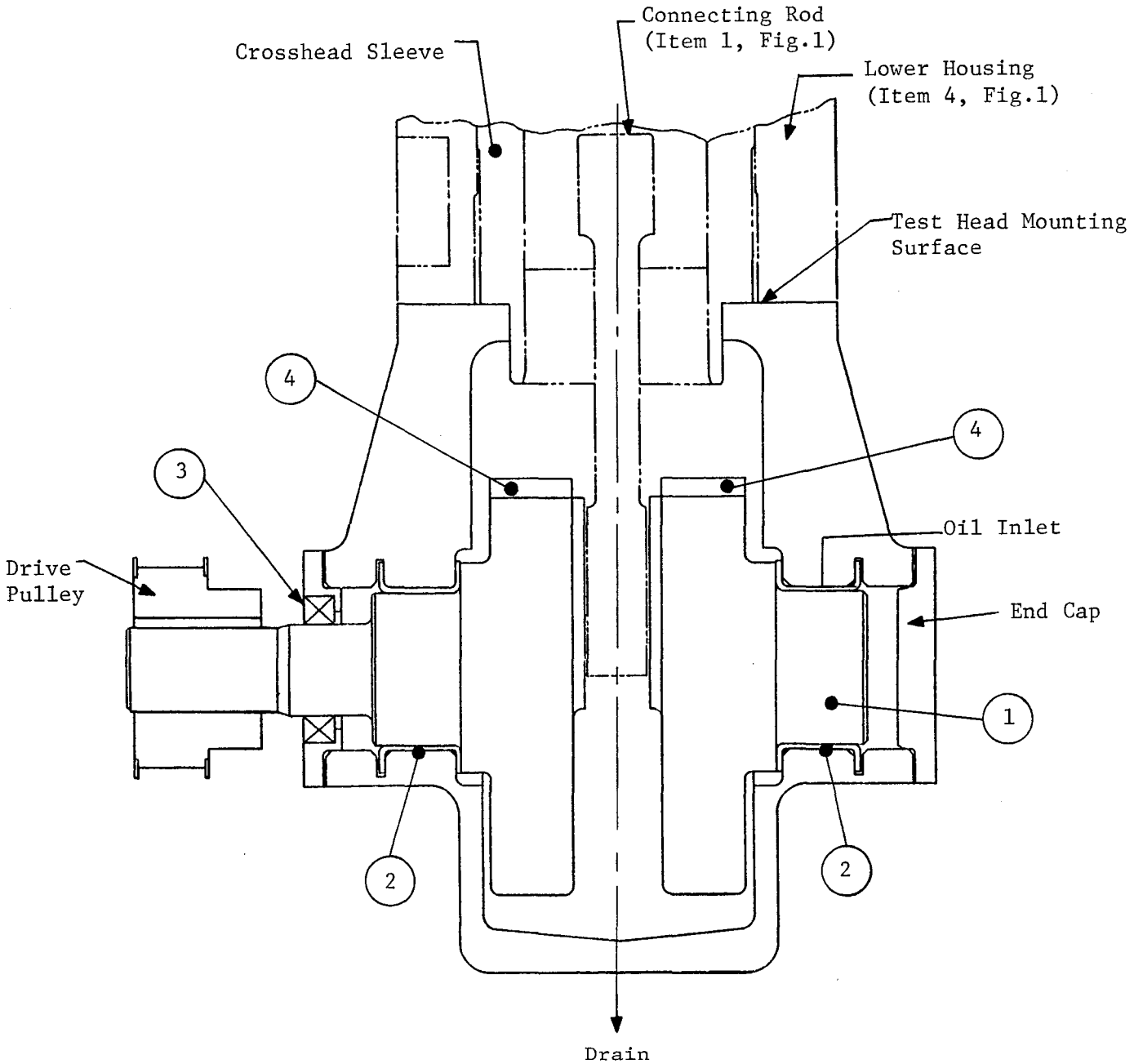

Fig. 2 Crankcase Assembly

crankshaft. Isolation mounts are attached underneath the base to prevent machine vibrations from being transmitted to the floor.

As described previously, individual cartridges provide a means for installing the pumping rings in the tester. Each cartridge is designed to accept pumping rings of the configuration shown in Figure 3. The cartridges are installed in the tester so that each pumps toward the other with the high-pressure discharge manifolds separated by a kap seal.

Figure 4 illustrates the pumping ring cartridge housing assembly. The pumping ring cartridge (1) is machined to accept the ring housing (2) and ring cap (3). The ring housing (2) and ring cap (3) form a subassembly for capturing the retaining flange of the oil pumping ring (4). Small clearances on the order of 0.076 to 0.127 mm (0.003 to 0.005 in.) are provided in the locations indicated to allow the pumping rings to align themselves when the cartridges are installed in the tester.

In order for the pumping rings to perform properly, they must be forced against the test rod at their thinnest cross sections. The force necessary to compress the rings against the rod is obtained by pressurizing behind an O ring (5), which is installed at the small end of the pumping ring. In operation, each pumping ring takes oil from the inlet manifold (A) and, by virtue of its pumping capability, discharges it into the high-pressure manifold (B). To prevent high-pressure oil from short circuiting back to the low-pressure side, an additional O ring (6) is installed over the ring housing. Some inlet oil circulates through the inlet manifold and exits the cartridge through the bypass port; additional oil exits the inlet manifold via the clearance space along the rod, thereby providing test-rod cooling.

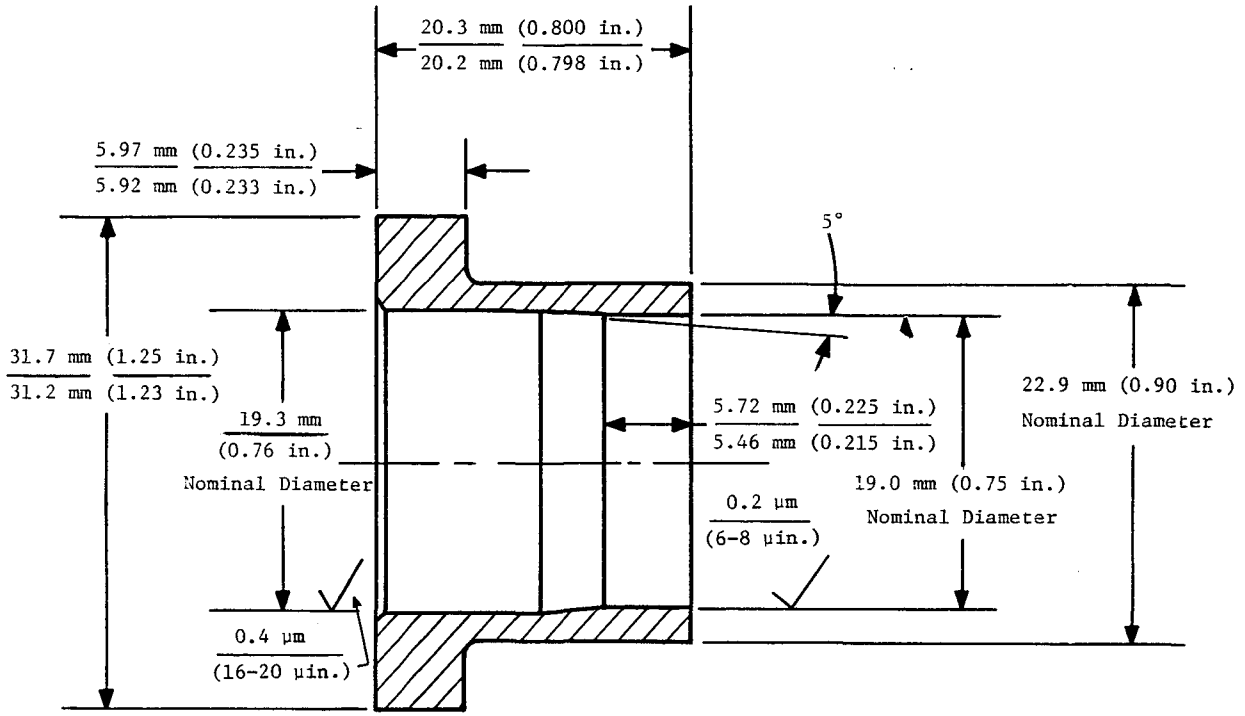

Fig. 3 Hydrodynamic Oil Pumping Ring Dimensions

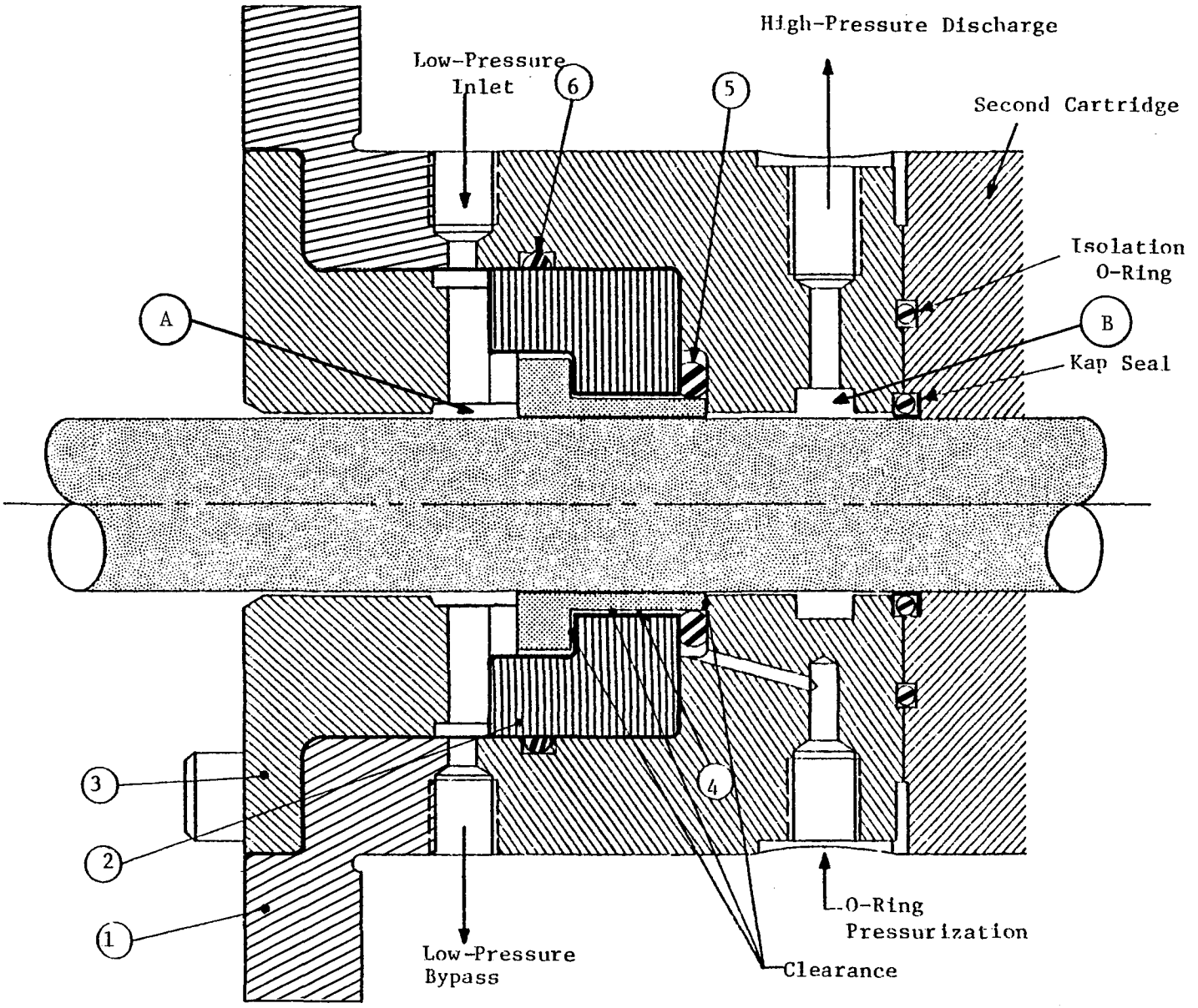

Fig. 4 Pumping Ring Cartridge Housing Assembly

This Page Intentionally Left Blank

4.0 TEST APPARATUS FABRICATION AND ASSEMBLY

4.1 Mechanical Assembly

As each component of the tester was assembled, photographs were taken to provide permanent visual records. Figure 5 shows the major crankcase components and identifies the construction of the two crankcase halves, the crankshaft, and the other incidental parts that make up the crankcase assembly. Figure 6 shows the assembled crankcase. The installation of the crankcase to the machine base is shown on Figure 7. In this photograph, the crankcase with the attached crosshead sleeve is assembled to the machine base; the isolation mounts are shown under the base, and the 5-hp, variable-speed motor is installed behind the belt guard.

Figure 8 pictorially presents the sequential assembly of the remainder of the tester. Figure 8a shows the lower housing installed on the crankcase while Figure 8b illustrates the lower bearing housing installed in position over the lower housing. Figures 8c and 8d show the installed positions of the cartridge housing and the upper bearing housing, respectively. Figure 8e presents the fully assembled, but unplumbed, tester. The installed tester, including controls, instrumentation and plumbing, is shown in Figure 9.

4.2 Fluid Systems

The hydraulic supply system is specifically designed to provide 20W40 oil to all required tester locations. The lubrication system schematic is shown as Figure 10. A parts' list for this system is included as Appendix A.

In general, a twin-pump arrangement, driven by a single motor, supplies high-pressure oil to the guide bearings and low-pressure oil to the pumping ring cartridges and the crankcase. Since the entire tester uses the same oil, the lubrication system is provided with a single scavange pump connected to the crankcase drain. The scavange pump return line contains a cooler for controlling oil temperatures during testing and an oil heater for bringing the system up to temperature quickly during start-up. Although some test instrumentation is shown on Figure 10, a separate instrumentation schematic is included as Figure 11.

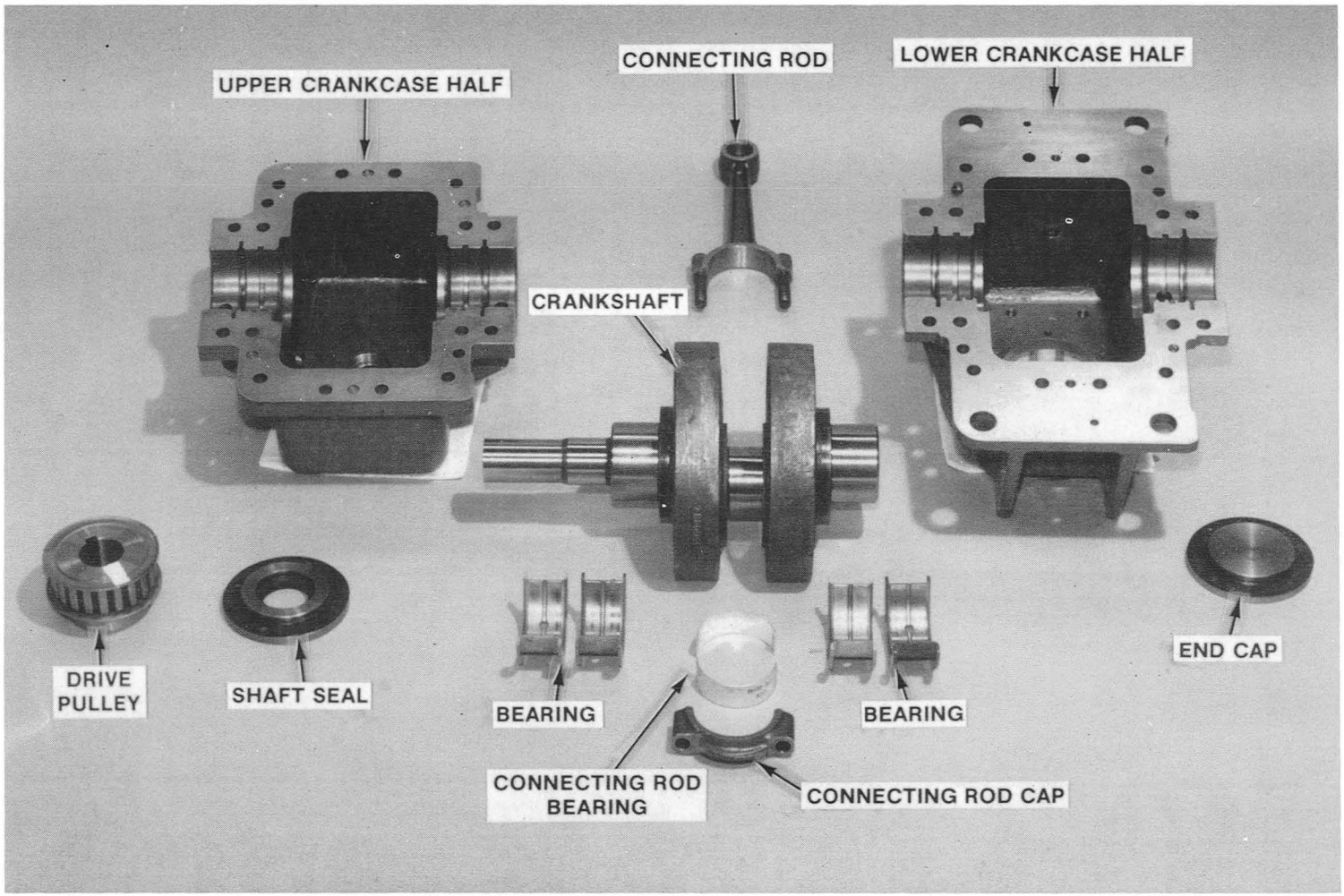

Fig. 5 Major Crankcase Components

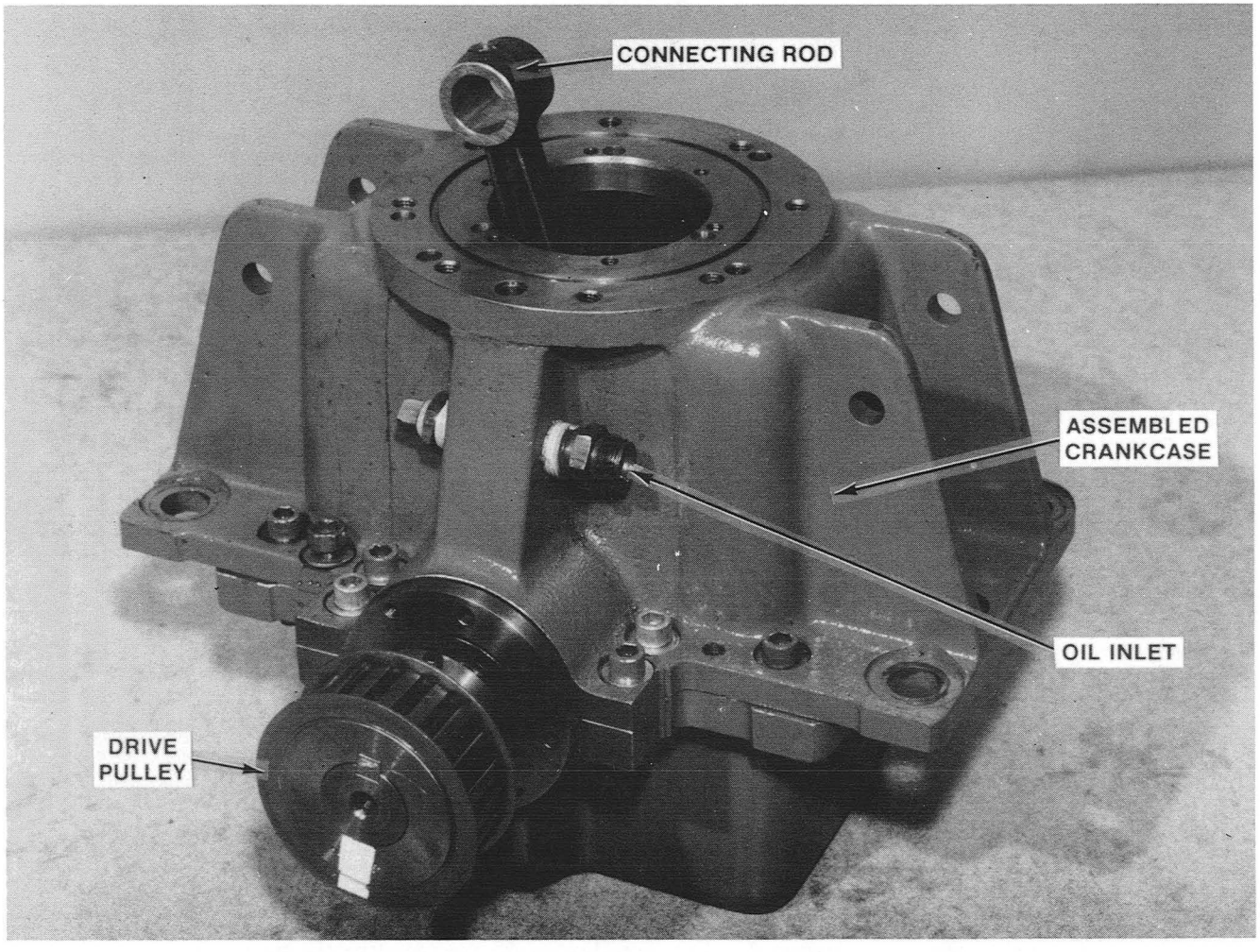

Fig. 6 Assembled Crankcase

This Page Intentionally Left Blank

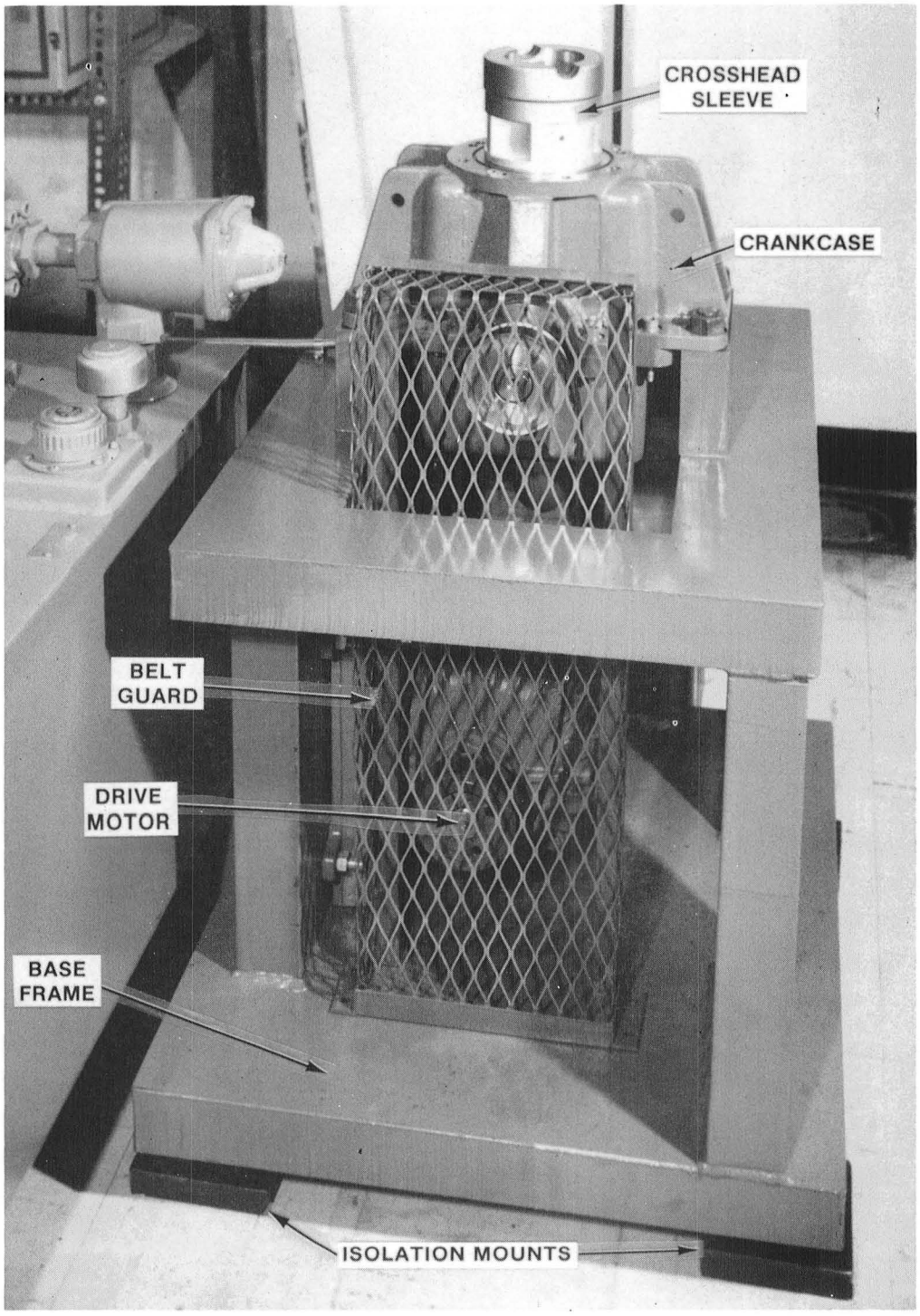

Fig. 7 Assembled Crankcase on Machine Base

This Page Intentionally Left Blank

Fig. 8a Installation of Lower Housing

This Page Intentionally Left Blank

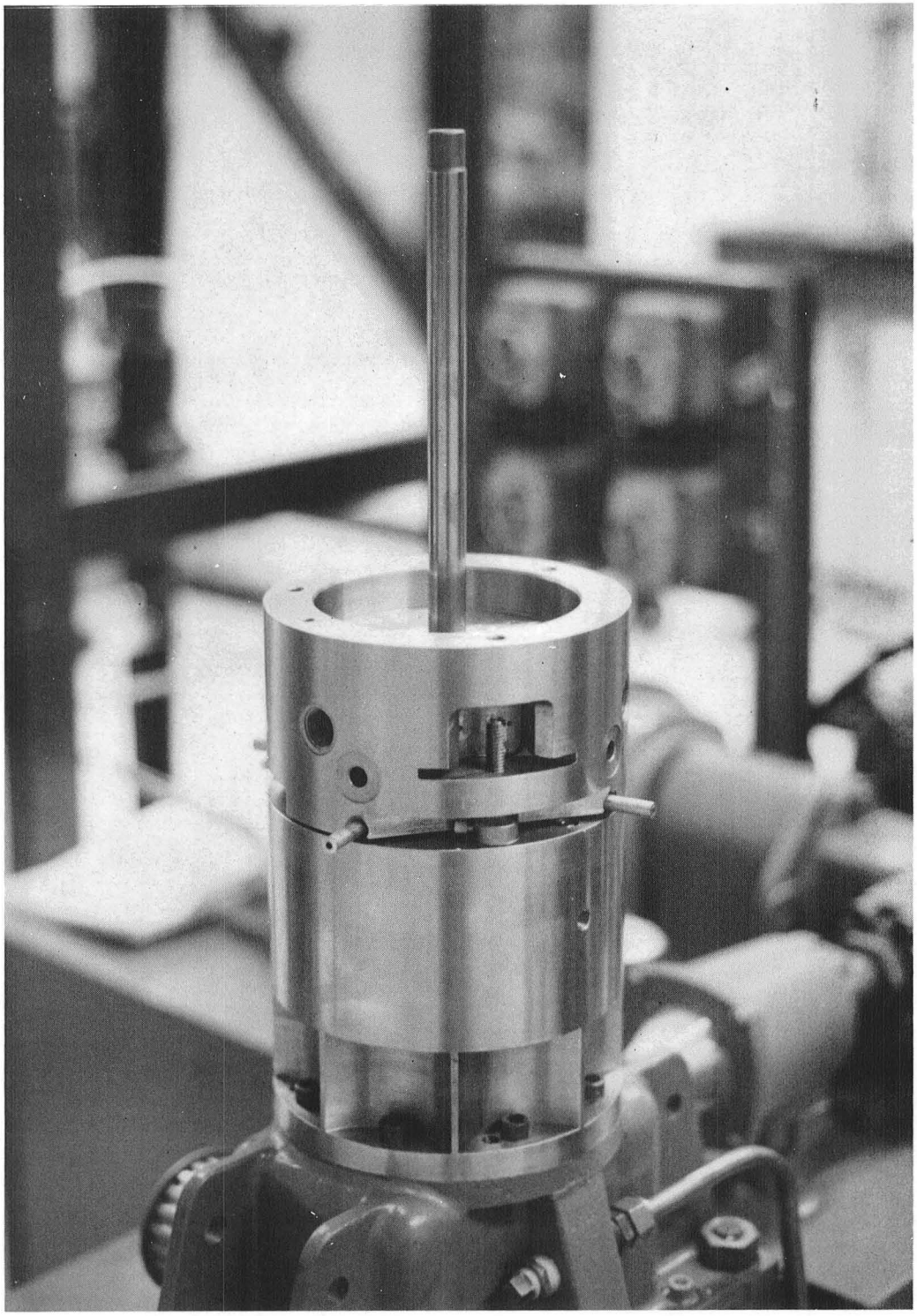

Fig. 8b Installation of Lower Bearing Housing

This Page Intentionally Left Blank

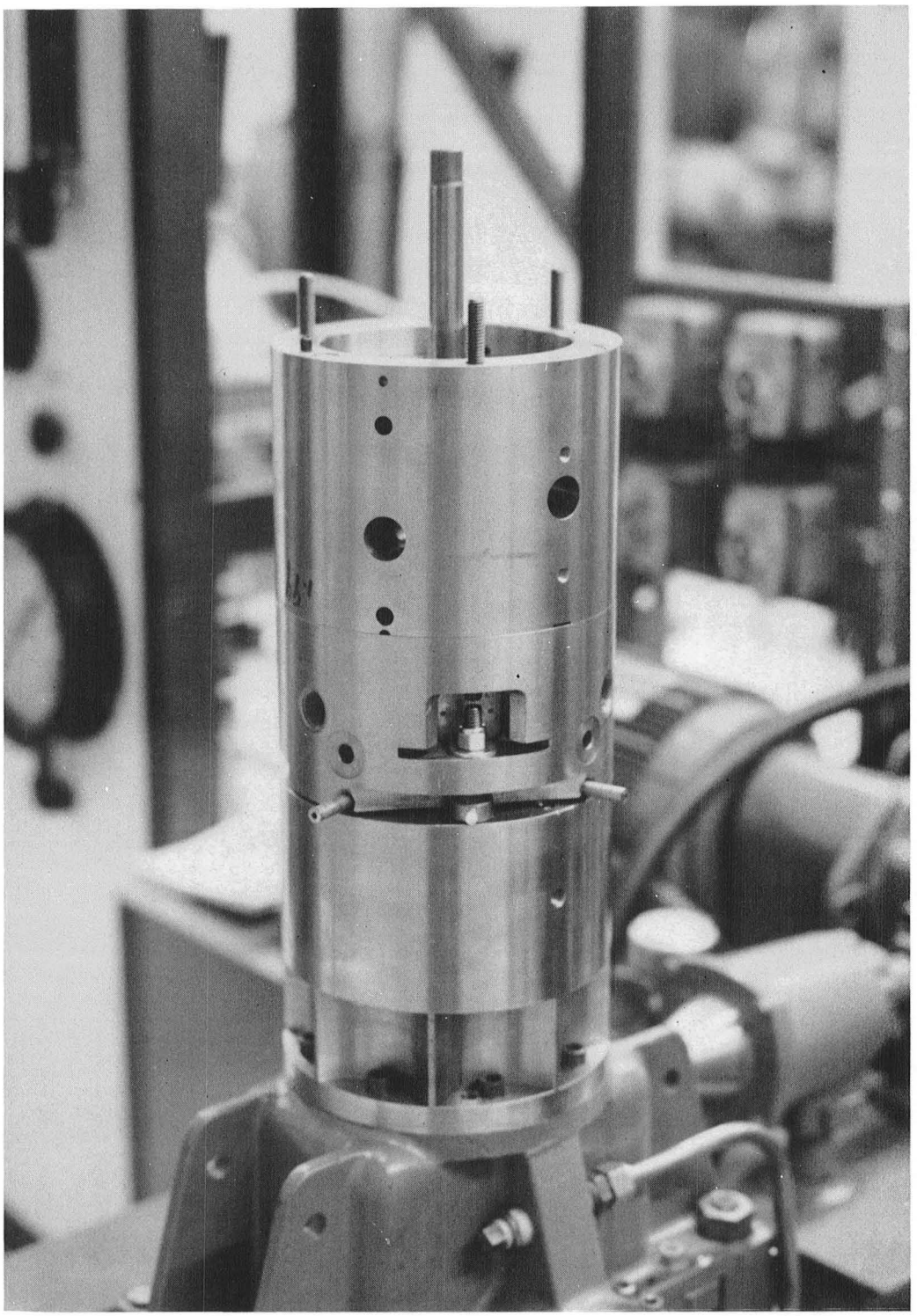

Fig. 8c Installation of Cartridge Housing

This Page Intentionally Left Blank

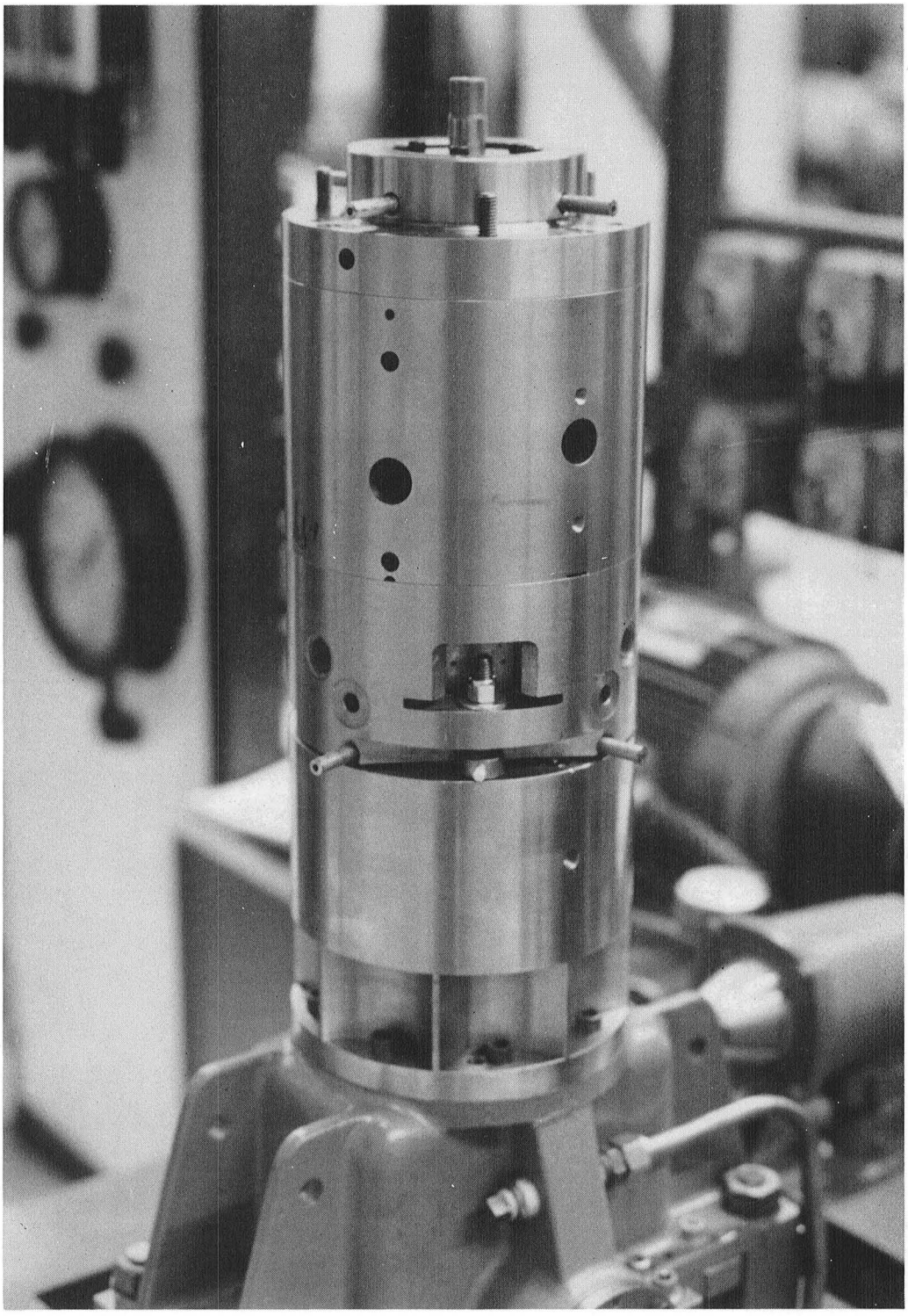

Fig. 8d Installation of Upper Bearing Housing

This Page Intentionally Left Blank

Fig. 8e Fully Assembled Tester

This Page Intentionally Left Blank

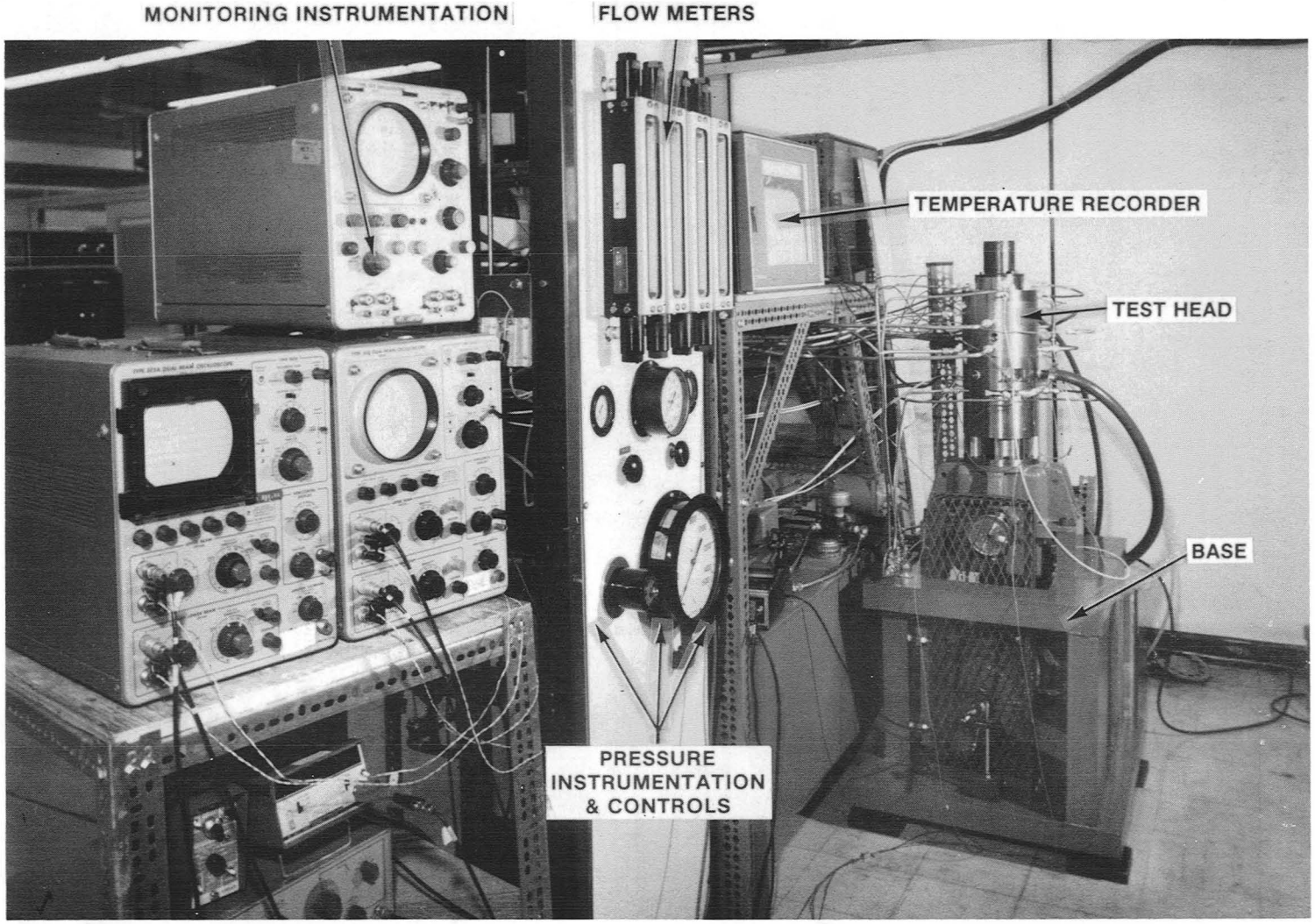

Fig. 9 Installed Tester

MTI-20241

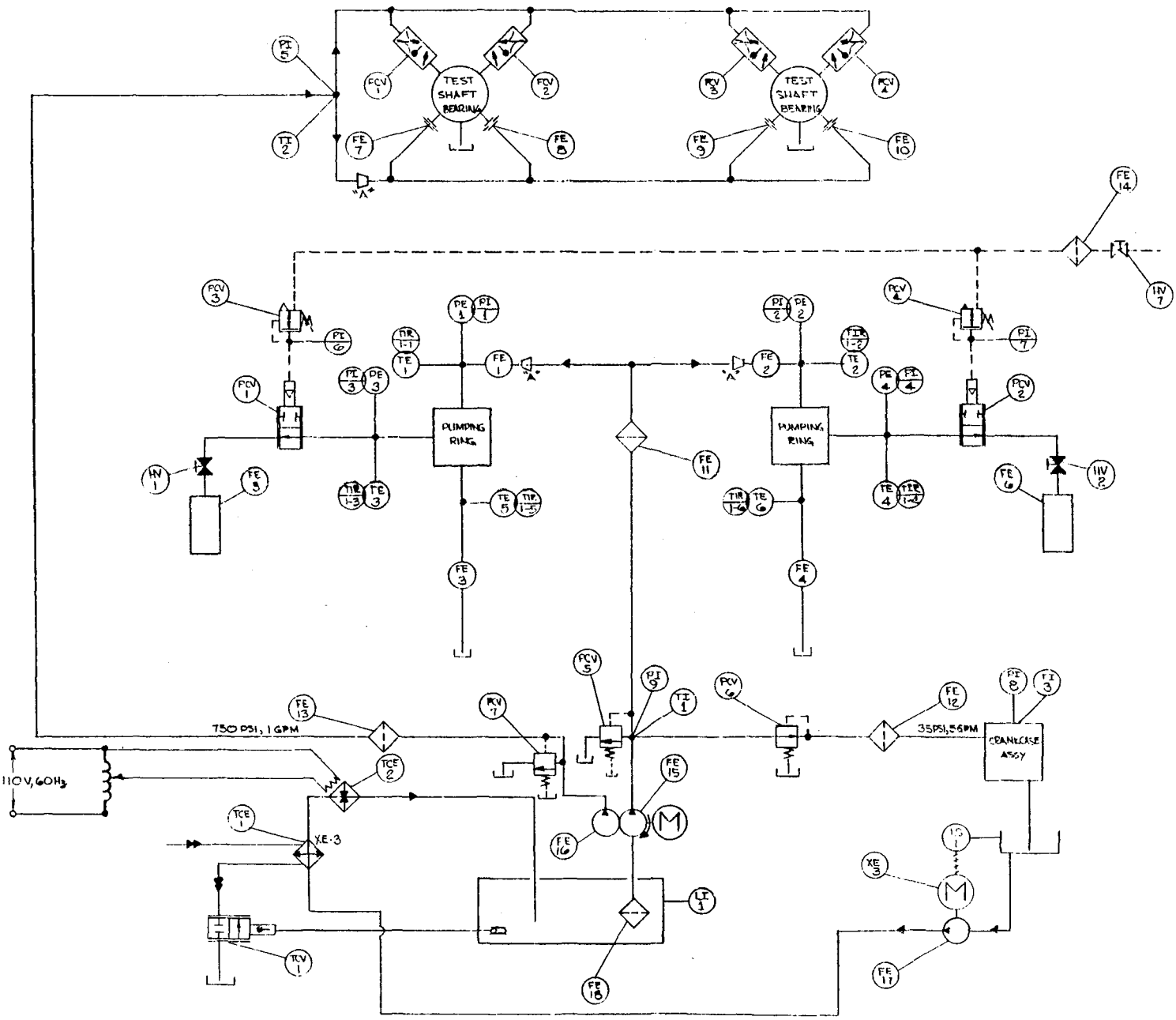

Fig. 10 Lubrication System Schematic

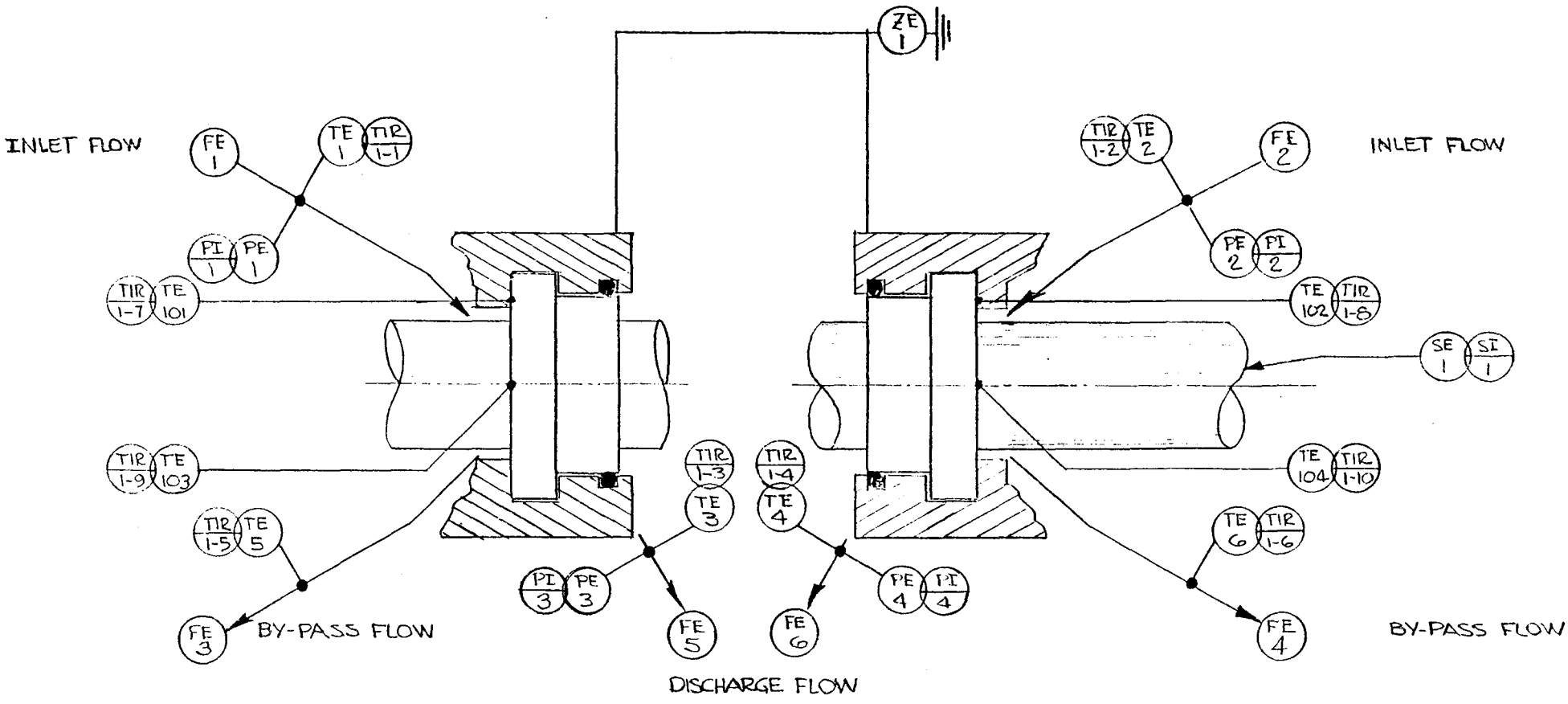

Fig. 11 Instrumentation Schematic

4.3 Instrumentation

An instrumentation system, as designed and built for the pumping ring tester, provides all the test data necessary to evaluate the pumping rings. The following instruments, which are identified on Figure 11, are listed below according to functions:

- Flow
  - FE-1, FE-2: Input to Pumping Rings
  - FE-3, FE-4: Bypass from Pumping Rings
  - FE-5, FE-6: Collection Beakers for Pumping Ring Flow

  } Direct-reading Float-type Flowmeters

- Pressure
  - PE-1, PE-2: Pressure Transducers for Inlet Flow to Pumping Rings 0.00-0.69 MPa (0-100 lb/in^2)
  - PE-3, PE-4: Pressure Transducers for Discharge Flow from Pumping Rings 0.00- 20.7 MPa (0-3000 lb/in.^{2})
  - PI-1, PI-2 PI-3, PI-4: Digital Voltmeters
- Temperature
  - TE-1, TE-2: Pumping Ring Inlet Flow Temperatures
  - TE-3, TE-4: Pumping Ring Discharge Flow Temperatures
  - TE-5, TE-6: Pumping Ring Bypass Flow Temperatures
  - TE-101 through TE-104: Pumping Ring Temperatures
  - TIR-1-1 through TIR-1-10: Multipoint Temperature Recorder
- Frequency
  - SE-1: Fiber-Optic Sensor
  - SI-1: Digital Frequency Meter
- Friction
  - ZE-1: Load Cell Transducer

5.0 PUMPING RING DESIGNS

Three pumping rings were evaluated during the experimental phase of the program. The three designs, identified on Figure 12, are discussed in detail as follows:

- Design #1 - Material: Tin-Based Babbitt (SAE 11)
  - Properties:

Modulus of Elasticity:	$E = 5.24 \times 10^4$ MPa (7.6×10^6 lb/in.^{2})
Poisson's Ratio:	$\gamma = 0.36$
Compressive Yield Strength:	$S_y = 42$ MPa (6100 lb/in.^{2})
Coefficient of Linear Expansion:	$\alpha = 23.4$ mm/mm/°C (13×10^6 in./in./°F)

  - Calculated Data (based on Thin Wall Theory) (ref. 5)

Load per Lineal in. @ 10.3 MPa (1500 lb/in.^{2}):	$V_o = 2.36 \times 10^4$ N/m (135 lb/in.)
Effective Length:	$L = 19.0$ mm (0.75 in.)
Radial Close-in:	$e_R = 0.028$ mm (0.0011 in.)
Initial Clearance:	$c_R = 0.018$ mm (0.0007 in.) (Room Temperature)
Maximum Hoop Stress:	$S_2 = 69$ MPa (10,029 lb/in.^{2})
Pumping Ring Wall Thickness:	$t = 1.98$ mm (0.078 in.)

- Design #2 - Material: Bearing Bronze (SAE 660)
  - Properties:

Modulus of Elasticity:	$E = 9.65 \times 10^4$ MPa (14×10^6 lb/in.^{2})
Poisson's Ratio:	$\gamma = 0.36$
Compressive Yield Strength:	$S_y = 186$ MPa (27,000 lb/in.^{2})
Coefficient of Linear Expansion:	$\alpha = 18 \times 10^{-6}$ mm/mm/°C (10×10^{-6} in./in./°F)

  - Calculated Data (based on Thin Wall Theory) (ref. 5)

Load per Lineal in. @ 10.3 MPa:	$V_o = 2.36 \times 10^4$ N/m (135 lb/in.)
Effective Length:	$L = 19.0$ mm (0.75 in.)
Radial Close-in:	$e_R = 0.025$ mm (0.001 in.)
Initial Clearance:	$c_R = 2.03 \times 10^{-2}$ mm (8×10^{-4} in.) (Room Temperature)

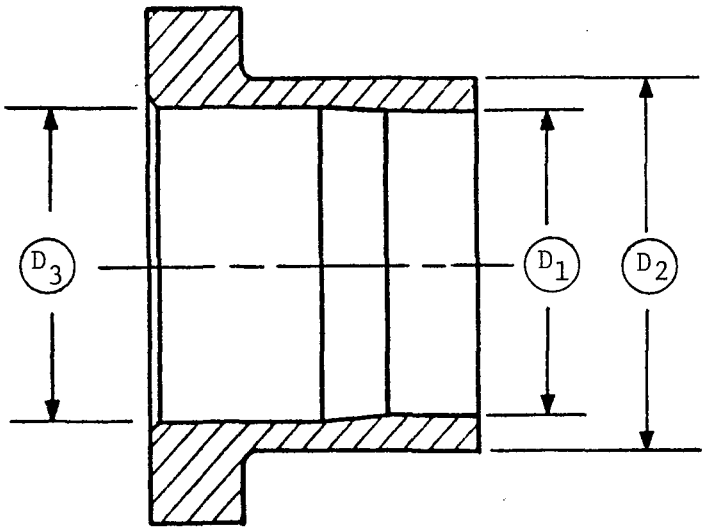

Ring	D_1 mm(in.)	D_2 mm(in.)	D_3 mm(in.)	Material
Design #1	19.086(0.7514)* 19.075(0.7510)	23.063(0.908) 23.012(0.906)	19.406(0.764)* 19.355(0.762)	Tin-Based Babbitt, SAE 11, Silver Plate+
Design #2	19.091(0.7516) 19.080(0.7512)	22.657(0.892) 22.606(0.890)	19.406(0.764) 19.355(0.762)	Bearing Bronze, CA932B/SAE660 (83% Cu, 7% Sn, 7% Pb)
Design #3	19.108(0.7523) 19.098(0.7519)	22.428(0.883) 22.377(0.881)	19.406(0.764) 19.355(0.762)	Mechanical Carbon Graphite(Union Carbide Grade CNF-J)

*Finish ID after Ag plate+
+Silver plate per AMS 2412 to obtain 0.0254 to 0.0762 mm (0.001 to 0.003 in.) plating thickness after machining.

Fig. 12 Hydrodynamic Oil Pumping Ring

Maximum Hoop Stress: S_2 = 186 MPa (27,000 lb/in.^{2})

Pumping Ring Wall Thickness: t = 1.78 mm (0.070 in.)

- Design #3 - Material: Mechanical Carbon Graphite (Union Carbide Grade CNF-J)

  - Properties:

    Modulus of Elasticity: E = 2.14 x 10^4 MPa (3.11 x 10^6 lb/in.^{2})

    Poisson's Ratio: γ = 0.29

    Compressive Yield Strength: S_y = 207 MPa (30,000 lb/in.^{2})

    Coefficient of Linear Expansion: α = 4.32 mm/mm/°C (2.4 x 10^{-6} in./in./°F

  - Calculated Data (based on Thin Wall Theory) (ref. 5)

    Load Per Lineal in. @ 10.3 MPa (1500 lb/in.^{2}): V_o = 2.36 x 10^4 N/m (1.35 lb/in.)

    Effective Length: L = 19.0 mm (0.75 in.)

    Radial Close-in: e_R = 0.025 mm (0.001 in.)

    Initial Clearance: c_R = 0.030 mm (0.0012 in.) (Room Temperature)

    Maximum Hoop Stress: S_2 = 207 MPa (27,000 lb/in.^{2})

    Pumping Ring Wall Thickness: t = 1.65 mm (0.065 in.)

All calculated close-ins were based upon the 10.3 MPa (1500 lb/in.^{2}) and a 3.17 mm (0.125 in.) ring width (assumed lineal contact was 2.29 mm (0.090 in.). In order to achieve the desired close-in at the end of the ring, it is possible that this pressure may require adjustment during any given test with any given ring.

The pumping rings ride on a 19 mm (0.75 in.) diameter test rod that is made from a solid bar of modified Nitralloy 135. The rod is case-hardened, ground and lapped to the following conditions:

- Surface Hardness: R_c = 64
- Roundness: ⌾ = 1.27 x 10^{-3} mm (0.00005 in.)
- Straightness: ⏤ = 8.33 x 10^{-3} mm/m (0.0001 in./ft)
- Surface Finish: √ = 0.062 μm (2.5 μin.)

A minimum of five (5) sample rings of each design were machined and inspected. Table 1 shows the final dimensions of bore and outer ring diameter for all the rings. From this table, specific rings of approximately the same bore dimensions were selected for testing.

TABLE 1

PUMPING RING DIMENSIONS

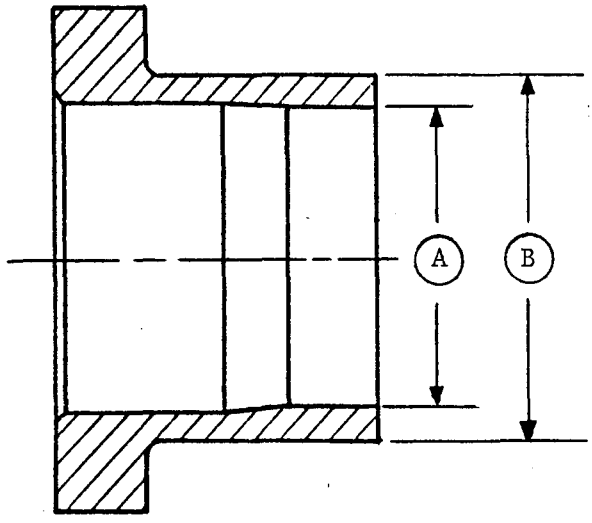

Design #	Material	Ring Identification Number						
		1	2	3	4	5	6	7
1	Tin-Based Babbitt							
	Diameter A	0.7512	0.7516	0.7513	0.7516	0.7520	0.7516	0.7517
	Diameter B	0.907	0.907	0.905	0.904	0.907	0.904	0.907
2	Bearing Bronze							
	Diameter A	0.7520	0.7515	0.7518	0.7520	0.7518		
	Diameter B	0.8915	0.8903	0.8895	0.8898	0.8905		
3	Mechanical Carbon Graphite							
	Diameter A	0.7523	0.7525	0.7525	0.7525	0.7527	0.7524	0.7525
	Diameter B	0.8825	0.8825	0.8818	0.8815	0.8825	0.8815	0.8825

Note: $\frac{\text{Diameter B} - \text{Diameter A}}{2}$ Wall Thickness of Pumping Ring

This Page Intentionally Left Blank

6.0 EXPERIMENTAL EVALUATION

Each of the three pumping ring designs was subjected to an experimental evaluation based on the test plan contained in Appendix B. As tester debugging progressed, it became evident that some changes in both the test plan and in the test procedures were required.

The most significant change required was in the maximum shaft speed at which the pumping rings were to be evaluated. Although the test drive was demonstrated to be capable of attaining a speed of 60 Hz, machinery vibration, due in part to excessive wrist pin clearance in the connecting rod, limited the test speed to 45 Hz. The two lower test speeds remained as originally specified so that all pumping ring tests were performed at 10, 35 and 45 Hz.

The second significant change was to the test procedure in which individual pumping ring flow rates were to be measured. The kap seal, previously identified on Figure 4, was intended to isolate the high-pressure discharge cavities of the two pumping rings. However, because of the lack of a substantial backup pressure, this seal did not perform the barrier function for which it was intended. After several attempts at making the kap seal functional, it was discarded entirely from the testing; as a result, all flow and friction force measurements taken for any data point represent the combined action of two rings.

As testing progressed, it became apparent that an adequate presentation of the flow-pressure characteristics of the pumping rings could not be obtained with only the three test pressures of 3.42 MPa (500 lb/in.^{2}), 6.85 MPa (1000 lb/in.^{2}), and 10.3 MPa (1500 lb/in.^{2}). For this reason, many additional pressure-flow data points were taken than were originally planned. These data provided a significantly better picture of pumping ring performance than could have been achieved with only the three pressure points listed in the test plan.

The following procedure was used to obtain all data point measurements:

1. Stabilize tester temperatures by circulating oil throughout the system with the tester speed maintained at 10 Hz, the pumping ring loading pressure set to zero (0), and the pumping ring discharge valve (PCV-1 & 2 on Figure 10) held open.
2. Set the tester speed to the proper value.
3. Set the pumping ring closing pressure to its proper level of 10.3 MPa (1500 lb/in.^{2}).
4. After stabilization, record all test data.
5. Close pumping ring discharge valve (PCV-1 & 2 on Figure 10). After stabilization, record all test data.
6. Readjust pumping ring discharge valve (PCV-1 & 2 on Figure 10) to obtain several intermediate test pressure points. After stabilization at each setting, record all test data.

6.1 Flow-Pressure Measurement Results

The quantity of test data collected for each ring design precluded the presentation of the flow-pressure evaluations on a combined basis. Therefore, these data are presented on an individual ring design basis in the following subsections.

6.1.1 Design #1 - Tin-Based Babbitt (SAE 11)

Flow-pressure test results for this ring design are presented on Tables 2, 3, and 4 and on Figures 13, 14, and 15. This ring performed the best of all the designs tested, producing the highest shut-off pressure of up to 11.0 MPa (1600 lb/in.^{2}). The shape of the flow-pressure curves generally conformed to expectations with the exception of some slight slope reversal at the lower pressure levels. The data points included in this test sequence are 1.1.1.1 through 3.3.3.1.

6.1.2 Design #2 - Bearing Bronze (SAE 660)

The Bearing Bronze pumping rings were evaluated at the same conditions as were the Tin-Based Babbitt rings. The results of these tests, however, were

TABLE 2

PUMPING RING DESIGN #1 - TIN-BASED BABBITT
(SAE 11)

Data Point 1.X.X.1

Ring Identification

#1 Ring - Upper Location
#3 Ring - Lower Location

Stroke = 25.4 mm (1.00 in.)							
Data Point	Frequency Hz	Oil Pressure MPa (lb/in^2)	Oil Temperature °C (°F)	Flow Inlet cm^3/sec (gal/min)	Bypass Flow cm^3/sec (gal/min)	Pumped Pressure MPa (lb/in^2)	Pumped Flow g/min
1.1.1.1	10	0.096 (14)	44 (111)	23.3 (0.37)	11.4 (0.18)	0.193 (28)	1.29
	10	0.096 (14)	42 (108)	23.3 (0.37)	11.4 (0.18)	1.03 (151)	1.30
	10	0.110 (16)	42 (107)	23.3 (0.37)	11.4 (0.18)	2.08 (302)	1.34
1.1.2.1	10	0.110 (16)	42 (107)	23.3 (0.37)	11.4 (0.18)	4.20 (610)	1.32
	10	0.096 (14)	43 (109)	22.1 (0.35)	10.1 (0.16)	5.38 (780)	1.26
	10	0.090 (13)	45 (12)	21.4 (0.34)	10.1 (0.16)	6.26 (908)	1.14
1.1.3.1	10	0.096 (14)	44 (111)	22.1 (0.35)	10.1 (0.16)	8.34 (1209)	0.77
	10	0.096 (14)	43 (110)	21.4 (0.34)	10.1 (0.16)	9.80 (1422)	0.38
1.2.1.1	35	0.090 (13)	42 (108)	20.1 (0.32)	10.1 (0.16)	0.324 (47)	4.56
	35	0.083 (12)	43 (110)	20.1 (0.32)	10.1 (0.16)	0.324 (47)	4.70
	35	0.069 (10)	49 (121)	20.1 (0.32)	10.1 (0.16)	2.09 (303)	4.56
1.2.2.1	35	0.069 (10)	48 (119)	18.9 (0.30)	9.46 (0.15)	4.26 (618)	3.56
	35	0.069 (10)	48 (118)	18.9 (0.30)	9.46 (0.15)	6.20 (900)	2.39
1.2.3.1	35	0.069 (10)	48 (118)	19.6 (0.31)	9.46 (0.15)	8.27 (1200)	0.43
1.3.1.1	45	0.069 (10)	52 (126)	18.9 (0.30)	8.83 (0.14)	0.345 (50)	5.50
	45	0.069 (10)	49 (121)	19.6 (0.31)	9.46 (0.15)	0.358 (52)	5.34
	45	0.069 (10)	51 (124)	19.6 (0.31)	8.83 (0.14)	2.45 (356)	5.48
1.3.2.1	45	0.069 (10)	51 (124)	18.9 (0.30)	8.83 (0.14)	4.80 (696)	5.10
	45	0.069 (10)	51 (124)	18.9 (0.30)	8.83 (0.14)	6.62 (960)	4.09
1.3.3.1	45	0.069 (10)	52 (125)	18.9 (0.30)	8.83 (0.14)	8.48 (1230)	2.95
	45	0.069 (10)	50 (123)	19.6 (0.31)	9.46 (0.15)	9.51 (1380)	0.691

TABLE 3

PUMPING RING DESIGN #1 - TIN-BASED BABBITT (SAE 11)

Data Point 2.X.X.1

Ring Identification

#1 Ring - Upper Location
#3 Ring - Lower Location

Stroke = 38.1 mm (1.50 in.)							
Data Point	Frequency Hz	Oil Pressure MPa (lb/in^2)	Oil Temperature °C (°F)	Flow Inlet cm^3/sec (gal/min)	Bypass Flow cm^3/sec (gal/min)	Pumped Pressure MPa (lb/in^2)	Pumped Flow g/min
2.1.1.1	10	0.055 (8)	49 (121)	15.8 (0.25)	7.56 (0.12)	0.21 (31)	1.82
	10	0.048 (7)	48 (119)	14.5 (0.23)	6.93 (0.11)	2.10 (304)	1.08
2.1.2.1	10	0.055 (8)	49 (120)	14.5 (0.23)	6.93 (0.11)	4.26 (618)	0.830
	10	0.055 (8)	49 (120)	15.1 (0.24)	6.93 (0.11)	6.45 (936)	0.330
	10	0.041 (6)	47 (117)	14.5 (0.23)	6.30 (0.10)	6.82 (990)	0.430
	10	0.034 (5)	51 (124)	14.5 (0.23)	6.30 (0.10)	6.95 (1008)	0.710
2.1.3.1	10	0.055 (8)	49 (121)	15.1 (0.24)	7.56 (0.12)	10.4 (1505)	0.440
	10	0.055 (8)	49 (120)	15.1 (0.24)	7.56 (0.12)	10.2 (1481)	0
2.2.1.1	35	0.055 (8)	47 (116)	15.8 (0.25)	10.1 (0.16)	0.37 (54)	7.26
	35	0.055 (8)	50 (123)	15.8 (0.25)	10.1 (0.16)	2.07 (300)	7.30
	35	0.055 (8)	50 (122)	15.8 (0.25)	10.1 (0.16)	3.51 (510)	6.78
2.2.2.1	35	0.055 (8)	49 (121)	15.1 (0.24)	7.56 (0.12)	5.30 (768)	5.47
	35	0.055 (8)	48 (118)	15.1 (0.24)	7.56 (0.12)	6.95 (1008)	3.32
2.2.3.1	35	0.055 (8)	47 (117)	15.8 (0.25)	10.1 (0.16)	8.69 (1260)	0.711
2.3.1.1	45	0.048 (7)	52 (126)	17.6 (0.28)	10.1 (0.16)	0.39 (56)	11.8
	45	0.048 (7)	54 (130)	18.9 (0.30)	10.1 (0.16)	2.81 (408)	10.9
2.3.2.1	45	0.055 (8)	54 (129)	18.9 (0.30)	10.1 (0.16)	4.88 (708)	10.3
	45	0.070 (10)	53 (128)	19.5 (0.31)	10.1 (0.16)	4.88 (708)	9.0
	45	0.055 (8)	54 (129)	18.9 (0.30)	10.7 (0.17)	6.95 (1008)	8.48
2.3.3.1	45	0.055 (8)	54 (130)	18.9 (0.30)	11.4 (0.18)	7.94 (1152)	6.57
	45	0.048 (7)	53 (128)	17.6 (0.28)	10.1 (0.16)	9.72 (1410)	5.37
	45	0.048 (7)	53 (128)	17.6 (0.28)	10.1 (0.16)	11.2 (1626)	0

TABLE 4

PUMPING RING DESIGN #1 - TIN-BASED BABBITT
(SAE 11)

Data Point 3.X.X.1

Ring Identification

#1 Ring - Upper Location
#3 Ring - Lower Location

Stroke = 50.8 mm (2.00 in.)							
Data Point	Frequency Hz	Oil Pressure MPa (lb/in^2)	Oil Temperature °C (°F)	Flow Inlet cm^3/sec (gal/min)	Bypass Flow cm^3/sec (gal/min)	Pumped Pressure MPa (lb/in^2)	Pumped Flow g/min
3.1.1.1	10	0.055 (8)	52 (126)	18.0 (0.29)	8.80 (0.14)	0.25 (36)	2.84
	10	0.028 (4)	50 (123)	15.1 (0.24)	6.93 (0.11)	2.07 (300)	2.67
3.1.2.1	10	0.055 (8)	50 (123)	17.6 (0.28)	8.80 (0.14)	4.14 (600)	2.54
	10	0.034 (5)	51 (124)	15.1 (0.24)	6.93 (0.11)	6.20 (900)	2.23
3.1.3.1	10	0.055 (8)	51 (124)	17.6 (0.28)	8.80 (0.14)	8.27 (1200)	1.84
	10	0.028 (4)	50 (122)	14.5 (0.23)	6.93 (0.11)	9.72 (1410)	1.36
3.2.1.1	35	0.062 (9)	51 (125)	18.0 (0.29)	8.19 (0.13)	0.44 (64)	16.4
	35	0.062 (9)	52 (126)	18.0 (0.29)	8.19 (0.13)	2.10 (304)	15.8
3.2.2.1	35	0.055 (8)	53 (127)	18.0 (0.29)	8.19 (0.13)	4.14 (600)	14.1
	35	0.028 (4)	53 (127)	15.1 (0.24)	6.30 (0.10)	6.20 (900)	8.80
3.2.3.1	35	0.028 (4)	53 (127)	15.1 (0.24)	6.93 (0.11)	8.27 (1200)	4.48
	35	0.028 (4)	53 (127)	15.1 (0.24)	6.93 (0.11)	9.93 (1440)	1.04
	35	-	-	-	-	10.6 (1530)	0
3.3.1.1	45	0.069 (10)	50 (123)	18.0 (0.29)	7.56 (0.12)	0.45 (65)	23.8
	45	0.028 (4)	49 (121)	14.5 (0.23)	5.67 (0.09)	2.81 (408)	22.0
3.3.2.1	45	0.055 (8)	52 (126)	17.6 (0.28)	7.56 (0.12)	5.58 (810)	20.0
3.3.3.1	45	0.034 (5)	50 (122)	15.1 (0.24)	6.30 (0.10)	8.27 (1200)	14.8
	45	0.028 (4)	50 (123)	15.1 (0.24)	5.67 (0.09)	9.72 (1410)	11.8
	45	0.069 (10)	47 (117)	18.9 (0.30)	7.56 (0.12)	10.7 (1548)	2.24
	45	0.069 (10)	49 (120)	18.0 (0.29)	7.56 (0.12)	11.0 (1600)	0

Design #1 Ring, Tin-Based Babbitt (SAE 11)
P_o: 10.3 MPa (1500 lb/in.^{2})
Stroke: 25.4 mm (1.00 in.)

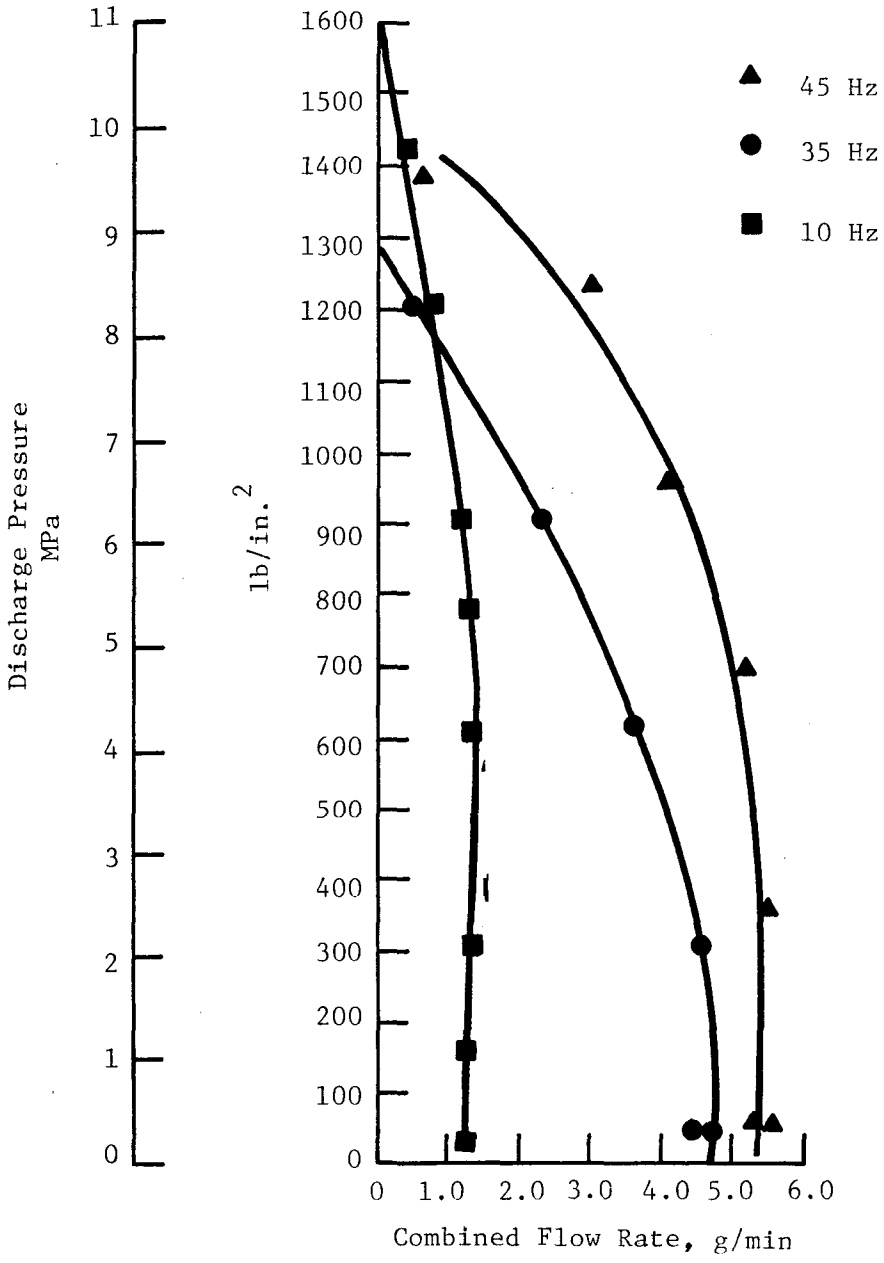

Fig. 13 Pressure-Flow Characteristic, Data Point 1.X.X.1

803322

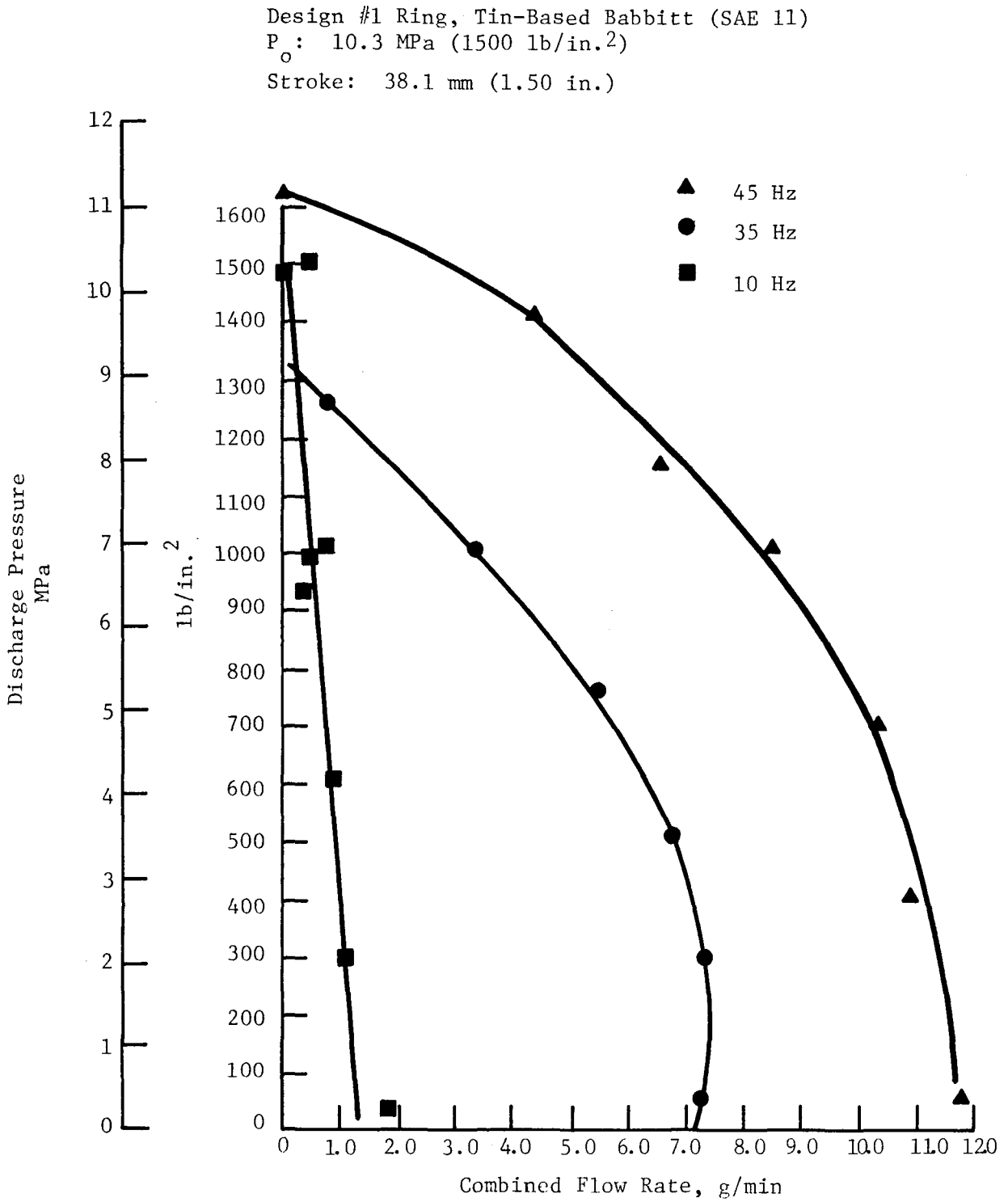

Fig. 14 Pressure-Flow Characteristic, Data Point 2.X.X.1

803323

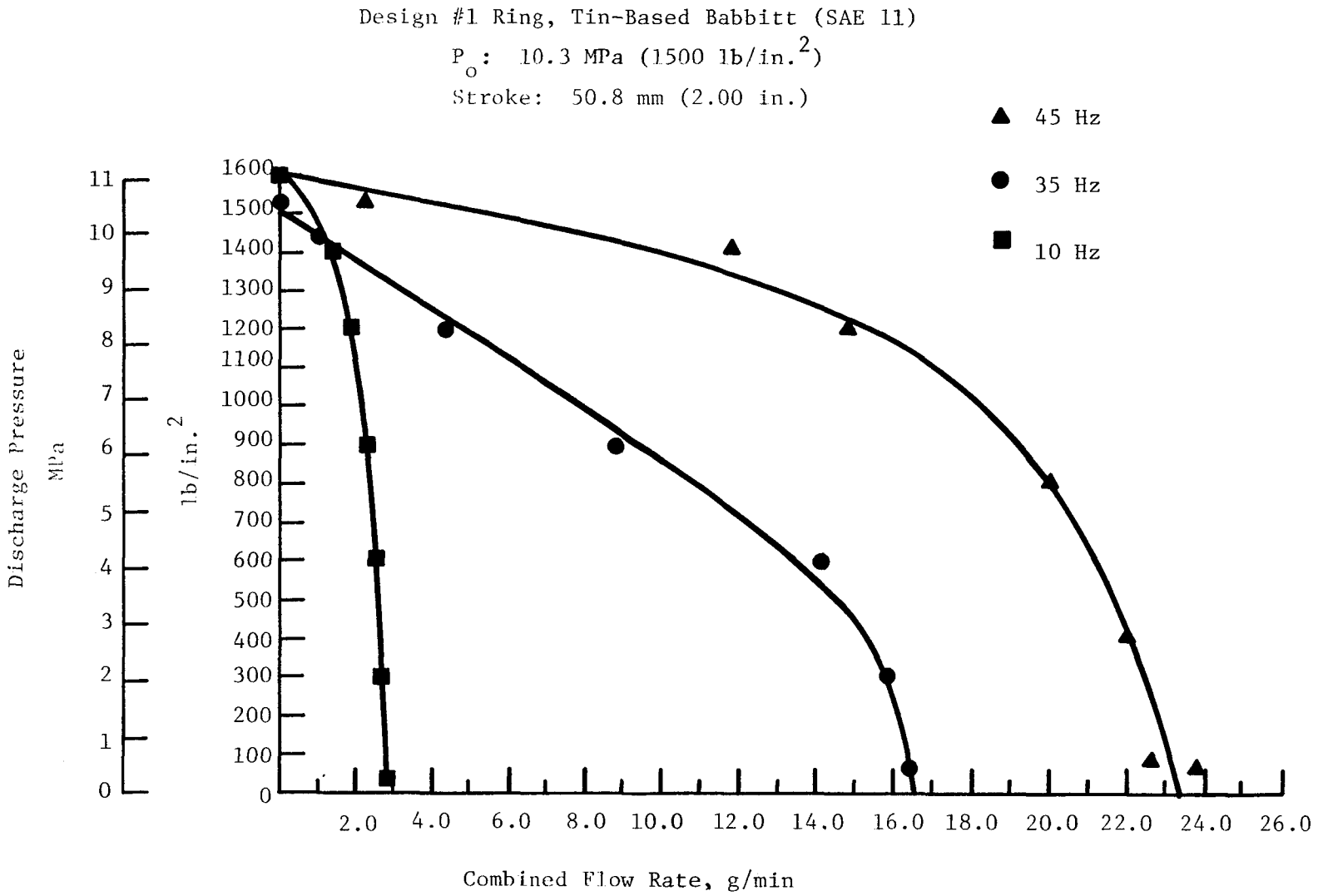

Fig. 15 Pressure-Flow Characteristic, Data Point 3.X.X.1

disappointing in that the Bearing Bronze rings did not generate any significant pressures. The test data for these rings, covering data points 1.1.1.2 through 3.3.3.2, showed the development of insignificant pressures that never exceeded 0.79 MPa (115 lb/in.^{2}). The results of the Bearing Bronze ring tests are shown on Tables 5, 6, 7 and Figure 16.

6.1.3 Design #3 - Mechanical Carbon Graphite (Union Carbide CNF-J)

The final set of data points scheduled to be tested in this program were points 1.1.1.3 through 3.3.3.3 for evaluation of Mechanical Carbon Graphite pumping ring performance. The results of these tests are shown on Tables 8, 9, 10 and on Figures 17, 18 and 19. Each pressure-flow curve determined for these rings generally followed the same shape produced by the Tin-Based Babbitt rings, but with some significant differences. The particular differences demonstrated by the Mechanical Carbon Graphite rings were (1) the lower shut-off pressure, (2) the higher open-end flow, and (3) the pronounced slope reversal exhibited by the pressure-flow curves at or near 4.83 MPa (700 lb/in.^{2}). Discussion of these results, as well as test results of the other ring designs, is presented in Section 8.0.

6.2 Friction Measurements

Losses generated by the pumping action of the test rings were determined from the measurement of friction forces as generated by the pumping action of the rings. The friction forces were measured using three force transducers that were placed between the cartridge housing and the lower bearing housing. A review of the tester assembly, shown as Figure 1, illustrates the position of these force transducers (8) relative to the cartridge housing (10) and the lower bearing housing (7).

Table 11 presents the friction force data as paired force level measurements; the first reading was taken without ring pressurization, while the second reading was taken after full pressurization to 10.3 MPa (1500 lb/in.^{2}). The difference between the two readings provides the effect of ring pumping on the total friction force seen by the cartridge housing. The friction readings, however, include not only the losses for the two unloaded rings but also the losses generated by the guide bearings and the shearing of

TABLE 5

PUMPING RING DESIGN #2 - BEARING BRONZE
(SAE 660)

Data Point 1.X.X.2

Ring Identification

#2 Ring - Upper Location
#1 Ring - Lower Location

Stroke = 25.4 mm (1.00 in.)							
Data Point	Frequency Hz	Oil Pressure MPa (lb/in^2)	Oil Temperature °C (°F)	Flow Inlet cm^3/sec (gal/min)	Bypass Flow cm^3/sec (gal/min)	Pumped Pressure MPa (lb/in^2)	Pumped Flow g/min
1.1.1.2	10	0.124 (18)	43 (110)	24.6 (0.39)	12.6 (0.20)	0	0.59
↓ 1.1.3.2	10	0.124 (18)	43 (110)	24.6 (0.39)	12.6 (0.20)	0	0
1.2.1.2	35	0.117 (17)	43 (110)	23.9 (0.38)	11.3 (0.18)	0.172 (25)	2.32
↓ 1.2.3.2	35	0.117 (17)	43 (110)	23.9 (0.38)	11.3 (0.18)	0.379 (55)	0
1.3.1.2	45	0.103 (15)	44 (111)	23.3 (0.37)	10.7 (0.17)	0.207 (30)	2.87
↓ 1.3.3.2	45	0.103 (15)	44 (111)	23.3 (0.37)	10.7 (0.17)	0.414 (60)	0

TABLE 6

PUMPING RING DESIGN #2 - BEARING BRONZE
(SAE 660)

Data Point 2.X.X.2

Ring Identification

#2 Ring - Upper Location
#1 Ring - Lower Location

Stroke = 38.1 mm (1.5 in.)							
Data Point	Frequency Hz	Oil Pressure MPa (lb/in^2)	Oil Temperature °C (°F)	Flow Inlet cm^3/sec (gal/min)	Bypass Flow cm^3/sec (gal/min)	Pumped Pressure MPa (lb/in^2)	Pumped Flow g/min
2.1.1.2	10	0.103 (15)	46 (115)	23.9 (0.38)	11.3 (0.18)	0.186 (27)	0.96
↓							
2.1.3.2	10	0.103 (15)	46 (115)	23.9 (0.38)	11.3 (0.18)	0.296 (43)	0
2.2.1.2	35	0.110 (16)	46 (115)	25.2 (0.40)	11.3 (0.18)	0.338 (49)	4.69
↓							
2.2.3.2	35	0.110 (16)	46 (115)	25.2 (0.40)	11.3 (0.18)	0.641 (93)	0
2.3.1.2	45	0.117 (17)	47 (117)	25.8 (0.41)	11.3 (0.18)	0.379 (55)	5.89
↓							
2.3.3.2	45	0.117 (17)	47 (117)	25.8 (0.41)	11.3 (0.18)	0.745 (108)	0

TABLE 7

PUMPING RING DESIGN #2 - BEARING BRONZE
(SAE 660)

Data Point 3.X.X.2

Ring Identification

#2 Ring - Upper Location
#1 Ring - Lower Location

Stroke = 50.8 mm (2.0 in.)							
Data Point	Frequency Hz	Oil Pressure MPa (lb/in^2)	Oil Temperature °C (°F)	Flow Inlet cm^3/sec (gal/min)	Bypass Flow cm^3/sec (gal/min)	Pumped Pressure MPa (lb/in^2)	Pumped Flow g/min
3.1.1.2	10	0.014 (2)	49 (121)	13.2 (0.21)	6.30 (0.10)	0.152 (22)	1.07
3.1.3.2	10	0.014 (2)	49 (121)	13.2 (0.21)	6.30 (0.10)	0.234 (34)	0
3.2.1.2	35	0.014 (2)	48 (118)	12.6 (0.20)	5.04 (0.08)	0.317 (46)	5.03
3.2.3.2	35	0.014 (2)	49 (120)	12.6 (0.20)	5.04 (0.08)	0.496 (72)	1.63
	35	0.014 (2)	48 (118)	12.6 (0.20)	5.04 (0.08)	0.648 (94)	0
3.3.1.2	45	0.028 (4)	49 (120)	15.8 (0.25)	5.67 (0.09)	0.365 (53)	7.13
	45	0.014 (2)	47 (117)	12.0 (0.19)	5.04 (0.08)	0.427 (62)	6.21
3.3.3.2	45	0.014 (2)	47 (117)	12.0 (0.19)	5.04 (0.08)	0.620 (90)	2.48
	45	0.014 (2)	47 (117)	12.0 (0.19)	5.04 (0.08)	0.779 (113)	0

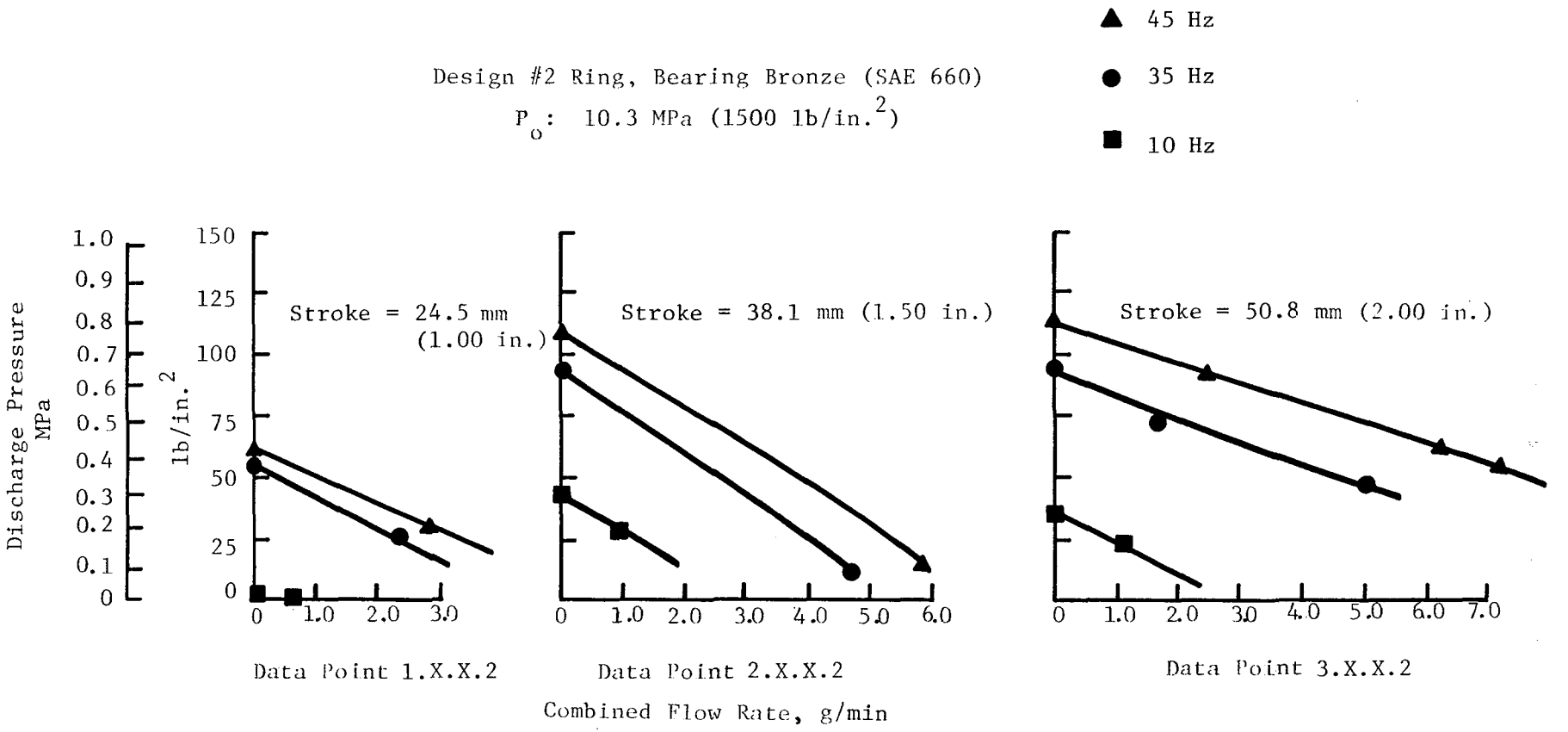

Fig. 16 Pressure-Flow Characteristic

TABLE 8

PUMPING RING DESIGN #3 - MECHANICAL CARBON GRAPHITE
(UNION CARBIDE GRADE CNF-J)

Data Point 1.X.X.3

Ring Identification

#4 Ring - Upper Location
#2 Ring - Lower Location

Stroke = 25.4 mm (1.00 in.)							
Data Point	Frequency Hz	Oil Pressure MPa (lb/in^2)	Oil Temperature °C (°F)	cm^3/sec (gal/min) Flow Inlet	Bypass Flow cm^3/sec (gal/min)	Pumped Pressure MPa (lb/in^2)	Pumped Fl g/min
1.1.1.3	10	0.062 (9)	50 (123)	18.9 (0.30)	8.19 (0.13)	0	1.11
	10	0.062 (9)	50 (122)	18.9 (0.30)	8.82 (0.14)	0.413 (60)	1.15
	10	0.055 (8)	50 (122)	18.9 (0.30)	8.19 (0.13)	0.503 (73)	1.25
	10	0.076 (11)	46 (115)	20.2 (0.32)	10.1 (0.16)	1.72 (250)	1.58
	10	0.076 (11)	46 (115)	20.2 (0.32)	10.1 (0.16)	3.45 (500)	1.71
1.1.2.3	10	0.055 (8)	49 (121)	17.6 (0.28)	8.82 (0.14)	4.48 (650)	1.36
	10	0.055 (8)	49 (121)	17.6 (0.28)	8.82 (0.14)	4.62 (670)	1.40
	10	0.124 (18)	42 (107)	23.9 (0.38)	10.7 (0.17)	5.34 (775)	1.86
	10	0.110 (16)	50 (123)	23.3 (0.37)	10.7 (0.17)	6.07 (880)	1.11
	10	0.110 (16)	43 (109)	23.9 (0.38)	10.7 (0.17)	6.34 (920)	0.54
1.1.3.3	10	0.062 (9)	50 (123)	20.2 (0.32)	8.19 (0.13)	7.11 (1032)	0
1.2.1.3	35	0.069 (10)	47 (116)	18.9 (0.30)	8.82 (0.14)	0	6.54
	35	0.069 (10)	47 (116)	18.9 (0.30)	8.82 (0.14)	0	6.78
	35	0.062 (9)	49 (121)	18.3 (0.29)	8.82 (0.14)	2.00 (290)	7.13
	35	0.062 (9)	49 (120)	18.3 (0.29)	8.82 (0.14)	2.14 (310)	7.19
1.2.2.3	35	0.062 (9)	48 (119)	18.3 (0.29)	8.82 (0.14)	4.48 (650)	7.40
	35	0.069 (10)	48 (118)	18.3 (0.29)	8.82 (0.14)	4.69 (680)	7.52
	35	0.076 (11)	46 (115)	18.9 (0.30)	8.82 (0.14)	5.52 (800)	6.80
	35	0.076 (10)	46 (114)	18.9 (0.30)	8.82 (0.14)	6.55 (950)	4.34
1.2.3.3	35	0.096 (14)	44 (111)	22.0 (0.35)	10.1 (0.16)	6.96 (1010)	2.42
	35	0.096 (14)	47 (116)	18.9 (0.30)	10.1 (0.16)	6.96 (1010)	1.65
	35	0.096 (14)	47 (116)	18.9 (0.30)	10.1 (0.16)	6.96 (1010)	1.68
	35	0.069 (10)	47 (116)	18.3 (0.29)	8.19 (0.13)	6.95 (1000)	0
1.3.1.3	45	0.096 (14)	43 (109)	21.4 (0.34)	9.45 (0.15)	0	8.06
	45	0.096 (14)	42 (107)	21.4 (0.34)	9.45 (0.15)	0	8.50
	45	0.096 (14)	49 (120)	21.4 (0.34)	9.45 (0.15)	2.00 (290)	8.80
	45	0.096 (14)	48 (118)	21.4 (0.34)	9.45 (0.15)	2.24 (325)	8.86
1.3.2.3	45	0.096 (14)	46 (115)	21.4 (0.34)	10.1 (0.16)	4.48 (650)	9.45
	45	0.096 (14)	44 (112)	21.4 (0.34)	10.1 (0.16)	4.69 (680)	9.30
	45	0.069 (10)	47 (117)	18.9 (0.30)	9.45 (0.15)	5.86 (850)	7.60
	45	0.069 (10)	47 (116)	18.9 (0.30)	9.45 (0.15)	6.20 (900)	6.56
1.3.3.3	45	0.096 (14)	40 (105)	18.3 (0.29)	10.1 (0.16)	7.37 (1069)	0

TABLE 9

PUMPING RING DESIGN #3 - MECHANICAL CARBON GRAPHITE
(UNION CARBIDE GRADE CNF-J)

Data Point 2.X.X.3

Ring Identification

#3 Ring - Upper Location
#2 Ring - Lower Location

Stroke = 38.1 mm (1.50 in.)							
Data Point	Frequency Hz	Oil Pressure MPa (lb/in^2)	Oil Temperature °C (°F)	Flow Inlet cm^3/sec (gal/min)	Bypass Flow cm^3/sec (gal/min)	Pumped Pressure MPa (lb/in^2)	Pumped Flow g/min
2.1.1.3	10	0.062 (9)	46 (115)	17.0 (0.27)	7.56 (0.12)	0.248 (36)	2.22
	10	0.055 (8)	46 (115)	17.0 (0.27)	7.56 (0.12)	1.48 (215)	2.42
	10	0.055 (8)	46 (115)	17.0 (0.27)	7.56 (0.12)	2.83 (411)	2.63
2.1.2.3	10	0.055 (8)	46 (115)	17.0 (0.27)	7.56 (0.12)	4.27 (619)	2.64
	10	0.055 (8)	46 (114)	17.0 (0.27)	7.56 (0.12)	5.68 (824)	2.47
	10	0.062 (9)	46 (115)	17.6 (0.28)	7.56 (0.12)	6.65 (964)	1.54
2.1.3.3	10	0.043 (7)	46 (115)	17.0 (0.27)	7.56 (0.12)	7.03 (1020)	0.90
	10	0.043 (7)	46 (115)	17.0 (0.27)	7.56 (0.12)	7.12 (1033)	0
2.2.1.3	35	0.069 (10)	47 (116)	18.9 (0.30)	8.82 (0.14)	0.414 (60)	12.2
	35	0.069 (10)	50 (123)	18.9 (0.30)	8.82 (0.14)	1.65 (240)	13.3
	35	0.069 (10)	48 (119)	18.9 (0.30)	8.82 (0.14)	3.52 (510)	13.3
2.2.2.3	35	0.076 (11)	49 (120)	19.5 (0.31)	8.82 (0.14)	4.84 (702)	13.7
	35	0.069 (10)	48 (118)	18.9 (0.30)	8.82 (0.14)	4.96 (720)	13.6
	35	0.062 (9)	51 (124)	18.9 (0.30)	8.82 (0.14)	5.79 (840)	11.6
	35	0.076 (11)	50 (123)	19.5 (0.31)	8.19 (0.13)	6.20 (900)	11.1
	35	0.069 (10)	47 (117)	18.9 (0.30)	8.82 (0.14)	7.16 (1038)	7.2
2.2.3.3	35	0.069 (10)	46 (115)	18.9 (0.30)	8.82 (0.14)	7.93 (1150)	0
2.3.1.3	45	0.083 (12)	48 (118)	20.8 (0.33)	8.82 (0.14)	4.41 (64)	16.9
	45	0.055 (8)	49 (121)	18.9 (0.30)	8.19 (0.13)	1.78 (258)	17.5
	45	0.083 (12)	52 (126)	20.8 (0.33)	8.82 (0.14)	3.52 (510)	18.8
2.3.2.3	45	0.083 (12)	52 (125)	20.8 (0.33)	8.82 (0.14)	4.96 (720)	18.0
	45	0.083 (12)	50 (122)	20.8 (0.33)	8.82 (0.14)	6.20 (900)	13.9
	45	0.055 (8)	50 (123)	18.9 (0.30)	8.19 (0.13)	6.95 (1008)	9.4
2.3.3.3	45	0.083 (12)	48 (118)	20.8 (0.33)	8.82 (0.14)	7.69 (1116)	0

TABLE 10

PUMPING RING DESIGN #3 - MECHANICAL CARBON GRAPHITE
(UNION CARBIDE GRADE CNF-J)

Data Point 3.X.X.3

Ring Identification

#3 Ring - Upper Location
#2 Ring - Lower Location

Stroke = 50.8 mm (2.00 in.)							
Data Point	Frequency Hz	Oil Pressure MPa (lb/in^2)	Oil Temperature °C (°F)	Flow Inlet cm^3/sec (gal/min)	Bypass Flow cm^3/sec (gal/min)	Pumped Pressure MPa (lb/in^2)	Pumped Flow g/min
3.1.1.3	10	0.03 (4)	50.6 (123)	13.8 (0.22)	6.30 (0.10)	0.22 (32)	2.64
	10	0.03 (4)	49.4 (121)	14.5 (0.23)	6.30 (0.10)	2.07 (300)	2.83
3.1.2.3	10	0.03 (4)	48.3 (119)	14.5 (0.23)	6.30 (0.10)	4.14 (600)	2.84
	10	0.03 (4)	48.3 (119)	13.8 (0.22)	6.30 (0.10)	5.58 (810)	1.84
	10	0.03 (4)	50.6 (123)	14.5 (0.23)	6.30 (0.10)	6.82 (990)	1.71
3.1.3.3	10	0.03 (4)	48.3 (119)	13.2 (0.21)	6.30 (0.10)	7.45 (1080)	0.64
	10	0.03 (4)	48.3 (119)	13.2 (0.21)	6.30 (0.10)	7.45 (1080)	0
3.2.1.3	35	0.07 (10)	47.8 (118)	13.8 (0.22)	6.30 (0.10)	0.40 (58)	14.7
	35	0.06 (9)	46.7 (116)	12.6 (0.20)	5.04 (0.08)	1.76 (255)	16.2
	35	0.06 (9)	46.7 (116)	12.6 (0.20)	5.04 (0.08)	3.52 (510)	16.7
	35	0.06 (9)	47.8 (118)	12.6 (0.20)	5.04 (0.08)	5.27 (765)	17.1
	35	0.06 (9)	48.3 (119)	12.6 (0.20)	5.04 (0.08)	6.93 (1005)	15.6
	35	0.06 (9)	49.4 (121)	12.6 (0.20)	5.04 (0.08)	7.65 (1110)	12.9
	35	0.06 (9)	49.4 (121)	12.6 (0.20)	5.04 (0.08)	8.27 (1200)	9.08
	35	0.06 (9)	49.4 (121)	12.6 (0.20)	5.04 (0.08)	8.98 (1302)	0
3.3.1.3	45	0.06 (8)	53.3 (128)	15.8 (0.25)	6.30 (0.10)	0.50 (73)	26.9
	45	0.03 (4)	48.3 (119)	13.8 (0.22)	5.04 (0.08)	2.07 (300)	29.1
3.3.2.3	45	0.03 (4)	49.4 (121)	13.8 (0.22)	5.04 (0.08)	4.14 (600)	28.4
	45	0.03 (4)	47.2 (117)	13.8 (0.22)	5.04 (0.08)	6.82 (900)	25.7
3.3.3.3	45	0.03 (4)	47.2 (117)	13.8 (0.22)	5.04 (0.08)	7.65 (1110)	13.6
	45	0.04 (6)	50.0 (122)	15.8 (0.25)	6.30 (0.10)	8.32 (1206)	2.35
	45	0.06 (8)	50.0 (122)	15.8 (0.25)	6.30 (0.10)	8.44 (1224)	0

Design #3 Ring, Mechanical Carbon Graphite (Union Carbine Grade CNF-J)
P_o: 10.3 MPa (1500 lb/in.^{2})
Stroke: 25.4 mm (1.00 in.)

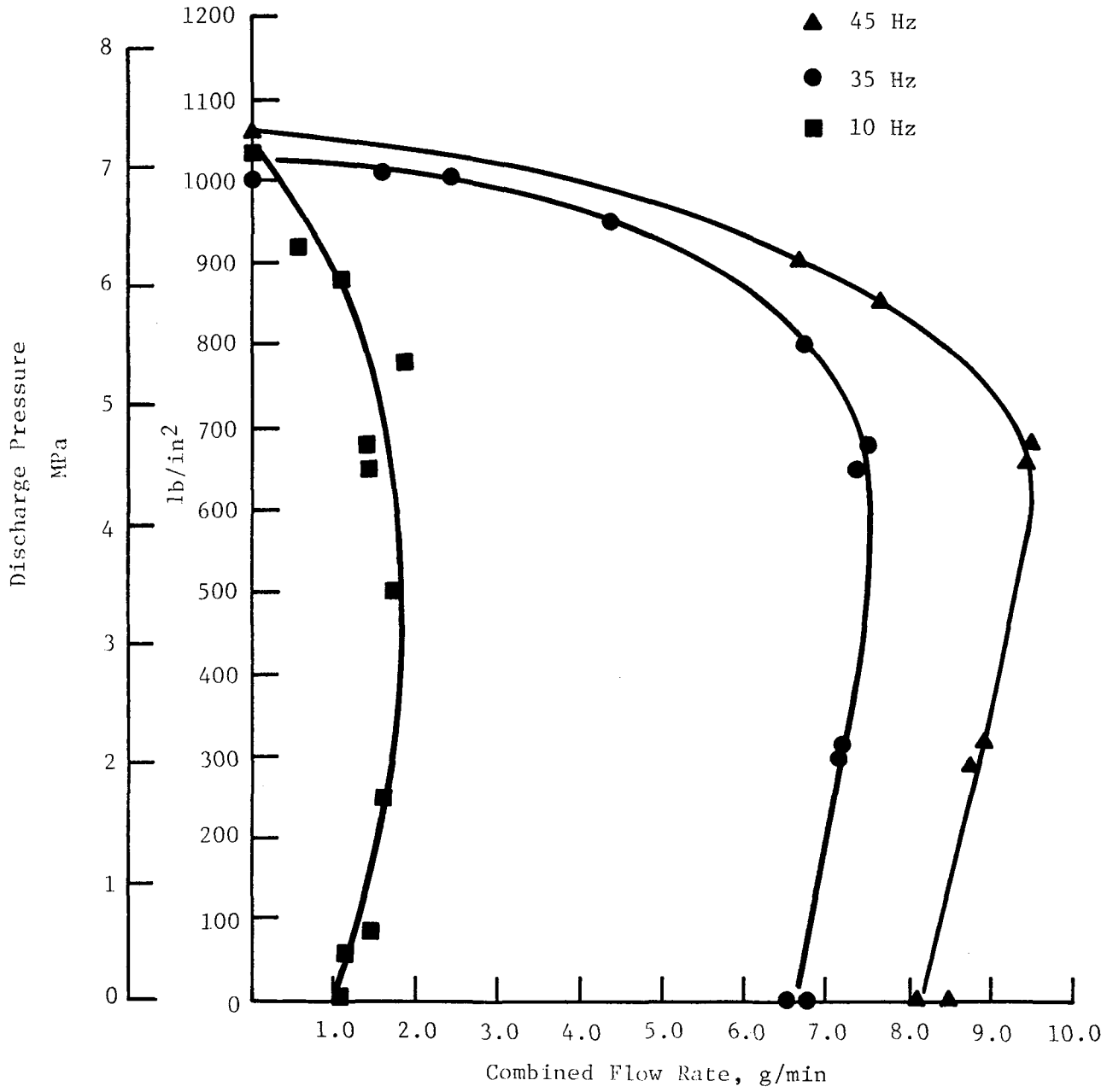

Fig. 17 Pressure-Flow Characteristic, Data Point 1.X.X.3

803319

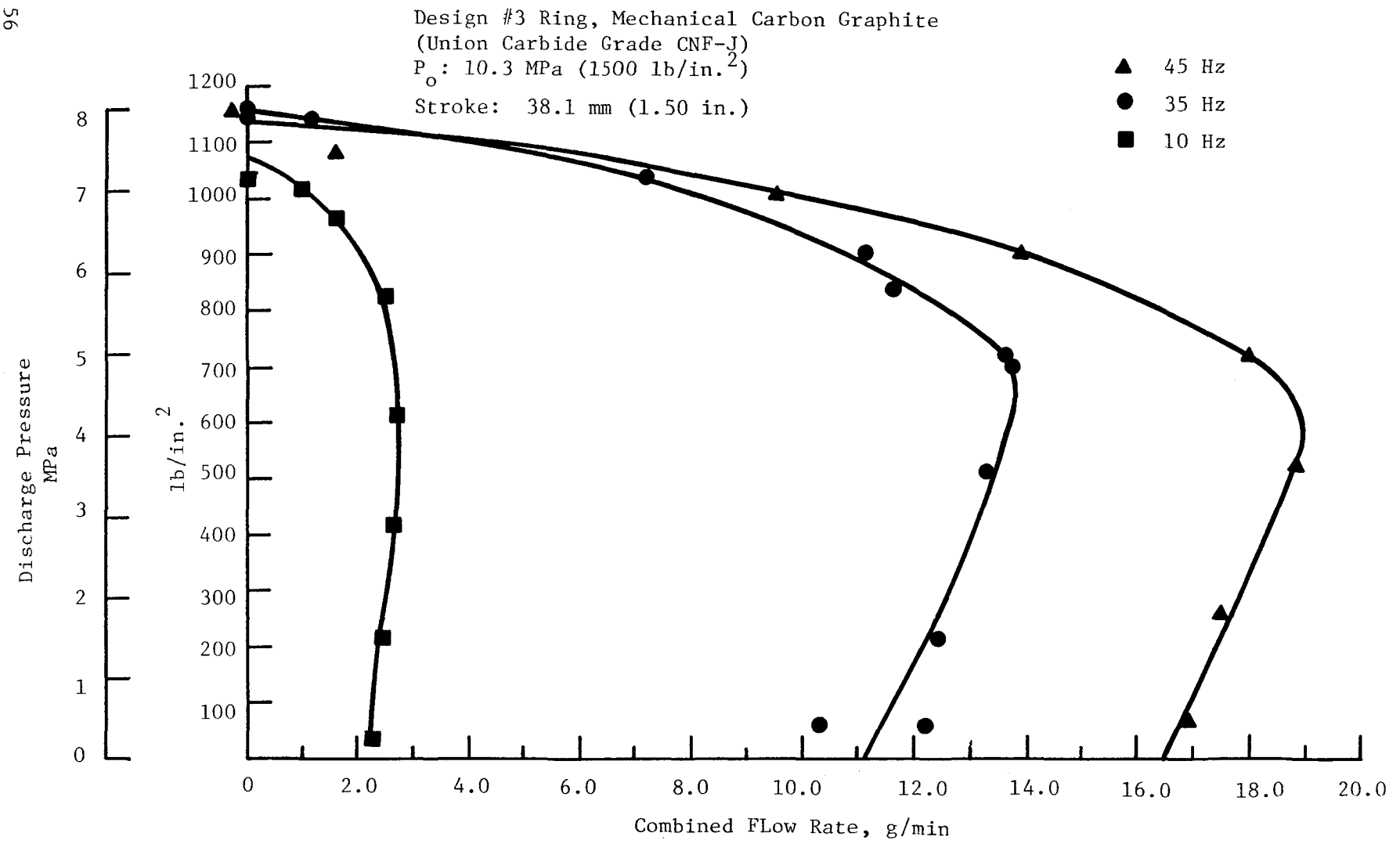

Fig. 18 Pressure-Flow Characteristic, Data Point 2.X.X.3

803321

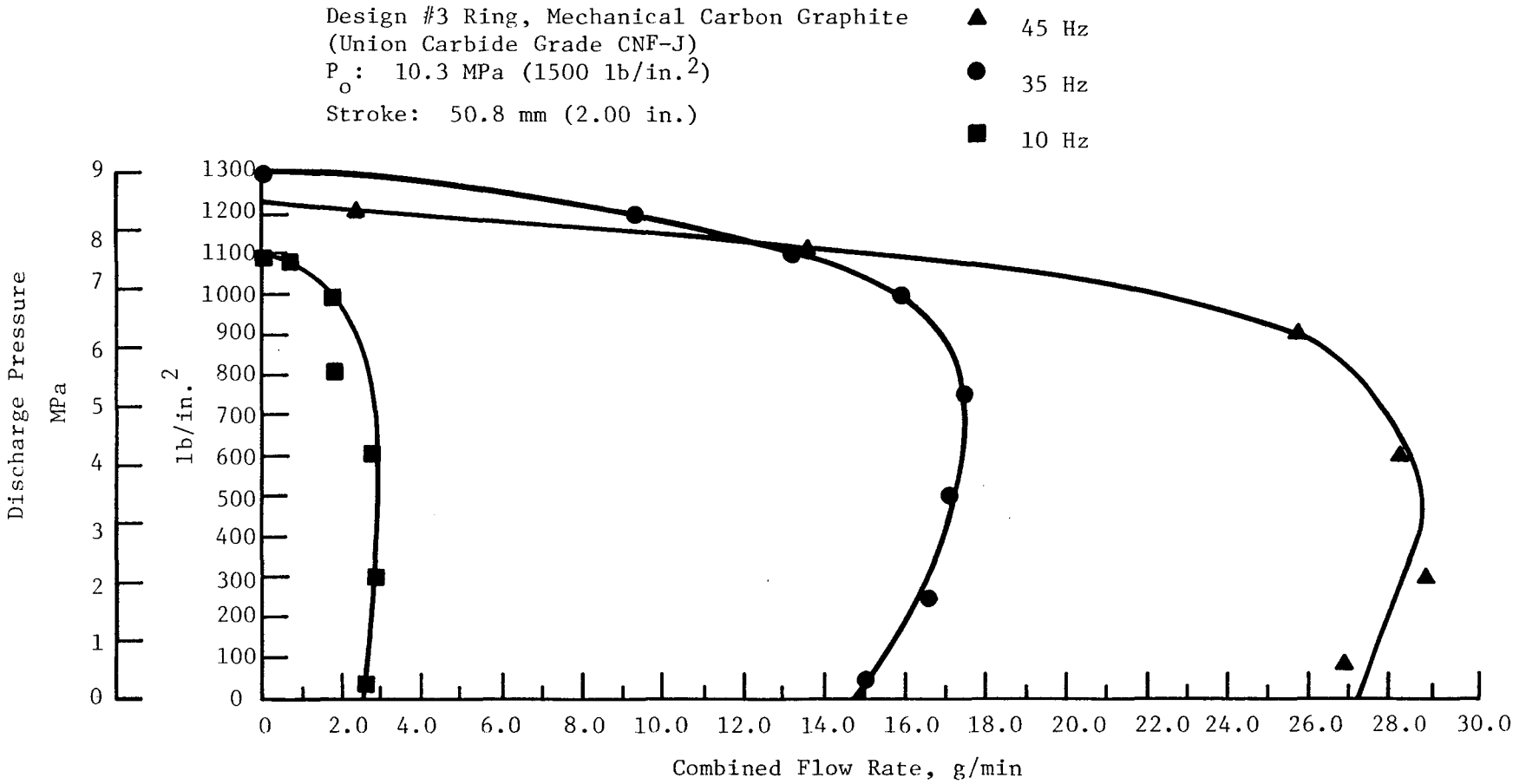

Fig. 19 Pressure-Flow Characteristic, Data Point 3.X.X.3

TABLE 11

HYDRODYNAMIC PUMPING RING - COMBINED PEAK FRICTION FORCE*

Stroke mm(in.)	Frequency Hz	Peak Force				Net Friction Force Change Due to Loading		Power Loss Due to Loading	
		Tin-Based Babbitt		Carbon Graphite **		Tin-Based Babbitt	Carbon Graphite	Tin-Based Babbitt	Carbon Graphite
		P_o = 0	P_o = 10.3 MPa (1500 lb/in.^{2})	P_o = 0	P_o = 10.3 MPa (1500 lb/in.^{2})				
		N (lb)	N (lb)	N (lb)	N (lb)	N (lb)	N (lb)	Watts (hp)	Watts (hp)
25.4 (1.00)	10	178 (40)	191 (43)	231 (52)	302 (68)	13 (3)	71 (16)	81 (0.109)	434 (0.519)
	35	89 (20)	118 (26)	111 (25)	133 (30)	27 (6)	22 (5)	570 (0.746)	475 (0.636)
	45	139 (31)	142 (32)	133 (30)	142 (32)	4.4 (1)	8.9 (2)	122 (0.164)	244 (0.327)
38.1 (1.50)	10	245 (55)	285 (64)	218 (49)	218 (49)	40 (9)	-0- (0)	366 (0.491)	-0- -0-
	35	294 (66)	356 (80)	231 (52)	231 (52)	53 (12)	-0- (0)	1709 (2.29)	-0- -0-
	45	400 (90)	436 (98)	285 (64)	302 (68)	36 (8)	18 (4)	1465 (1.96)	732 (0.982)
50.8 (2.00)	10	156 (35)	169 (38)	187 (42)	334 (75)	13 (3)	142 (32)	163 (0.218)	1736 (2.33)
	35	249 (55)	294 (66)	302 (68)	356 (80)	49 (11)	76 (17)	2089 (2.80)	3228 (4.33)
	45	276 (62)	320 (72)	409 (92)	436 (98)	44 (10)	36 (8)	2441 (3.27)	1953 (2.62)

*Forces are generated by two pumping rings acting together

**Carbon graphite ring #2 was replaced with Carbon Graphite ring #5 for friction tests at the 38.1 mm (1.50 in.) stroke

the cooling oil along the reciprocating shaft. For this reason, the individual ring loss readings cannot be used as the direct measure of ring loss but must be used in conjunction with each other to arrive at an effective loss value.

6.3 Temperature Measurements

Each data point evaluation included the measurement of several temperatures associated with the pumping rings. The measured temperatures included not only the actual operating temperatures of the rings undergoing test, but also the temperatures found in the supply and discharge oil flows.

The design of the tester provided for a large quantity of oil to bypass through the pumping ring location in order to bathe the test shaft with cooling oil. This design also provided a large thermal mass for cooling purposes and, as a result, the bulk oil temperature and the ring temperatures showed only very small differences. At no time did the ring temperature differ from the oil inlet temperature by more than 1 to 2°C (2 to 4°F). The oil discharge temperature taken outside the tester was usually 8 to 16°C (14 to 29°F) below the inlet temperature.

6.4 Additional Testing

A nonscheduled test to examine the effect of a reduced ring clamping pressure (P_o) was performed on the Mechanical Carbon Graphite rings at the 50.8 mm (2.00 in.) stroke, at a tester speed of 35 Hz, and at a P_o of 6.85 MPa (1000 lb/in.^{2}). The results of this test are shown on Table 12 and Figure 20. Included on Figure 20 is the test result for the Carbon Graphite ring with the normal P_o of 10.3 MPa (1500 lb/in.^{2}); it is evident from this figure that the reduced clamping pressure produced the more expected flow-pressure curve without the slope reversal experienced by the same rings at the higher P_o. The dead-ended pressure, however, was substantially reduced by the lower P_o, which at the same time produced a much higher open-ended flow rate.

6.5 Test Specimens

The test shaft and all of the pumping rings used for test purposes were photographed at the conclusion of the test program. A close-up view of the

TABLE 12

PUMPING RING DESIGN #3 - MECHANICAL CARBON GRAPHITE
(UNION CARBIDE GRADE CNF-J)

Reduced Clamping Pressure

Ring Identification

#3 Ring - Upper Location
#2 Ring - Lower Location

P_o = 6.85 MPa (1000 lb/in.^{2}) Stroke = 50.8 mm (2.00 in.)							
Data Point	Frequency Hz	Oil Pressure MPa (lb/in^2)	Oil Temperature °C (°F)	Flow Inlet cm^3/sec (gal/min)	Bypass Flow cm^3/sec (gal/min)	Pumped Pressure MPa (lb/in^2)	Pumped Flow g/min
-	35	0.06 (9)	50 (122)	12.6 (0.20)	5.04 (0.08)	0.58 (85.2)	31.9
	35	0.06 (9)	50 (122)	12.6 (0.20)	5.04 (0.08)	0.58 (85.2)	31.0
	35	0.06 (9)	49 (121)	12.6 (0.20)	5.04 (0.08)	1.76 (255)	30.4
	35	0.06 (9)	49 (121)	12.6 (0.20)	5.04 (0.08)	3.52 (510)	23.2
	35	0.06 (9)	49 (121)	12.6 (0.20)	5.04 (0.08)	4.52 (660)	6.97
	35	0.06 (9)	49 (121)	12.6 (0.20)	5.04 (0.08)	4.81 (702)	0

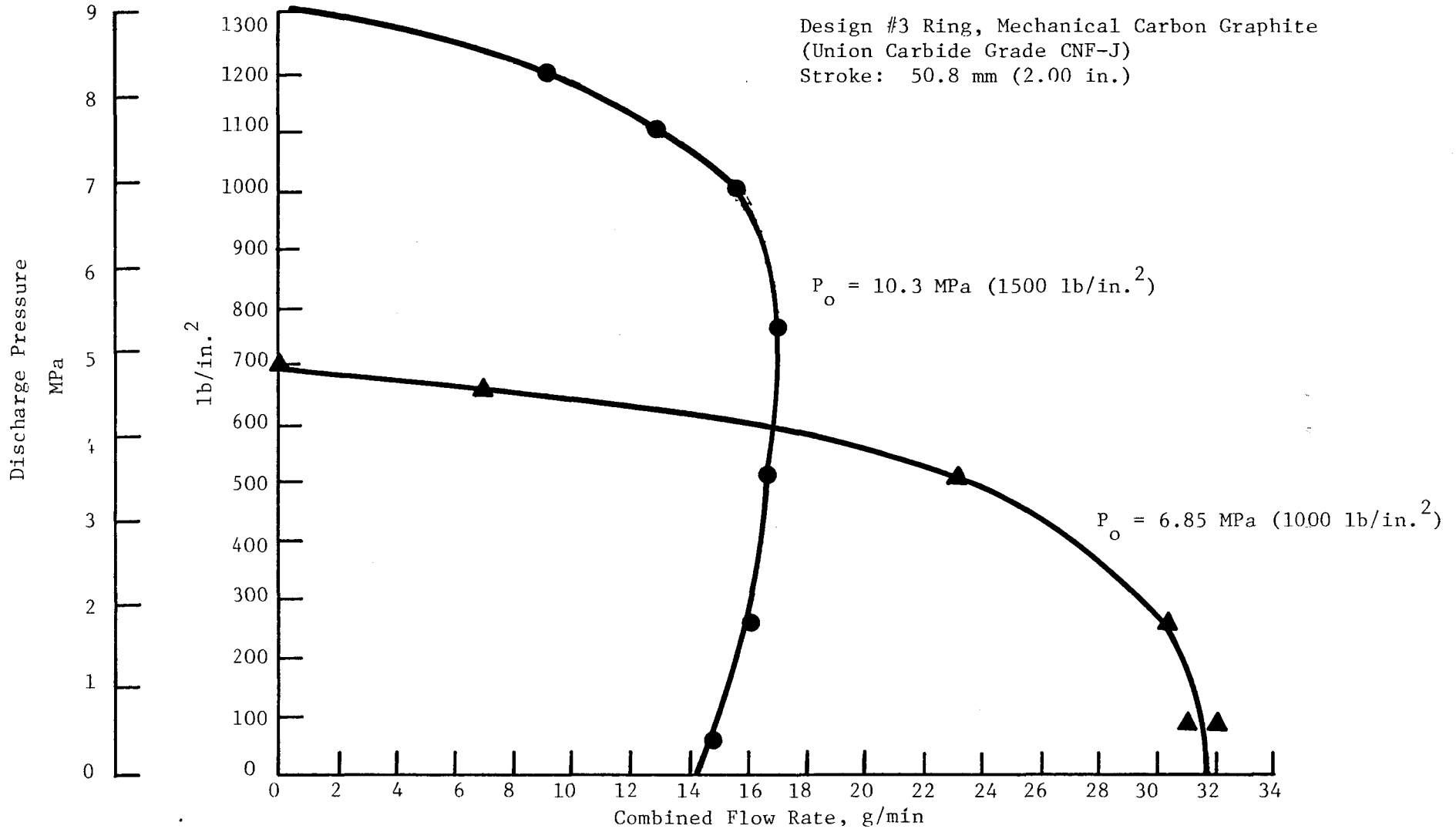

Fig. 20 Effect of Reduced Ring Clamping Pressure

803326

end-of-stroke pattern on the test shaft is presented on Figure 21. Although the wear pattern is optically visible, a measurement of the amount of material removed at each wear track (attempted with a surface analyzer) was undetectable; thus representing no apparent shaft material removal.

Photographs of all the pumping rings installed in the tester are shown in Figures 22 through 24. Figure 22 shows the #1 and #3 Tin-Based Babbitt rings, which demonstrated the highest pumped pressure capability and showed a nearly uniform wear surface over the entire length of their close-fitting bore area, including some longitudinal scratches. The Bearing Bronze rings, shown in Figure 23, illustrate the lack of a definite wear track on either the #1 or #2 ring. While these rings had an elasticity modulus highest of all the rings tested, they demonstrated practically no pumping capability, a result which is commensurate with the lack of close-in wear seen in the photographs.

Each of the four Mechanical Carbon Graphite rings photographed in Figure 24 shows a narrow wear band at or near the edge of the close-fitting bore area. Unlike the Tin-Based Babbitt rings, the wear bands on the Mechanical Carbon Graphite rings are clearly defined. Two of the Mechanical Carbon Graphite rings broke at their close-in ends. Ring #4 broke during disassembly after the conclusion of data point 1.X.X.3 (25.4 mm (1.00 in.) stroke); ring #2 broke during tester disassembly after data points 2.X.X.3 and 3.X.X.3 and the unassigned data point were completed. In order to obtain friction data not recorded during the original testing for the data point, ring #3 replaced ring #2 for a tester reassembly at the 2.X.X.3 data point.

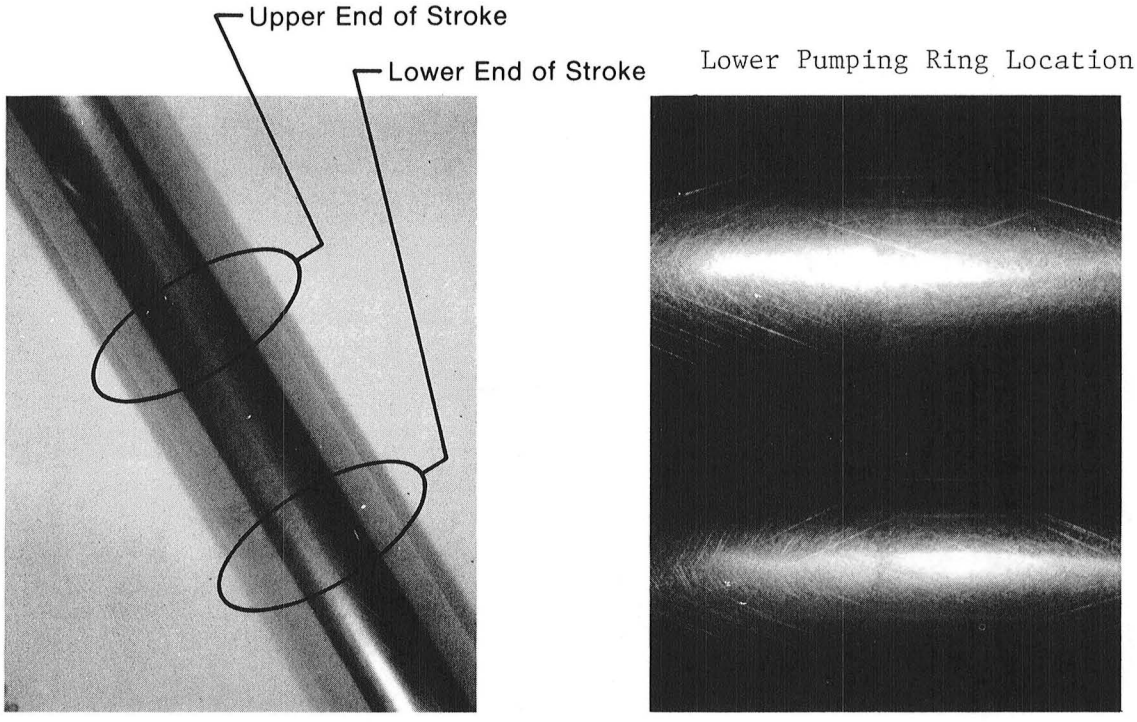

End of Stroke
Magnification = X1.67

End of Stroke
Magnification = X9.75

Fig. 21 End-of-Stroke Pattern on Test Shaft

This Page Intentionally Left Blank

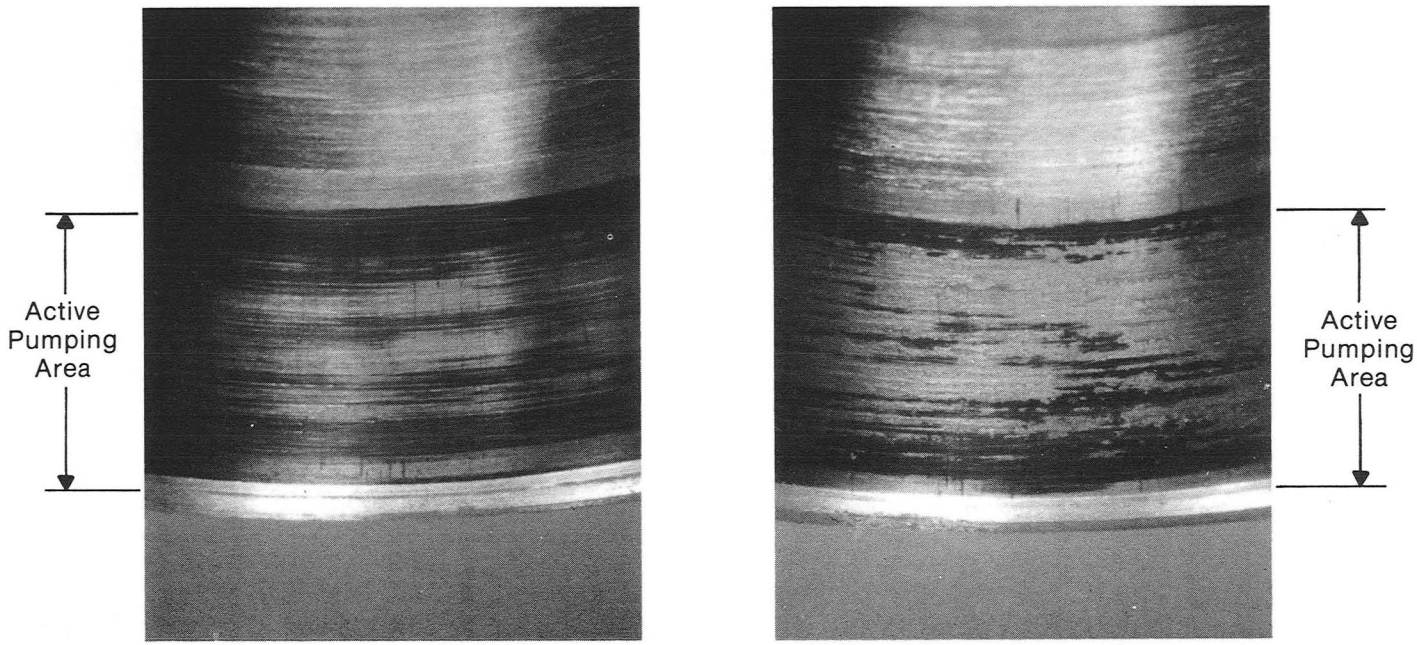

Ring #1, Upper Location

Ring #3, Lower Location

Fig. 22 Tin-Based Babbitt Pumping Rings After Testing
(Magnification = X9.75)

MTI-20315

This Page Intentionally Left Blank

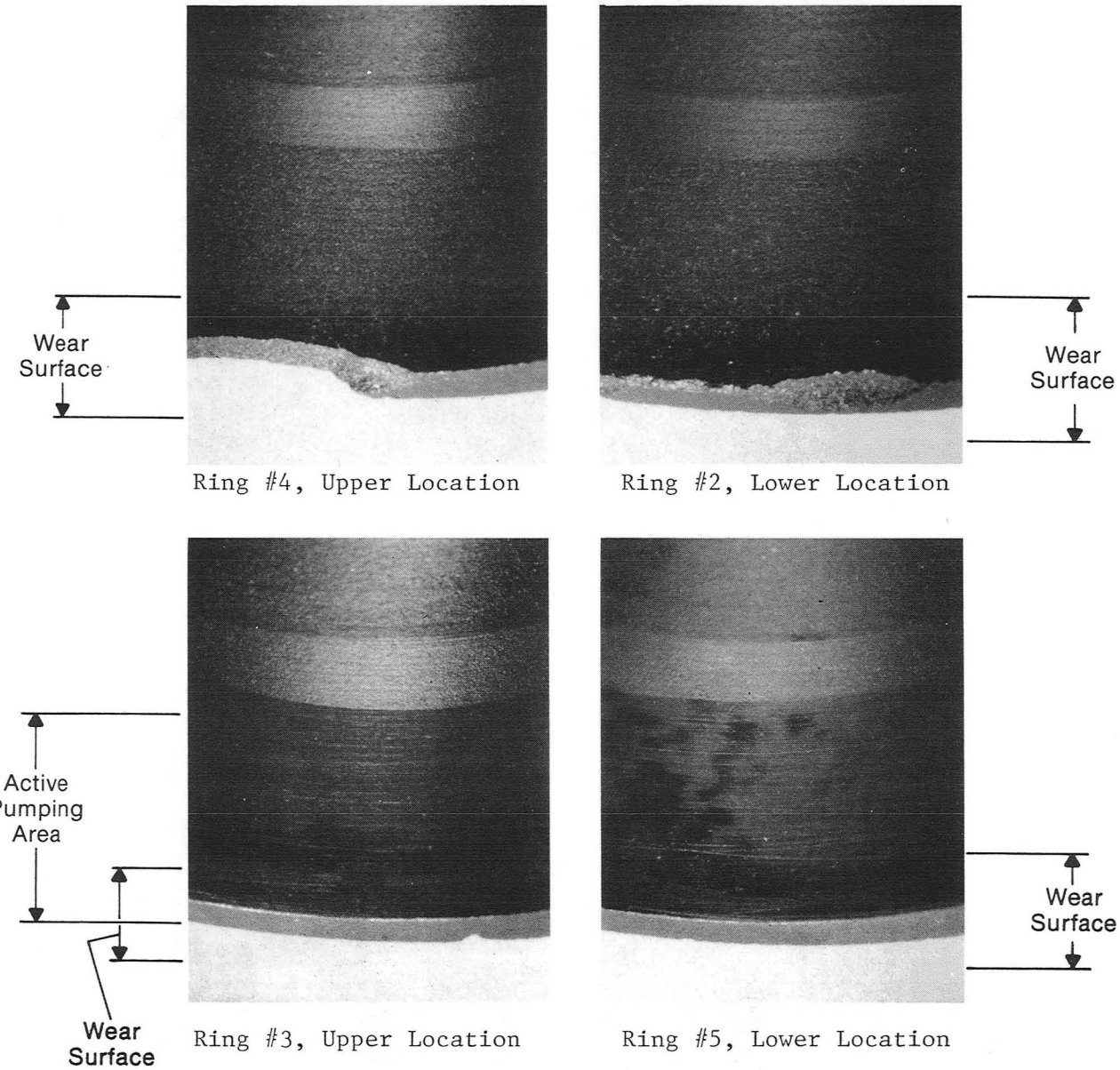

Fig. 23 Mechanical Carbon Graphite Pumping Rings After Testing
(Magnification = X9.75)

MTI-20301

This Page Intentionally Left Blank

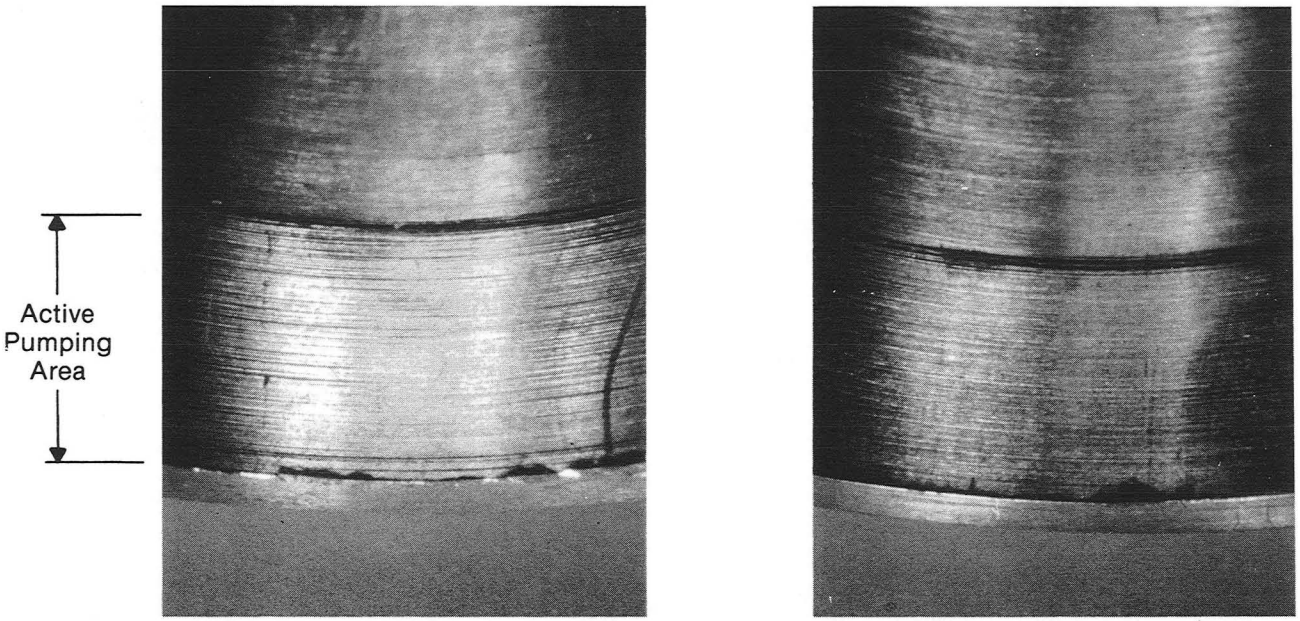

Ring #2, Upper Location

Ring #1, Lower Location

Fig. 24 Bearing Bronze Pumping Rings After Testing
(Magnification = X9.75)

This Page Intentionally Left Blank

7.0 PUMPING RING ANALYSIS

The model used to represent the pumping rings that were tested is shown schematically in Figure 25. The ring is assumed to be undercut at x = 0 so that the hydrodynamic film starts there and ends at x = L. The ring is assumed to be clamped at $x = -L_1$ and loaded at a distance e from the end with the uniform pressure p_0. The no-load clearance on the ring is assumed to be a constant value c and the thickness of the ring t is assumed to be small compared with the mean radius R.

The elastic deflection under the loading p_0 develops a wedge that results in hydrodynamic pressure generation in balance with the loading and the elastic restraint at the equilibrium operating position during the forward stroke. During the backward stroke, the conditions are such that the ring is in rubbing contact with the shaft. The equations governing the deflection of an axisymmetric shell under bending can be found in many texts (ref. 6). The equations for the radially inward deflection w are as follows:

$$\frac{E\,t^3}{12(1-\nu^2)}\frac{d^4w}{dx^4} + \frac{Et}{R^2}w = -P(x) \tag{1}$$

where E denotes the elastic modulus, ν the Poisson's Ratio, and P(x) the radially outward loading that may be expressed in terms of the applied loading p_0 and the hydrodynamic pressure p as

$$P(x) = \begin{cases} 0, & -L_1 \leq x \leq 0 \\ p, & 0 \leq x < L - e \\ p-p_0, & L - e \leq x \leq L. \end{cases} \tag{2}$$

The hydrodynamic pressure p is determined from the solution to Reynolds Equation

$$\frac{dp}{dx} = 6\,\mu\,u_0\,\frac{h-k}{h^3} \tag{3}$$

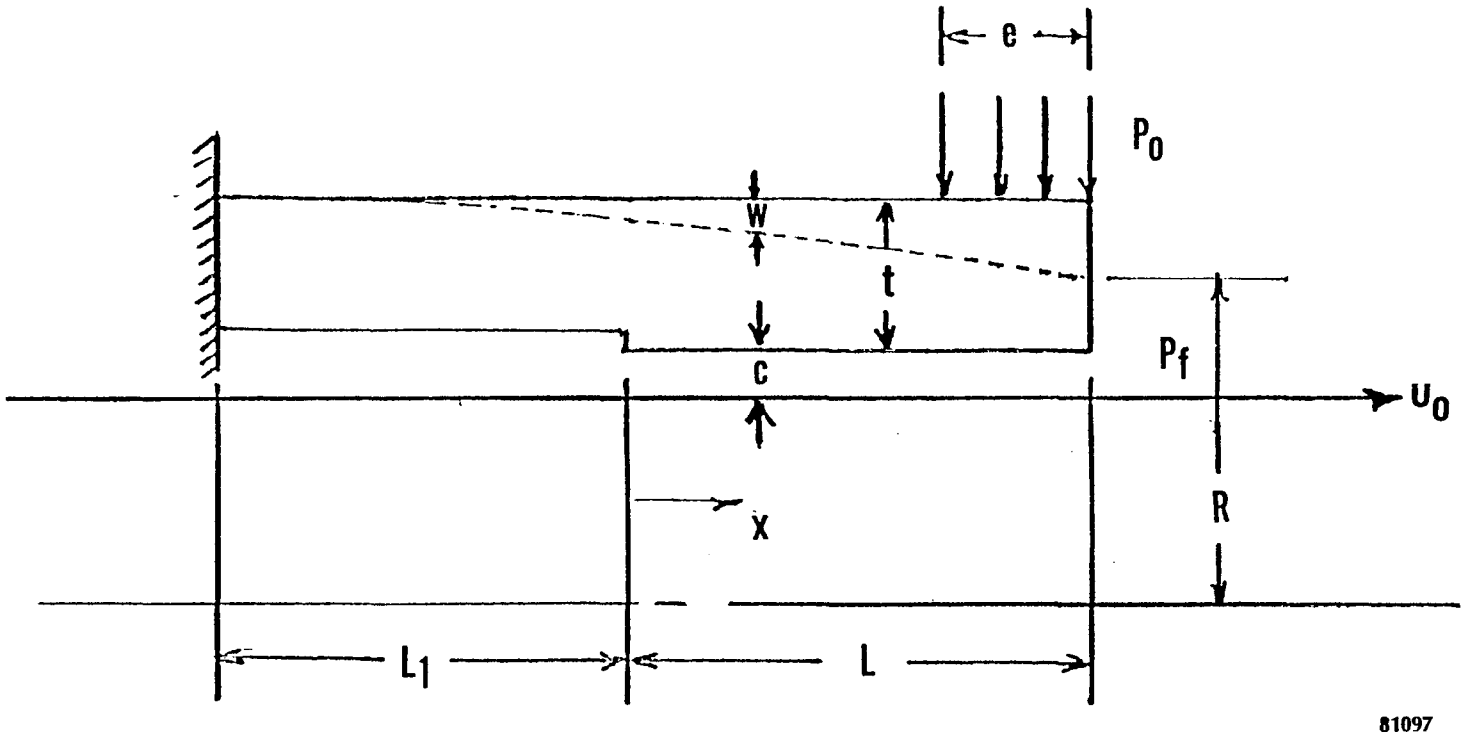

Fig. 25 Model for Pumping Ring Analysis

where μ is the fluid viscosity, k a constant of integration related to the flow, and u_0 is the average speed, which is related to the frequency N and the stroke S by

$$u_0 = 2NS$$

This velocity represents the average of the sinusoidal velocity over half cycle. Since the system contains two opposing pumping rings, it is double-acting and the velocity u_0 is assumed to prevail over the entire period of operation. In this manner, the transient problem is approximated and greatly simplified into a steady-state process. The film thickness h appearing in Equation (3) is related to the deflection w by

$$h = c - w, \quad 0 \leq x \leq L$$

The system of equations given by Equations (1) through (3) represents a fifth-order set of differential equations requiring five boundary conditions, in addition to a sixth condition for the evaluation of the constant k appearing in Equation (3), Two conditions result from the clamped-end requirement at $x = -L_1$

$$w = \frac{dw}{dx} = 0 \qquad \text{at } x = -L_1$$

Two conditions result from the prescribed pressures at x = 0 and L

$$p = 0 \text{ at } x = 0 \qquad\qquad p = p_f \text{ at } x = L$$

where p_f is the sealed pressure. The remaining two conditions relate to the free-end condition at x = L, requiring no moment and shear,

$$\frac{d^2w}{dx^2} = \frac{d^3w}{dx^3} = 0.$$

The above system of equations can be expressed in terms of the following dimensionless variables and parameters

$$\tilde{p} = \frac{c^2}{6\mu u_0 L} p \ , \qquad \tilde{p}_0 = \frac{c^2}{6\mu u_0 L} p_0 \ , \qquad \tilde{p}_f = \frac{c^2}{6\mu u_0 L} pf \ ,$$

$$\xi = \frac{x}{L}, \qquad \varepsilon = \frac{e}{L}, \qquad \tilde{L}_1 = \frac{L_1}{L}$$

$$\beta = \frac{6\mu u_0}{c^2}\frac{R^2}{ctE}$$

$$\alpha = \frac{t^2R^2}{12L^4(1-\nu^2)}, \qquad K = \frac{Q}{\pi R u_0 C}$$

where β represents a coupled elastohydrodynamic parameter, α is a geometric parameter that is an index of the bending induced to hoop stress induced deflections, and K is a dimensionless volumetric flow rate. The deflections are expressed in terms of a dimensionless film thickness function $\tilde{h}$ defined as

$$\tilde{h} = \begin{cases} 1 - \frac{w}{c}, & \xi < 0 \\ \frac{h}{c}, & \xi \geq 0 \end{cases} \tag{4}$$

The dimensionless differential equations for $\tilde{h}$ and $\tilde{p}$ in terms of the above quantities are

$$\alpha \frac{d^4\tilde{h}}{d\xi^4} + \tilde{h} = \begin{cases} 1 & -L_1 < \xi < 0 \\ 1 + \beta\tilde{p}, & 0 < \xi < 1 - \varepsilon \\ 1 + \beta(\tilde{p}-\tilde{p}_0) & 1 - \varepsilon < \xi < 1 \end{cases} \tag{5}$$

$$\frac{d\tilde{p}}{d\xi} = \frac{\tilde{h} - K}{\tilde{h}^3} \tag{6}$$

with the boundary conditions

$$\tilde{p}(0) = 0, \quad \tilde{p}(1) = \tilde{p}_f \tag{7}$$

$$\tilde{h}(-\tilde{L}_1) = 1, \quad \tilde{h}'(-\tilde{L}_1) = 0, \quad \tilde{h}''(1) = \tilde{h}'''(1) = 0 \tag{8}$$

In addition, since the thickness, t, is assumed constant and there are no concentrated loads, quantities $\tilde{h}$, $\tilde{h}'$, $\tilde{h}''$, and $\tilde{h}'''$ are continuous in the entire interval $-L_1 < \xi < 1$.

Equations (5) and (6) are solved simultaneously with the fourth-order Runge-Kutta method.

The equations are integrated backward from $\xi = 1$. The equations $\tilde{h}''(1)$, $\tilde{h}'''(1)$ and $\tilde{p}(1)$ are prescribed by Equations (7) and (8). For any given values of $\tilde{h}(1)$, $\tilde{h}'(1)$, and K, the following may be computed: $\tilde{h}(-\tilde{L}_1)$ and $\tilde{p}(0)$. This results in three nonlinear equations of the form

$$\tilde{p}(0) = F_1(\tilde{h}(1), \tilde{h}'(1), K) = 0$$

$$\tilde{h}(-L_1) = F_2(\tilde{h}(1), \tilde{h}'(1), K) = 1$$

$$\tilde{h}'(-L_1) = F_3(\tilde{h}(1), \tilde{h}'(1), K) = 0$$

which are inverted numerically by the secant method. The solutions so obtained provide dimensionless values of the film thickness profile, the pressure profiles and the flow rates for prescribed values of the parameters α, β, $\tilde{p}_0$, $\tilde{p}_f$, ε, and $\tilde{L}_1$.

A set of comparisons between theoretical predictions and experimental results for a geometry simulating the Mechanical Carbon Graphite pumping rings as closely as possible is presented in Section 8.0. Parametric studies for a free pumping ring are described below. For a free-ended pumping ring, the boundary conditions at $x = -L_1$ are replaced by the conditions that $h''(0) = h'''(0) = 0$, which corresponds to a vanishing of the shear force and moment at $x = 0$. A dimensionless central case is taken for the parametric study that roughly approximates the Mechanical Carbon Graphite ring. The parameter values are $\alpha = 0.032$, $\beta = 0.16$, $\tilde{p}_0 = 6$ and $\varepsilon = 0.5$.

The results of the parametric studies are given in Figures 26 through 34 in the form of film thickness and pressure as functions of position at various sealed pressures. Values of the dimensionless volumetric flow rate, K, are given with their associated pressure curves. At high loads and low sealed pressures, the pressures tend to follow the same curve until very close to the high-pressure end of the ring, where the pressure rapidly approaches the sealed pressure. The flow rates do not vary significantly with sealed pressure at low sealed pressures.

Figure 26 shows the pressures and film thicknesses for the central case. Figures 27, 28, and 29 show the effect of varying α. Figures 30 through 33 show the effects of the hydrodynamic parameters on pumping ring behavior. In each of these cases β and $\tilde{p}_0$ are varied, keeping the product $\beta\tilde{p}_0 = 0.9$. This corresponds to varying speed or viscosity while keeping the applied loading constant. Flow rates at low to moderate sealed pressures can be seen to increase with increasing viscosity and to increase markedly with increasing speed. As seen in Figure 33, the pressure and deformation profiles at very low speeds are almost independent of sealed pressures, except when extremely close to the high-pressure end. Finally, Figure 34, when compared with Figure 26, shows the effect of decreasing the loading, while keeping the other parameters fixed. A relatively small decrease in the load tends to result in higher flows at low sealed pressures and, in addition, markedly decreases the maximum pressure that can be sealed. As is discussed later, the loading is a very sensitive parameter to seal performance.

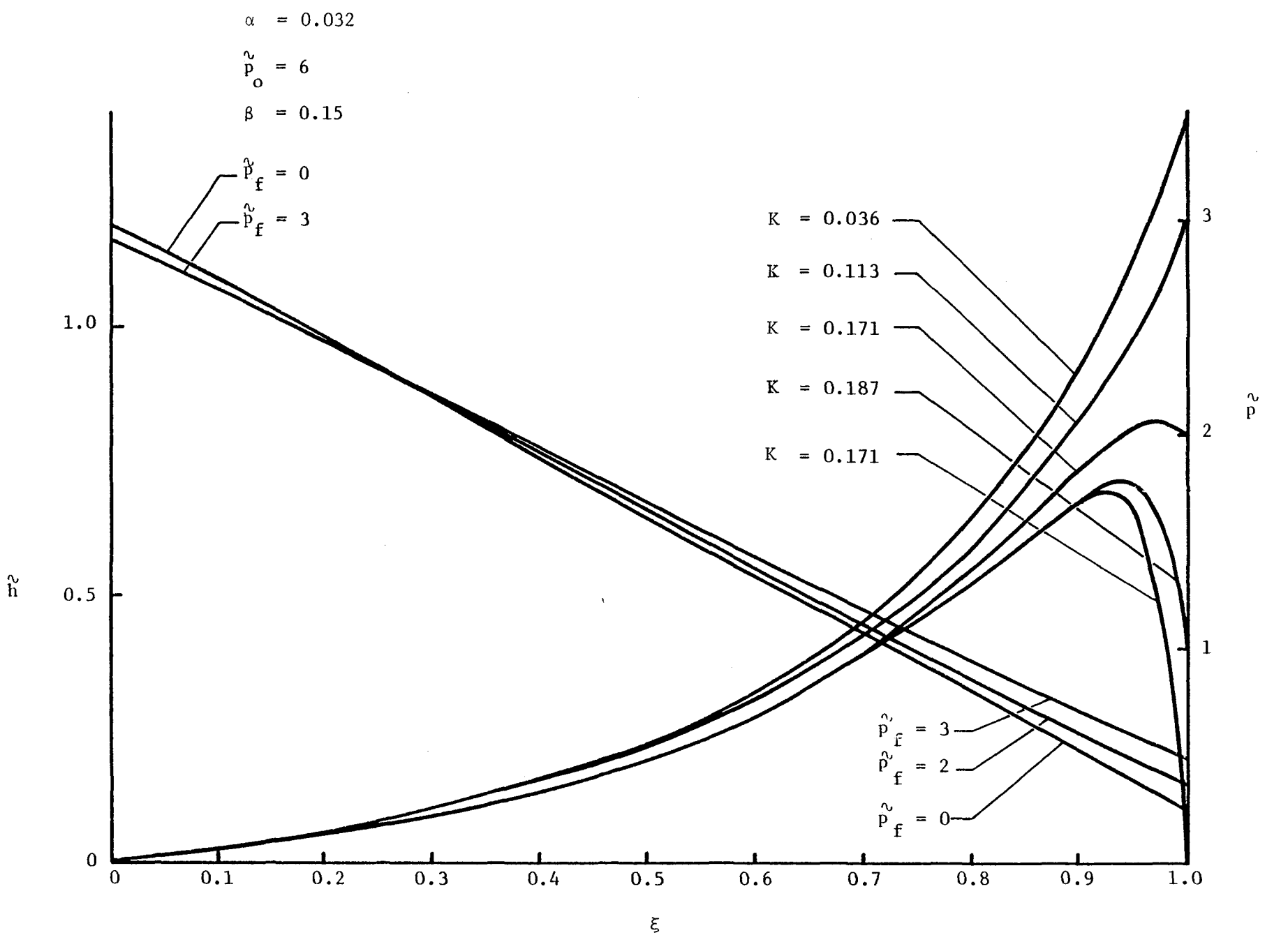

Fig. 26 Pressure and Film Thickness, Central Case

803604

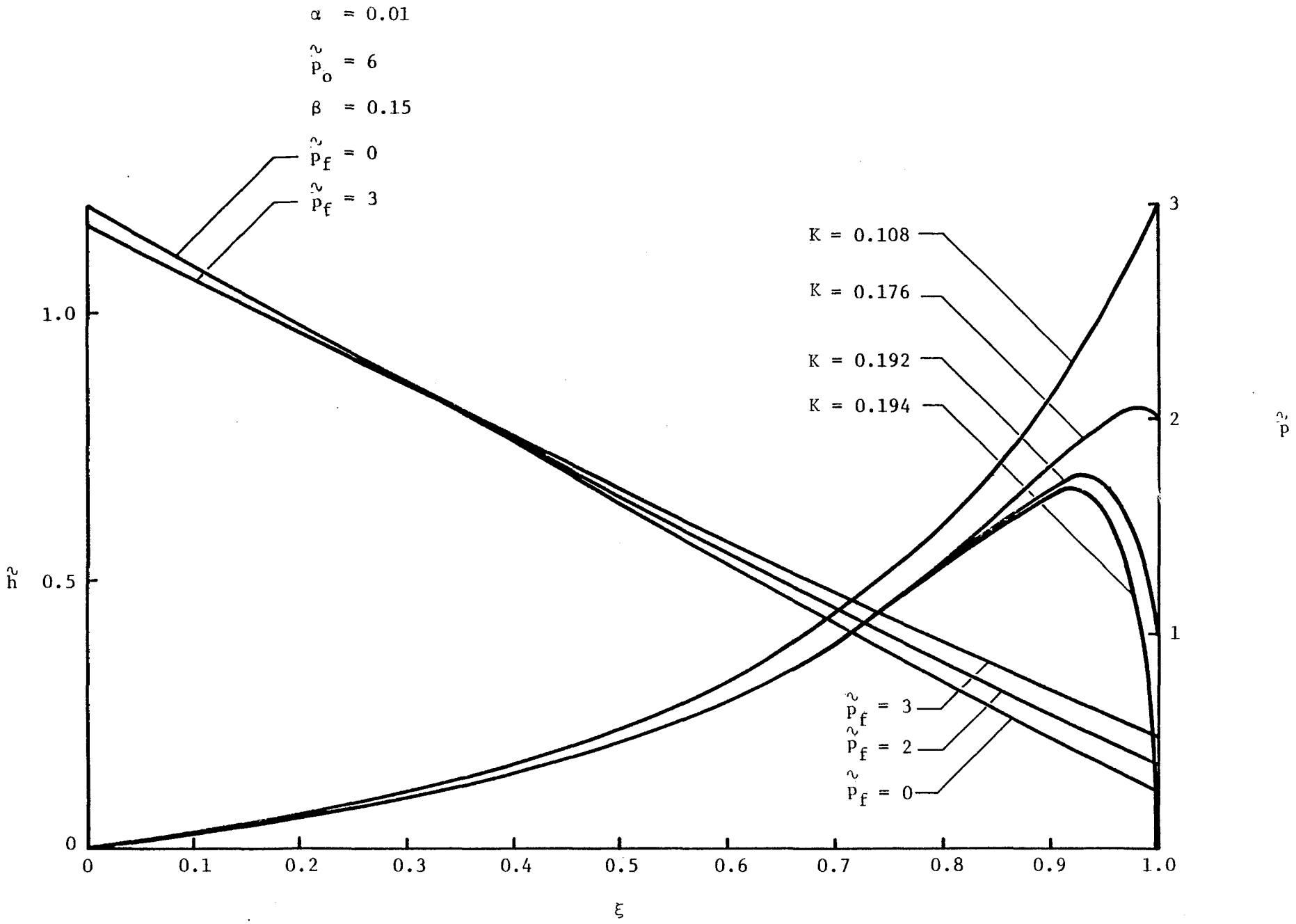

Fig. 27 Pressure and Film Thickness, α = 0.01

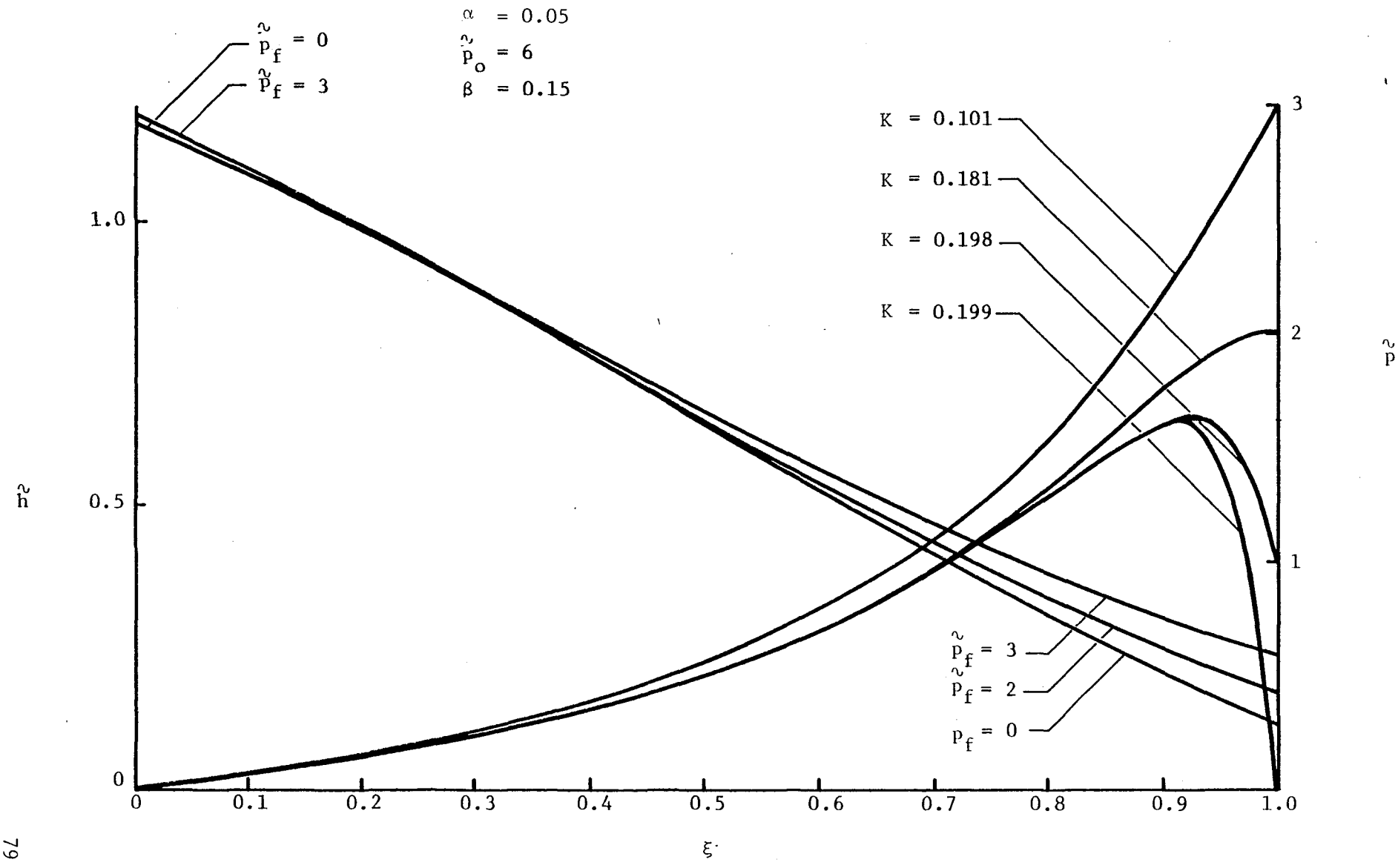

Fig. 28 Pressure and Film Thickness, α = 0.05

803605

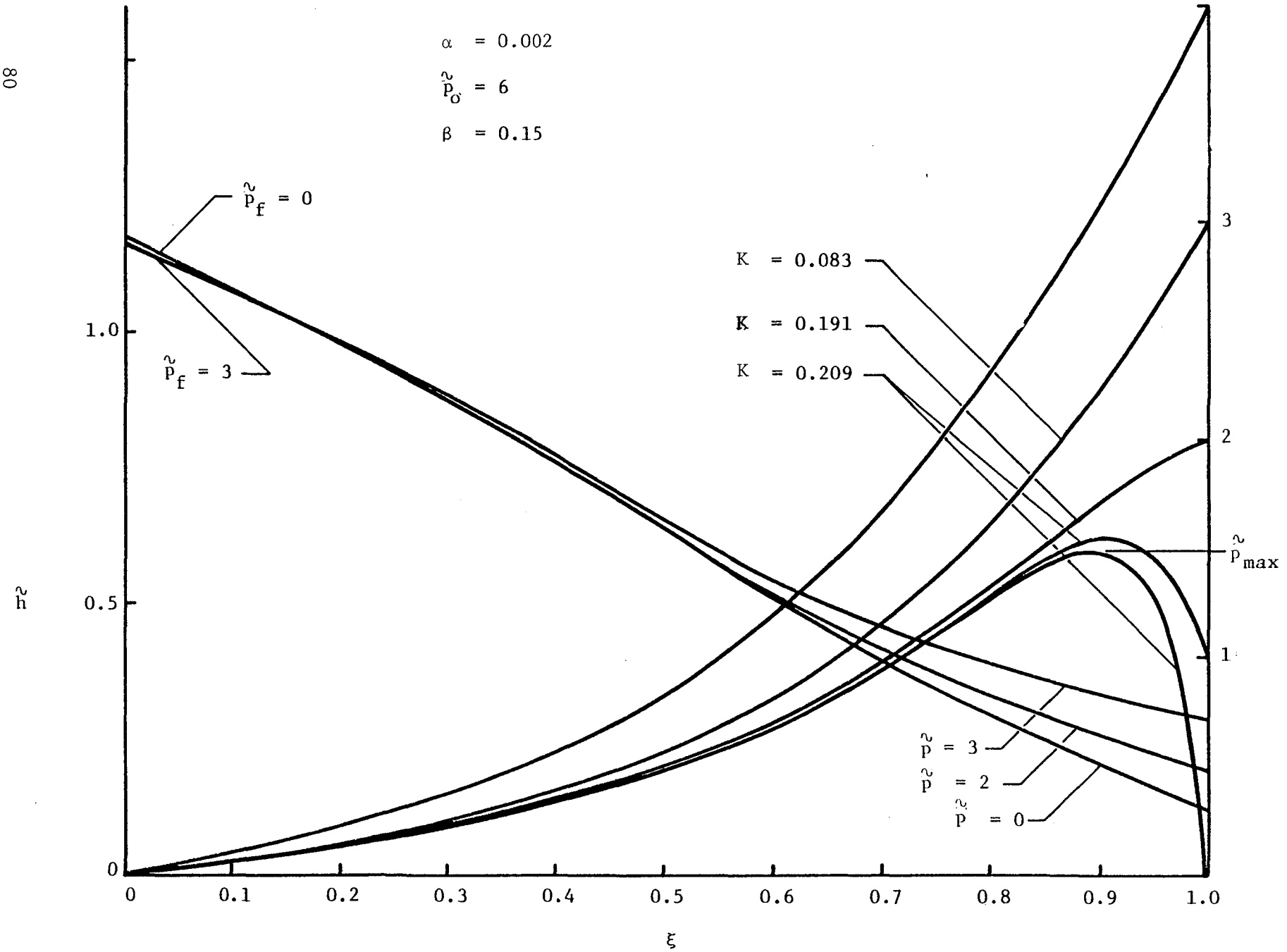

803603

Fig. 29 Pressure and Film Thickness, α = 0.002

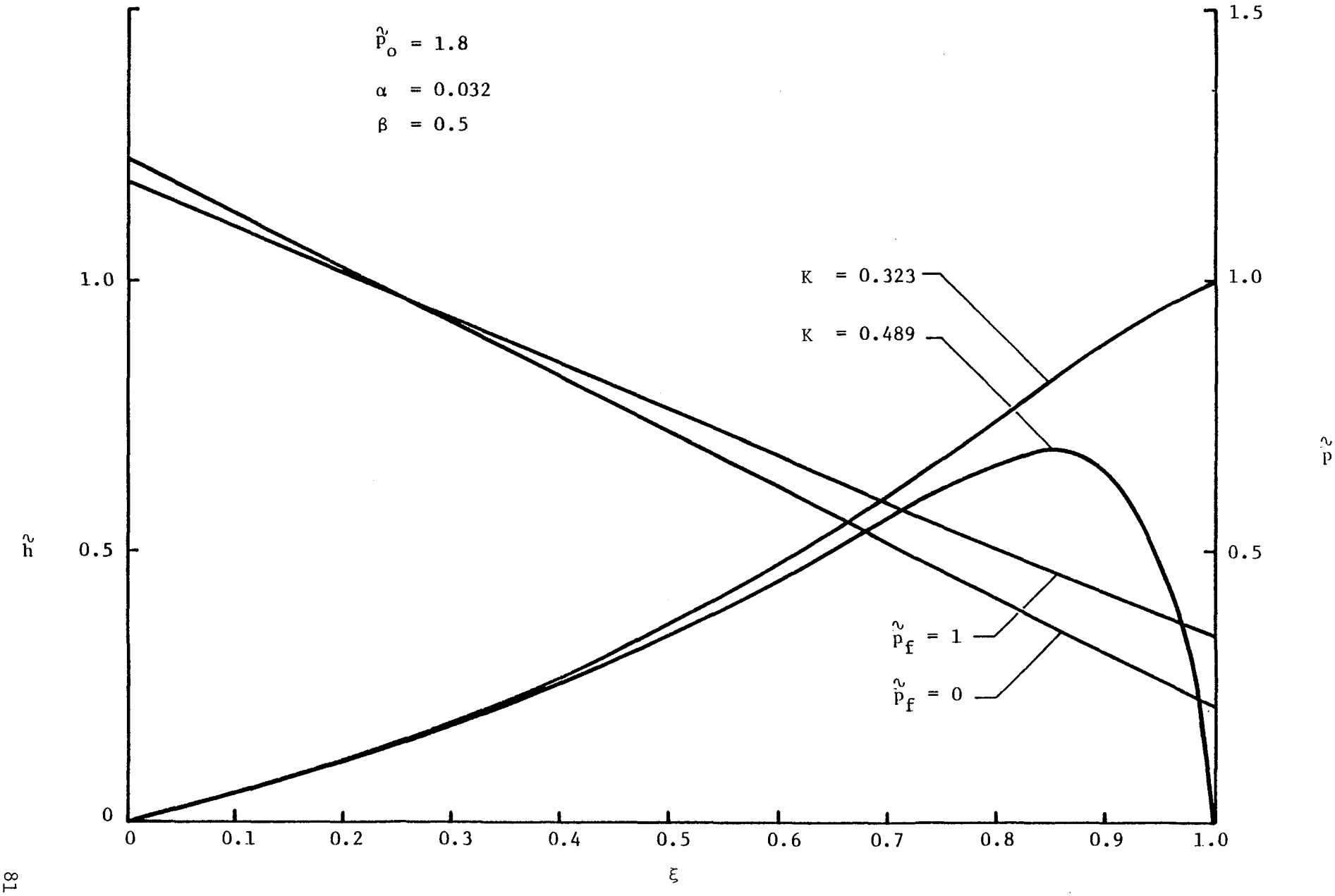

803601

Fig. 30 Pressure and Film Thickness, β = 0.5, $\beta\tilde{p}_o$ = 0.9

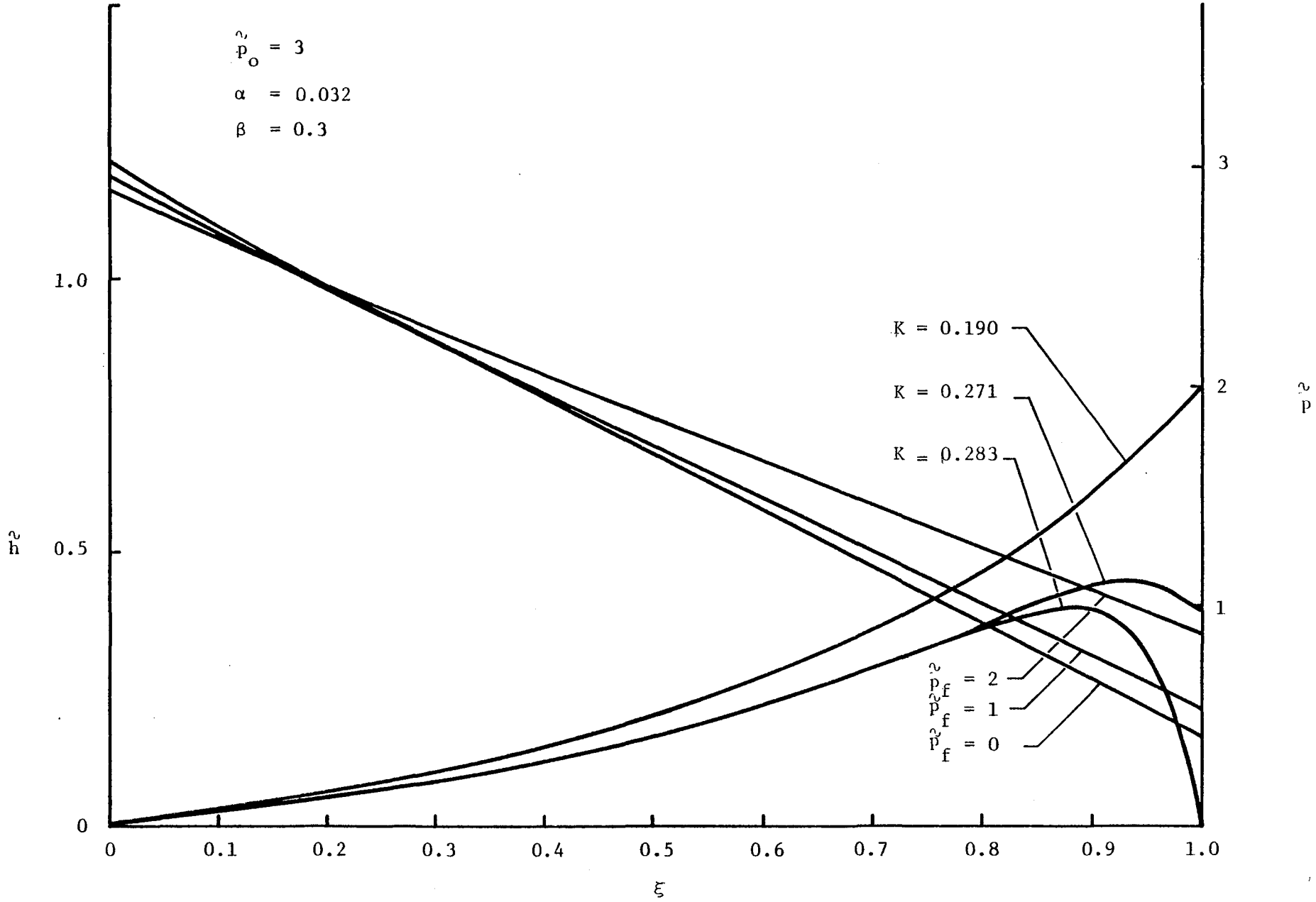

Fig. 31 Pressure and Film Thickness, $\beta = 0.3$, $\beta\tilde{p}_o = 0.9$

803606

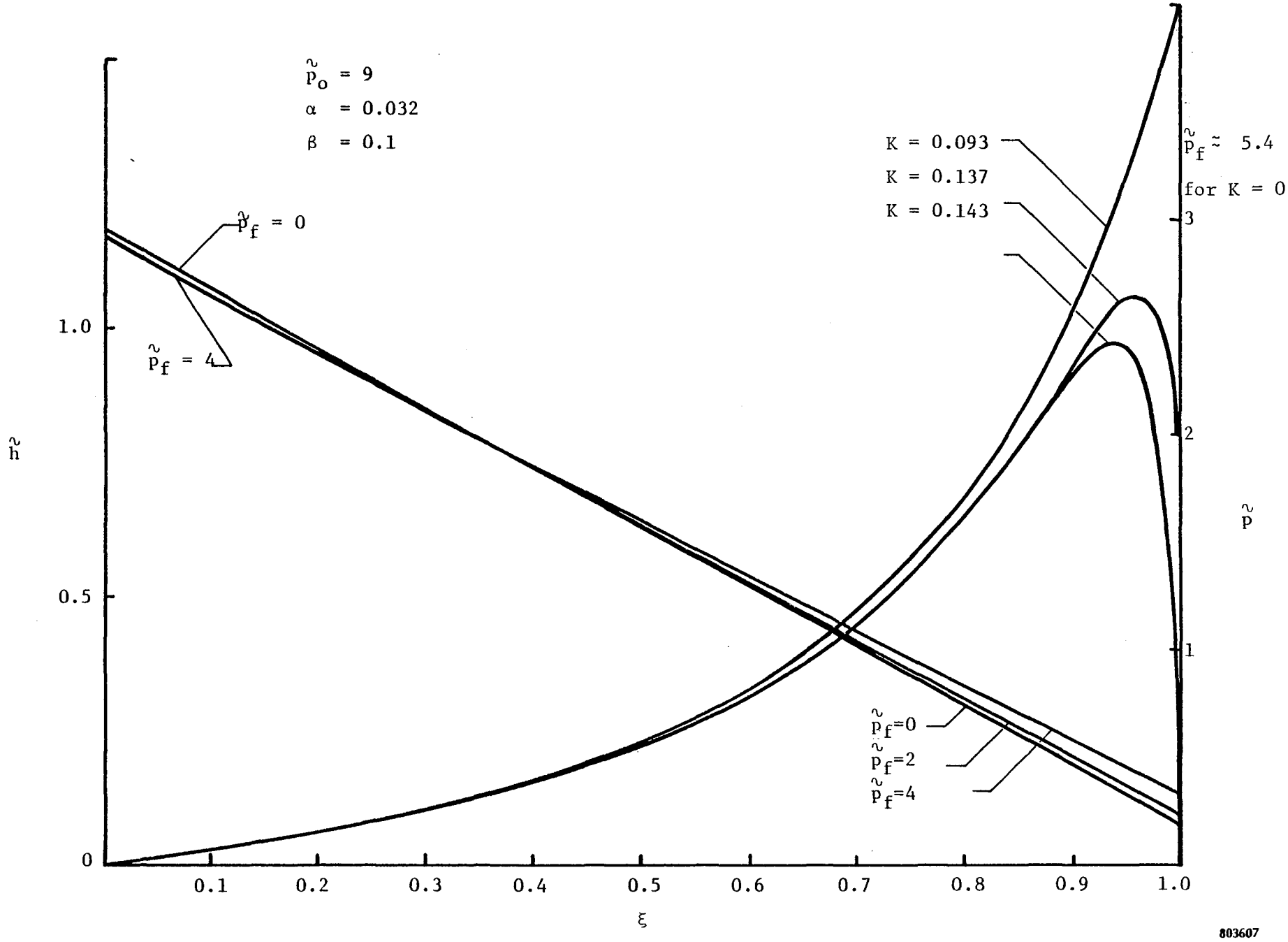

Fig. 32 Pressure and Film Thickness, β = 0.1, $\beta\tilde{p}_o$ = 0.9

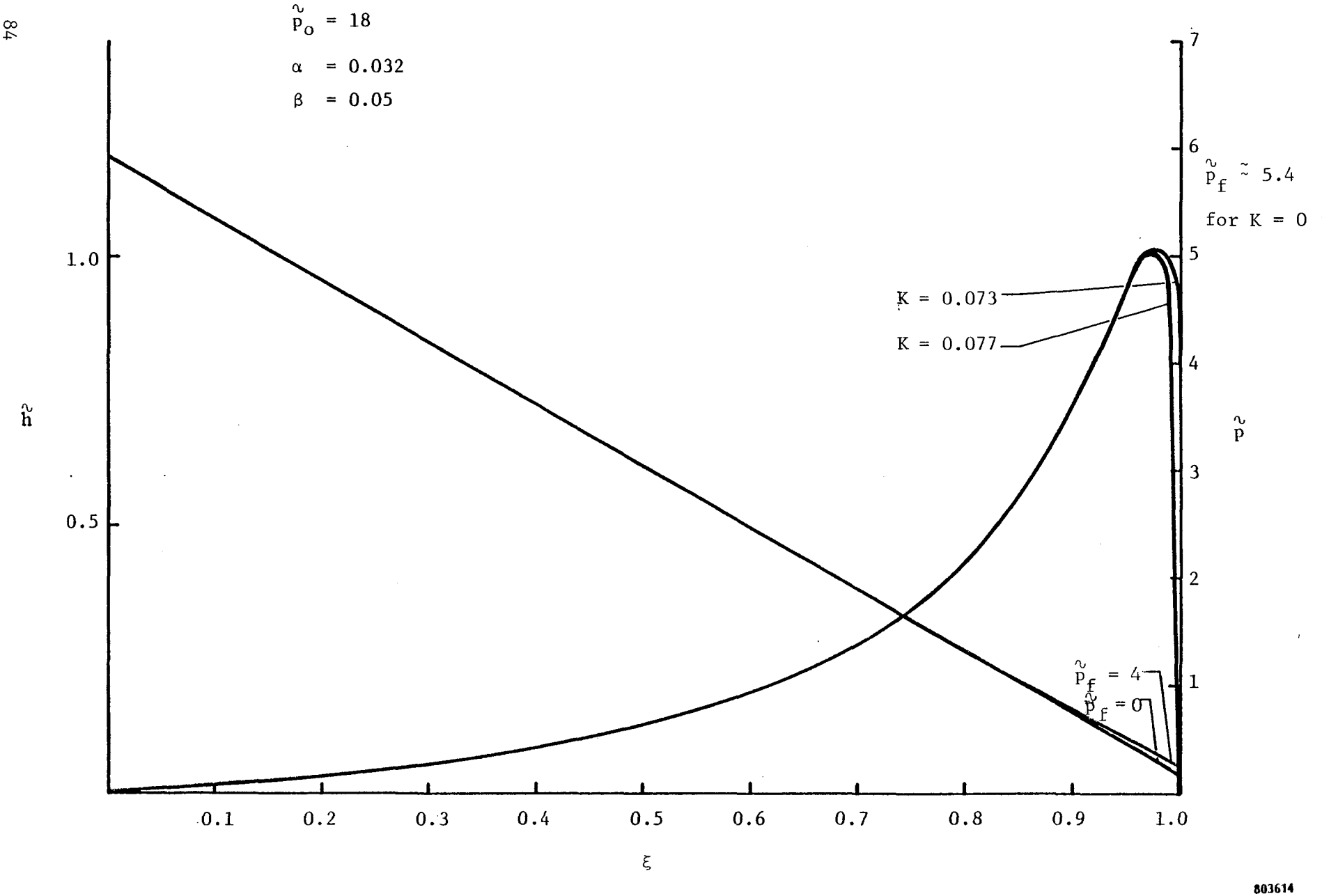

Fig. 33 Pressure and Film Thickness, β = 0.05, $\beta\tilde{p}_o$ = 0.9

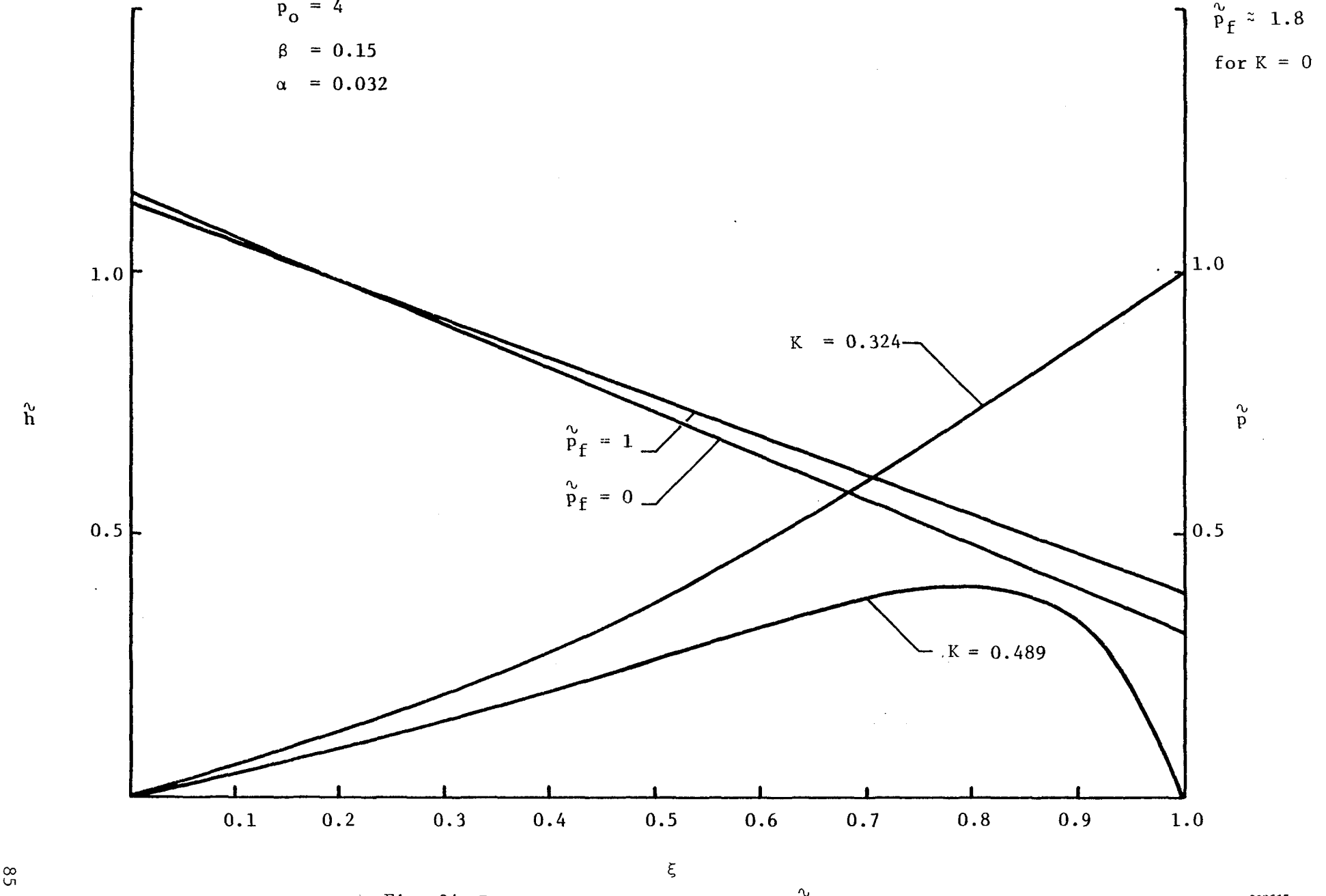

Fig. 34 Pressure and Film Thickness, $\tilde{p}_o = 4.0$

803615

This Page Intentionally Left Blank

8.0 COMPARISON BETWEEN THEORY AND EXPERIMENT

Analytically produced curves showing the sealed pressure-flow rate performances of the Mechanical Carbon Graphite pumping rings are presented on Figures 35 through 39. The experimental data for the Mechanical Carbon Graphite pumping rings are shown by the points superimposed on these curves. All data in Figure 35 correspond to a 25.4 mm (1.00 in.) stroke; Figure 36 to a 38.1 mm (1.50 in.) stroke; and Figure 37 to a 50.8 mm (2.00 in.) stroke. The three sets of points on each figure were taken at frequencies of 10 Hz, 35 Hz and 45 Hz. Solid lines appearing on the figures denote theoretical predictions, which were obtained for a set of property values corresponding to a Mechanical Carbon Graphite ring and a 20W40 oil at a temperature of 49°C (120°F). The property values and geometrical parameters used to characterize the ring are given on Table 13.

The theory tends to overpredict the flow at high speeds and underpredict the flow at lower speeds. Errors in the absolute value of the predicted flow are partially attributable to uncertainties in the clearance, elastic modulus and mean viscosity that were used in the computations. The more severe speed variations predicted by theory, as compared with those that were measured, are believed to result from thermal effects. At higher speeds, increased viscous heating results in a lower local viscosity, which, in turn, decreases the film thickness, thereby reducing the flow rate from that predicted isothermally.

The predicted lack of flow variation with sealed pressure at low pressures results from the balance between the applied pressure gradient, which tends to increase the film, and the flow. The equilibrium between the elastic deflections and the hydrodynamic pressure gives rise to the result that the flow at low pressures is independent of the pressure. The observed increases in flow with increasing sealed pressure are also believed to be the result of thermal effects. The isothermal theory predicts the flow rate at low pressures to be independent of pressure and to increase with increasing viscosity. As the sealed pressure is increased, the film thickness increases and the shear rate (hence, the amount of viscous heating) tends to decrease, resulting in a lower temperature and, in turn, a higher viscosity

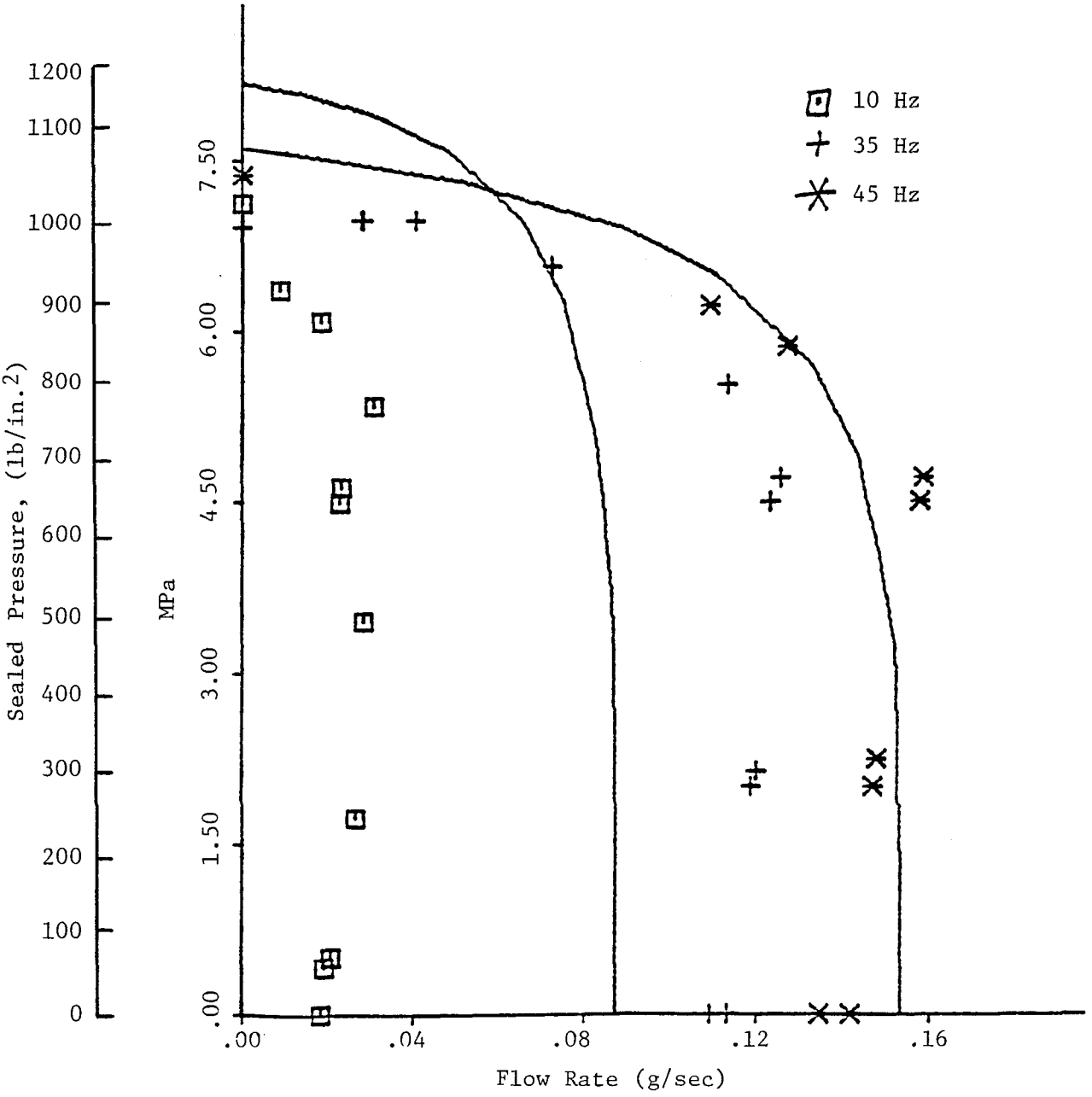

Fig. 35 Pressure-Flow Relationship, Stroke = 25.4 mm

81098

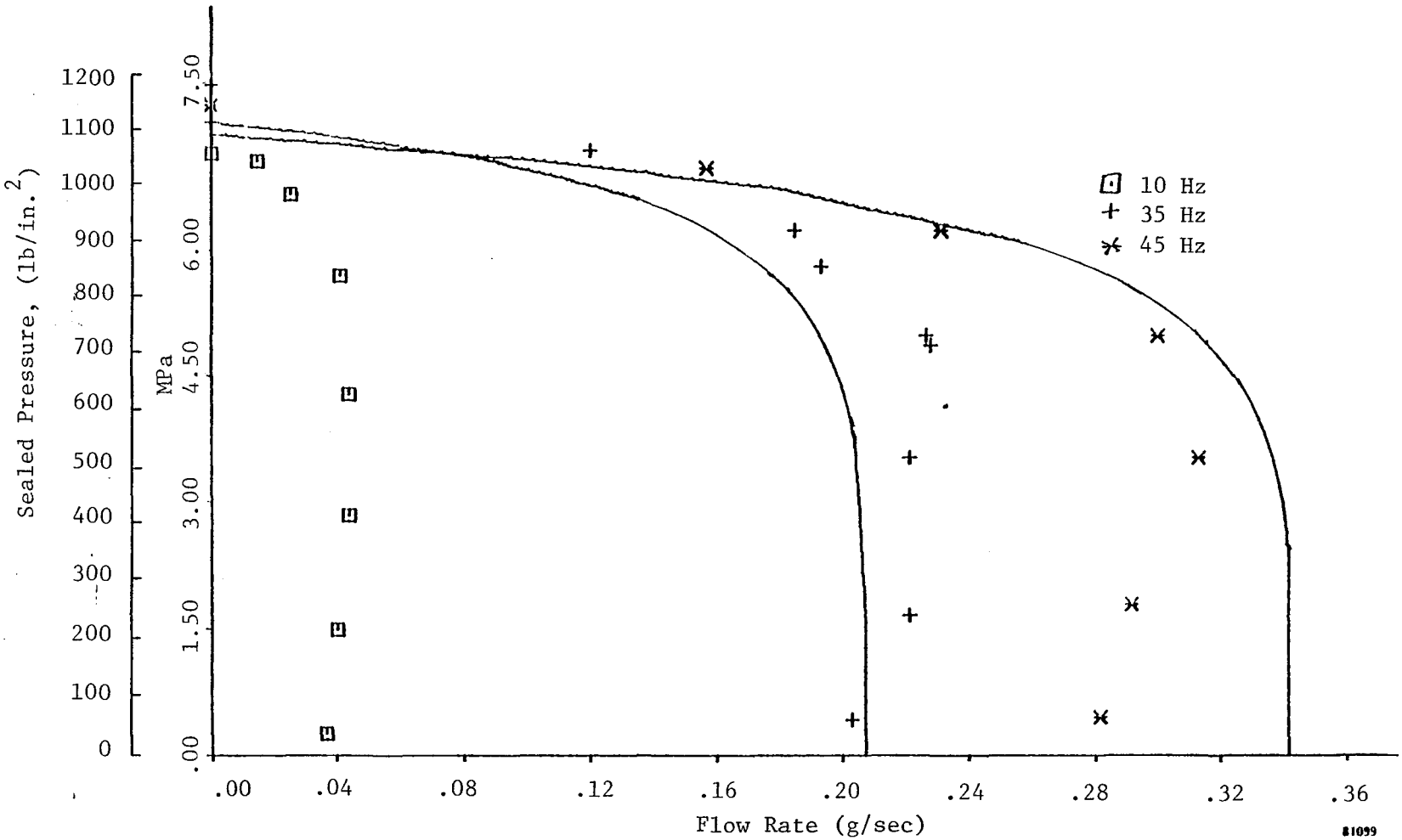

Fig. 36 Pressure-Flow Relationship, Stroke = 38.1 mm

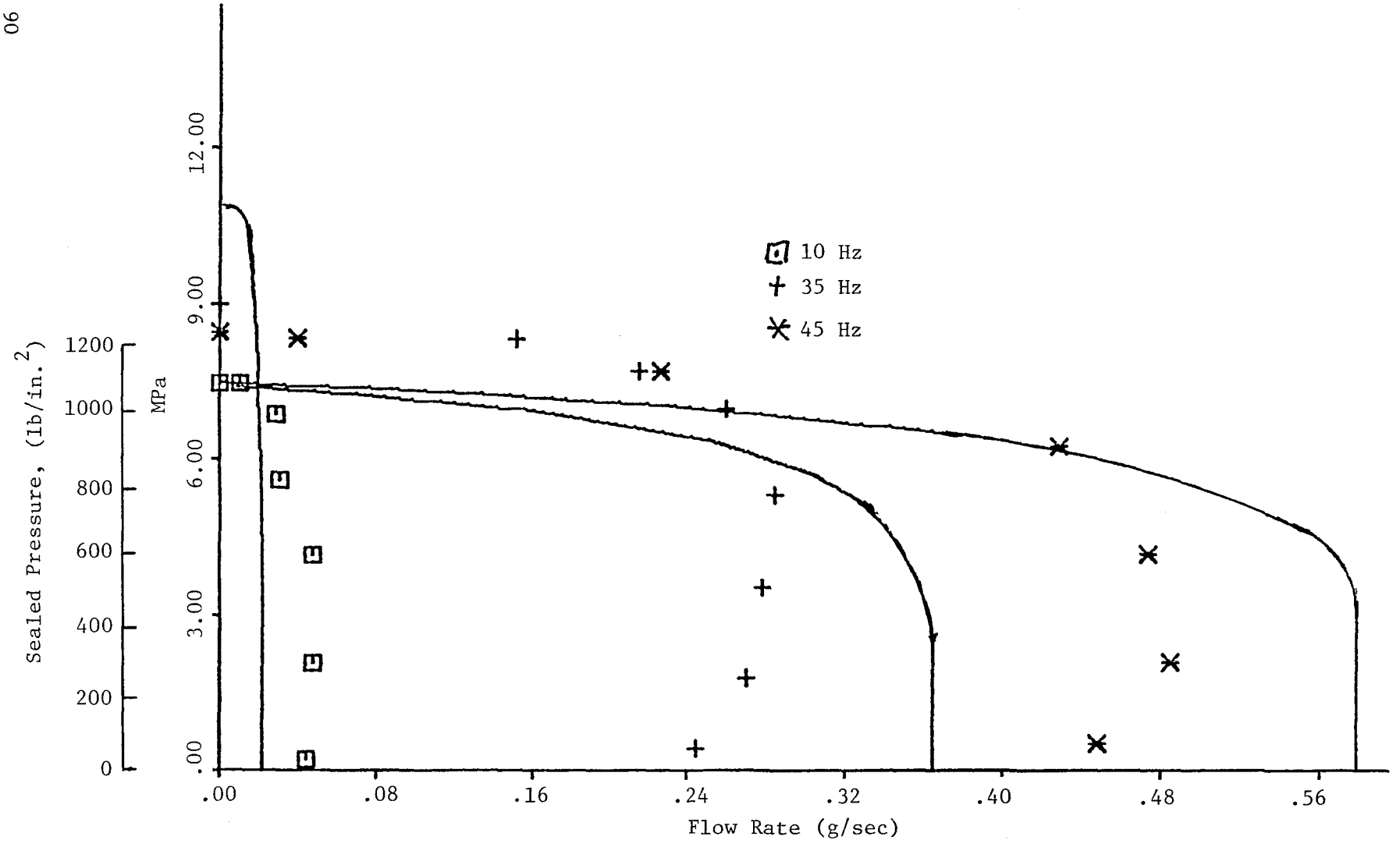

Fig. 37 Pressure-Flow Relationship, Stroke = 50.8 mm

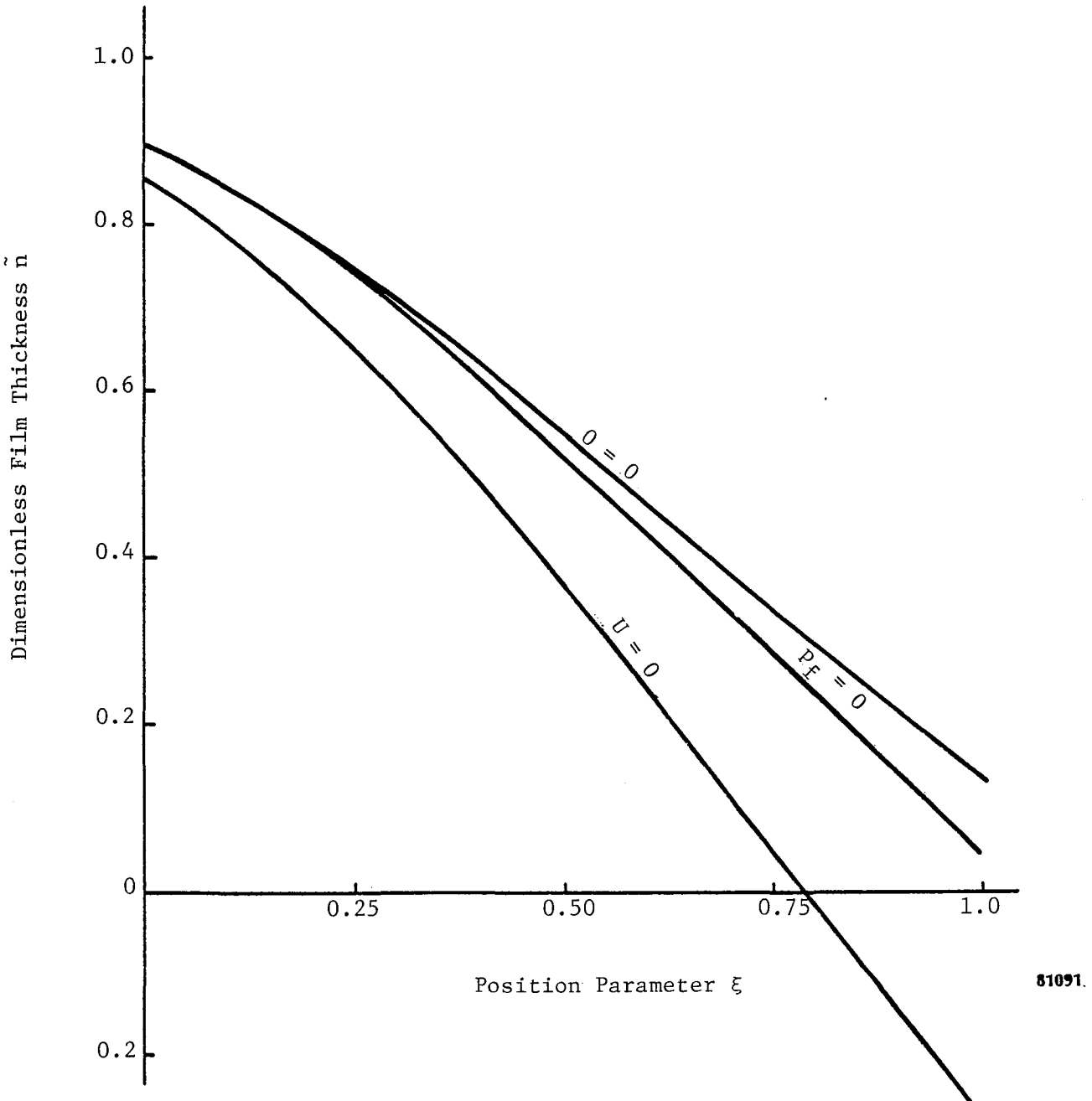

Fig. 38 Dimensionless Film Thickness Profiles, Stroke = 25.4 mm

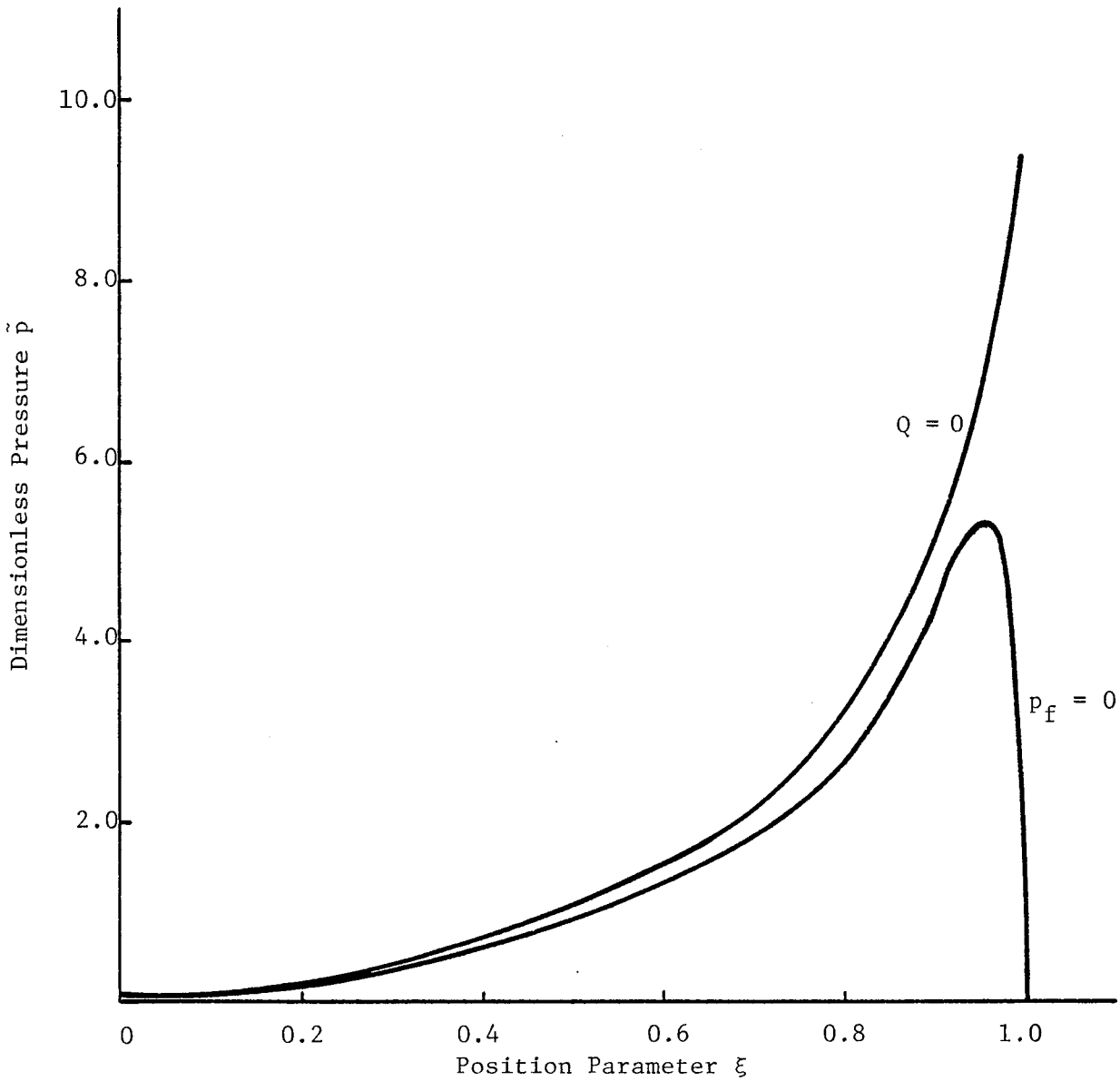

Fig. 39 Dimensionless Pressure Profiles

TABLE 13

GEOMETRY AND PROPERTY VALUES USED IN OBTAINING SOLUTIONS

Oil Viscosity:	μ = 8.3 cp @ 49°C (1.2×10^{-6} $\frac{\text{lb-sec}}{\text{in.}^2}$)
Oil Density:	ρ = 0.9 g/cm^3 (0.32 lb/in.^{3})
Elastic Modulus (Carbon Graphite):	E = 2.14×10^4 MPa (3.11×10^6 lb/in.^{2})
Poisson's Ratio:	ν = 0.29
Loading Length:	e = 0.292 cm (0.114 in.)
Length (Ref. Figure 12):	L_1 = 0.876 cm (0.345 in.)
Hydrodynamic Land Length:	L = 0.559 cm (0.220 in.)
Radius:	R = 1.04 cm (0.409 in.)
Mean Thickness:	t = 0.16 cm (0.63 in.)
Operating Clearance (at temperature):	c = 2.8×10^{-3} cm (1.10×10^{-3} in.)

and higher flow rate. This should result in the observed increase in flow with increased sealed pressure.

A plot of the predicted dimensionless film thickness as a function of position for a 25.4 mm (1.00 in.) stroke at frequency of 45 Hz is shown in Figure 38. The curve labeled u = 0 corresponds to the deformation of the ring that occurs under the applied loading at zero speed without the restraint of the shaft. The negative values of $\tilde{h}$ correspond to an interference fit. The results show a maximum interference of 27% of the clearance. The curve labeled $p_f = 0$ corresponds to the predicted film thickness profile under hydrodynamic conditions with no sealed pressure. The minimum film thickness here is appproximately one-third of the value for the case noted by Q = 0, which represents the film thickness profile at zero flow rate. The general shape of the film thickness profile at these two extremes is similar. The pressures shown in Figure 39 are very close to each other over 90% of the region of hydrodynamic operation; over the last 10%, the pressure rapidly approaches its boundary value. Similar behavior would be observed at intermediate sealed pressures.

The predicted flow rates are very sensitive to the parameters influencing the degree of interference (the applied loading, clearance, thickness, radius and elastic modulus). The hydrodynamic pressures must generate a force sufficient to eliminate the interference and to provide a positive film thickness; this force must be roughly proportional to the interference fit. A 27% increase in the applied loading would double the interference, thereby approximately doubling the hydrodynamic forces needed to generate a film. These hydrodynamic forces could only be developed at very small film thicknesses and, thus, would result in low flow rates.

In designing a pumping ring, it is quite evident that optimum parameter values exist. For a very rigid ring with relatively small deflections, as exemplified by the Bearing Bronze rings, an insufficient hydrodynamic wedge develops, thereby eliminating any significant pumping since flow during the backstroke approaches that of the forward stroke. At relatively high interference fits, as found with the Mechanical Carbon Graphite

rings, the possible sealed pressures are very high and the flow rates relatively low. However, due to the high loading during the return stroke and the small film thicknesses during the forward stroke, wear may become a more significant problem. Between these two extremes lies a ring design which pumps to high pressures, is capable of pumping a significant amount of oil and, yet, does not produce a high rod interference. In the test program presented in this report, the Tin-Based Babbitt rings exhibited this type of performance.

For the present Mechanical Carbon Graphite ring design at low speeds (10 Hz at a 25.4 mm (1.00 in.) stroke), film thicknesses of the order of a few microinches are predicted. To arrive at an optimum design, a sufficient interference fit must be used to meet the sealed pressure requirements but not to significantly exceed them.

This Page Intentionally Left Blank

9.0 CONCLUSIONS AND RECOMMENDATIONS FOR FURTHER STUDY

The pumping ring concept under investigation has the capability of delivering flow and maintaining high sealed pressures in reciprocating systems. Comparisons between theory and experiment indicate a fair degree of qualitative, and some quantitative, agreement. The present theory should provide an initial design tool for the selection of optimum rings for further testing.

Further analytical work is needed for the inclusion of both thermal and transient effects, as well as for the determination of flow during the backstroke for more lightly loaded rings. In addition, for short rings, the effect of ring starvation at the end of the backstroke should be considered since the ring will not be filled until the shaft traverses more than the length of the ring during the forward stroke.

This Page Intentionally Left Blank

APPENDIX A

PARTS LIST FOR HYDRAULIC SUPPLY SYSTEM

NASA PUMPING RING LUBRICATION SYSTEM SCHEMATIC: 642D030

ITEM IDENTIFICATION	NAME	FUNCTION
FCV-1	Flow Control Valve	Test Shaft Bearing Oil Supply
FCV-2	Flow Control Valve	Test Shaft Bearing Oil Supply
FCV-3	Flow Control Valve	Test Shaft Bearing Oil Supply
FCV-4	Flow Control Valve	Test Shaft Bearing Oil Supply
FE-1	Flow Meter	Pumping Ring Inlet Flow Rate
FE-2	Flow Meter	Pumping Ring Inlet Flow Rate
FE-3	Flow Meter	Pumping Ring Bypass Flow Rate
FE-4	Flow Meter	Pumping Ring Bypass Flow Rate
FE-5	Oil Collection Beaker	Pumping Ring Discharge Flow Rate
FE-6	Oil Collection Beaker	Pumping Ring Discharge Flow Rate
FE-7	Orifice	Test Shaft Bearing Oil Supply
FE-8	Orifice	Test Shaft Bearing Oil Supply
FE-9	Orifice	Test Shaft Bearing Oil Supply
FE-10	Orifice	Test Shaft Bearing Oil Supply
FE-11	Oil Filter	Pumping Ring Oil Supply Filter
FE-12	Oil Filter	Crankcase Oil Supply Filter
FE-13	Oil Filter	Test Shaft Bearing Oil Supply Filter

APPENDIX A (CONT'D)

ITEM IDENTIFICATION	NAME	FUNCTION
FE-14	Air Filter	Control Air Filter
FE-15	Oil Pump	Crankcase/Pumping Ring
FE-16	Oil Pump	Test Shaft Bearings
FE-17	Oil Pump	Scavange Pump
FE-18	Filter	Supply Pump Scavange
HV-1	Shut-off Valve	Canister Fill
HV-2	Shut-off Valve	Canister Fill
LI-1	Level Indicator	Reservoir Level
LS-1	Level Switch	Scavange Pump Control
PCV-1	Air-Operated Needle Valve	Pumping Ring Discharge Control
PCV-2	Air-Operated Needle Valve	Pumping Ring Discharge Control
PCV-3	Air Pressure Regulator	Pumping Ring Discharge Control Air
PCV-4	Air Pressure Regulator	Pumping Ring Discharge Control Air
PCV-5	Pressure Regulator	Pumping Ring Supply Control
PCV-6	Pressure Regulator	Crankcase Supply Control
PCV-7	Pressure Regulator	Journal Bending Supply Control
PE-1	Pressure Transducer	Pumping Ring Inlet Oil Pressure
PE-2	Pressure Transducer	Pumping Ring Inlet Oil Pressure
PE-3	Pressure Transducer	Pumping Ring Discharge Oil Pressure
PE-4	Pressure Transducer	Pumping Ring Discharge Oil Pressure

APPENDIX A (CONT'D)

ITEM IDENTIFICATION	NAME	FUNCTION
PI-1	Pressure Indicator	Pumping Ring Inlet Oil Pressure
PI-2	Pressure Indicator	Pumping Ring Inlet Oil Pressure
PI-3	Pressure Indicator	Pumping Ring Discharge Oil Pressure
PI-4	Pressure Indicator	Pumping Ring Discharge Oil Pressure
PI-5	Pressure Indicator	Journal Bearing Supply Pressure
PI-6	Pressure Indicator	Control Air Pressure
PI-7	Pressure Indicator	Control Air Pressure
PI-8	Pressure Indicator	Crankcase Supply Pressure
PI-9	Pressure Indicator	Pumping Ring Regulated Pressure
TE-1	Thermocouple	Pumping Ring Inlet Oil Temperature
TE-2	Thermocouple	Pumping Ring Inlet Oil Temperature
TE-3	Thermocouple	Pumping Ring Discharge Oil Temperature
TE-4	Thermocouple	Pumping Ring Discharge Oil Temperature
TE-5	Thermocouple	Pumping Ring Bypass Oil Temperature
TE-6	Thermocouple	Pumping Ring Bypass Oil Temperature
TI-1	Thermometer	Supply Pump Discharge Temperature
TI-2	Thermometer	Journal Bearing Inlet Temperature
TI-3	Thermometer	Crankcase Inlet Temperature
TCE-1	Heat Exchanger	Reservoir Oil Cooler
TCE-2	Heat Exchanger	Reservoir Oil Heater

APPENDIX A (CONT'D)

ITEM IDENTIFICATION	NAME	FUNCTION
TCV-1	Control Valve	Reservoir Temperature Control
TIR-1	Temperature Recorder	All Temperatures

APPENDIX B

TEST PLAN

HYDRODYNAMIC PUMPING RING EVALUATION

NASA Contract DEN3-119

1.0 OBJECTIVE

The objective of the Hydrodynamic Pumping Ring Test Program is to evaluate performance of various pumping ring designs over a range of speeds, reciprocating shaft stroke lengths (peak to peak) and pumping ring discharge pressures.

2.0 TEST PARAMETERS

2.1 Variable Parameters

The test parameters to be varied during a test sequence will include:

Variable	Magnitude
• Reciprocating Rod Stroke:	24.4 mm (1.00 in.), 38.1 mm (1.50 in.), 50.8 mm (2.00 in.)
• Rotational Frequency:	10 Hz, 35 Hz, 60 Hz
• Pumping Ring Discharge Pressure:	3.45 MPa (500 lb/in.^{2}), 6.89 MPa (1000 lb/in.^{2}), 10.3 MPa* (1500 lb/in.^{2})
• Pumping Ring Design:	Brass, Babbitt, Carbon Graphite (four rings of each design)

2.2 Fixed Parameters

The test parameters to remain fixed for all test sequences will be:

• Pumping Ring Supply Pressure:	0.41 MPa (60 lb/in.^{2})
• Pumping Ring Oil:	20W40 (Mobil DELVAC)
• Oil Supply Temperature:	49°C (120°F)

*This is a target pressure, the maximum pressure obtainable will constitute the third pressure test point.

3.0 TEST MEASUREMENTS

The independent and dependent test parameters will include:

Quantity	Instrument
• Pumping Ring Supply Pressure	Pressure Transducer
• Pumping Ring Supply Temperature	Thermocouple
• Pumping Ring Supply Flow Rate	Variable Area Flow Meter
• Reciprocating Shaft Frequency	Light Sensor/Frequency Meter
• Pumping Ring Temperature	Thermocouple
• Pumping Ring Discharge Pressure	Pressure Transducer
• Pumping Ring Discharge Temperature	Thermocouple
• Pumping Ring Discharge Flow Rate	By Collection Means
• Pumping Ring Supply Pass Temperature	Thermocouple
• Pumping Ring Supply by Flow Rate	Variable Area Flow Meter

The above parameters will be measured on each of two identical pumping ring designs which will be tested and measured simultaneously.

4.0 TEST MATRIX

Table B-1 presents the test matrix to be implemented by this test plan.

A failed test pumping ring will be replaced by an unused ring at the data point when the failure has occurred. That particular data point will be repeated and the test sequence continued to completion or until all rings of the same design have failed.

TEST MATRIX

HYDRODYNAMIC PUMPING RING TEST PROGRAM

Sequence 1.XXX	Stroke mm (in.)	Frequency Hz	Pressure, MPa ($lb/in.^2$)	Design (642C007)
1.1.1.1	25.4 (1.0)	10	3.45 (500)	P1
1.2.1.1		35		
1.3.1.1		60		
1.1.2.1		10	6.89 (1000)	
1.2.2.1		35		
1.3.2.1		60		
1.1.3.1		10	10.3 (1500)	
1.2.3.1		35		
1.3.3.1		60		
1.1.1.2	25.4 (1.0)	10	3.45 (500)	P2
1.2.1.2		35		
1.3.1.2		60		
1.1.2.2		10	6.89 (1000)	
1.2.2.2		35		
1.3.2.2		60		
1.1.3.2		10	10.3 (1500)	
1.2.3.2		35		
1.3.3.2		60		
1.1.1.3	25.4 (1.0)	10	3.45 (500)	P3
1.2.1.3		35		
1.3.1.3		60		
1.1.2.3		10	6.89 (1000)	
1.2.2.3		35		
1.3.2.3		60		
1.1.3.3		10	10.3 (1500)	
1.2.3.3		35		
1.3.3.3		60		

Sequence 2.X.X.X identical to 1.X.X.X except stroke is now 38.1 mm (1.50 in.)

Sequence 3.X.X.X identical to 1.X.X.X except stroke is now 50.8 mm (2.00 in.)

This Page Intentionally Left Blank

APPENDIX C

NOMENCLATURE

D = Rod diameter

E = Elastic modulus

K = Dimensionless flow rate, $\frac{Q}{\pi R u_0 C}$

L = Hydrodynamic land width

L_1 = Effective distance from fixed end to start of film

$\tilde{L}_1$ = Dimensionless length, L_1/L

N = Reciprocating frequency

$P(x)$ = Radial loading function (See Eq. 2)

Q = Volumetric flow rate

Q_m = Mass flow rate

R = Mean ring radius

S = Rod stroke

c = Radial clearance

e = Axial length over which ring closure pressure acts

h = Film thickness

$\tilde{h}$ = Dimensionless film function (Eq. 4)

k = Constant in Reynolds equation

p = Hydrodynamic pressure

$\tilde{p}$ = Dimensionless hydrodynamic pressure, $\frac{C^2}{6\mu u_0 L} p$

p_f = Sealed pressure

$\tilde{p}_f$ = Dimensionless sealed pressure, $\frac{C^2}{6\mu u_0 L} p_f$

p_0 = Ring closure pressure

$\tilde{p}_0$ = Dimensionless closing pressure, $\frac{C^2}{6\mu u_0 L} p_0$

t = Thickness of ring

u_0 = Average velocity (2NS)

NOMENCLATURE (Cont'd)

w = Elastic deflection

x = Position variable

α = Geometric bending parameter, $\dfrac{t^2R^2}{12L^4(1-\nu^2)}$

β = Elastohydrodynamic parameter, $\dfrac{6\mu u_0}{C^2}\dfrac{R^2}{CtE}$

ε = Dimensionless loading length, e/L

μ = Viscosity

ν = Poisson's ratio

ξ = Dimensionless position variable x/L

REFERENCES

1. "Assessment of the State of Technology of Automotive Stirling Engines," DOE/NASA/0032-79/4, NASA CR-159631, MTI 79-ASE77RE2, September 1979. Prepared for NASA LeRC under Contract DEH 3-32.

2. Kuzma, D.C., "Analysis of Pumping Rings," Journal of Lubrication Technology, April 1971, pp. 287-292.

3. Zull, L.M., and Kettleborough, C.F., "An Elastohydrodynamic Analysis of Transient Pumping Ring Operation," Journal of Lubrication Technology, April 1975, pp. 195-201.

4. Theeuwes, G.J.A., "Dynamic Seals in Stirling Engines," Sixteenth Summary Report, Highway Vehicle Systems, Contractors' Coordination Meeting, sponsored by the Department of Energy, September 1979, pp. 289-297.

5. Roark, R.J., "Formulas for Stress and Strain," Chapter 12, Pressure Vessels and Pipes, p. 302.

6. Timoshenko, S., and Woinowsky-Krieger, S., "Theory of Plates and Shells," McGraw-Hill Book Company, New York, 1959.

1. Report No.	2. Government Accession No.	3. Recipient's Catalog No.
NASA CR-165271		

4. Title and Subtitle	5. Report Date
AN EXPERIMENTAL EVALUATION OF OIL PUMPING RINGS	April 1981
	6. Performing Organization Code

7. Author(s)	8. Performing Organization Report No.
Martin W. Eusepi, Jed Walowit, Maurice Cohen	MTI 81TR3
	10. Work Unit No.

9. Performing Organization Name and Address	11. Contract or Grant No.
Mechanical Technology Incorporated 968 Albany-Shaker Road Latham, New York 12110	DEN3-119
	13. Type of Report and Period Covered
12. Sponsoring Agency Name and Address	Contractor Report
National Aeronautics and Space Administration Washington, D.C. 20546	14. Sponsoring Agency Code DOE/NASA/0119-81/1

15. Supplementary Notes

Final Report. Prepared under Interagency Agreement EC-77-A-31-1040.
Project Manager, Robert E. Cunningham
Structures and Mechanical Technologies Division, NASA-Lewis Research Center
Cleveland, Ohio 33315

16. Abstract

This report covers the design and construction of a reciprocating test vehicle to be used in evaluating hydrodynamic oil pumping rings. In addition, this report presents experimental test data for three pumping ring designs that were constructed from Tin-Based Babbitt (SAE 11), Bearing Bronze (SAE 660), and Mechanical Carbon Graphite (Union Carbide Grade CNF-J). Data of pumped flow rate versus delivered pressure, as well as friction loss, are reported for the following conditions: frequencies of 10, 35 and 45 Hz; strokes of 25.4 mm (1.00 in.), 38.1 mm (1.50 in.) and 50.8 (2.00 in.); oil inlet temperatures of 49°C (120°F); and pumping ring close-in pressures of 10.3 MPa (1500 lb/in.^{2}). A 20W40 automotive oil was used for all tests. The maximum delivered pressure was 11 MPa (1600 lb/in.^{2}). An analysis of hydrodynamic oil pumping rings was performed and the results of the analysis were compared to measured test data.

17. Key Words (Suggested by Author(s))	18. Distribution Statement
Hydrodynamic Oil Pumping Ring Reciprocating Shaft High-Pressure Oil Pump	Unclassified-Unlimited Star Category 37 DOE Category UC-96

19. Security Classif. (of this report)	20. Security Classif. (of this page)	21. No. of Pages	22. Price*
Unclassified	Unclassified	109	

* For sale by the National Technical Information Service, Springfield, Virginia 22151

MTI-17983

NASA-C-168 (Rev. 6-71)